Article

VDAC2 loss elicits tumour destruction and inflammation for cancer therapy

https://doi.org/10.1038/s41586-025-08732-6

Received: 7 April 2024

Accepted: 3 February 2025

Published online: 19 March 2025

Open access

Check for updates

Sujing Yuan[1,4], Renqiang Sun[1,4], Hao Shi[1], Nicole M. Chapman[1], Haoran Hu[1], Cliff Guy[1], Sherri Rankin[1], Anil KC[1], Gustavo Palacios[1], Xiaoxi Meng[1], Xiang Sun[1], Peipei Zhou[1], Xiaoyang Yang[2], Stephen Gottschalk[3] & Hongbo Chi[1]✉

Tumour cells often evade immune pressure exerted by CD8$^+$ T cells or immunotherapies through mechanisms that are largely unclear[1,2]. Here, using complementary in vivo and in vitro CRISPR–Cas9 genetic screens to target metabolic factors, we established voltage-dependent anion channel 2 (VDAC2) as an immune signal-dependent checkpoint that curtails interferon-γ (IFNγ)-mediated tumour destruction and inflammatory reprogramming of the tumour microenvironment. Targeting VDAC2 in tumour cells enabled IFNγ-induced cell death and cGAS–STING activation, and markedly improved anti-tumour effects and immunotherapeutic responses. Using a genome-scale genetic interaction screen, we identified BAK as the mediator of VDAC2-deficiency-induced effects. Mechanistically, IFNγ stimulation increased BIM, BID and BAK expression, with VDAC2 deficiency eliciting uncontrolled IFNγ-induced BAK activation and mitochondrial damage. Consequently, mitochondrial DNA was aberrantly released into the cytosol and triggered robust activation of cGAS–STING signalling and type I IFN response. Importantly, co-deletion of STING signalling components dampened the therapeutic effects of VDAC2 depletion in tumour cells, suggesting that targeting VDAC2 integrates CD8$^+$ T cell- and IFNγ-mediated adaptive immunity with a tumour-intrinsic innate immune-like response. Together, our findings reveal VDAC2 as a dual-action target to overcome tumour immune evasion and establish the importance of coordinately destructing and inflaming tumours to enable efficacious cancer immunotherapy.

Immunotherapies such as adoptive cell therapy (ACT) and immune checkpoint blockade (ICB) show considerable clinical benefits for cancer treatment[1,2]. CD8$^+$ T cells contribute to the cancer–immunity cycle and immunotherapeutic effects[3] by releasing cytotoxic granules[4] and producing pro-inflammatory cytokines[5]. In particular, IFNγ contributes to tumour control by increasing tumour antigen presentation and production of chemokines that mediate immune cell recruitment and remodelling of the tumour microenvironment (TME). Accordingly, IFNγ signalling is key to the immunotherapeutic success of ACT and ICB[6,7]. Nonetheless, immunotherapies do not achieve sustained clinical responses in most patients with solid tumours[1,2,8], with loss-of-function mutations in IFNγ-pathway-related genes accounting for such therapeutic resistance in a small population of patients[9,10]. As it remains unclear how the majority of cancers evade immunosurveillance[11], targeting the mechanisms that overcome tumour resistance to IFNγ and CD8$^+$ T cell-induced cytotoxic effects holds promise for inducing potent anti-tumour effects and maximizing immunotherapeutic responses.

The TME is characterized by nutrient competition and metabolic communication between cancer cells and immune cells that contribute to the tumour immune escape[12–15]. Furthermore, targeting metabolism-associated processes, including electron flow through mitochondrial complex I[16] or autophagy[17], in cancer cells reinvigorates anti-tumour immunity and ICB. However, we lack a systemic understanding of the molecules or pathways in tumour cells that mediate immune escape, including those related to metabolism and associated signalling events.

VDAC2 mediates tumour immune evasion

To identify metabolism-associated factors underlying tumour immune evasion, we transduced Cas9- and ovalbumin (OVA)-expressing B16F10 (B16-OVA) melanoma cells with a single guide RNA (sgRNA) library targeting 3,017 metabolism-associated genes[18], and performed CRISPR drop-out screens[19] under conditions of T cell-mediated immune pressure (Fig. 1a and Methods). sgRNAs targeting *Vdac2* were among the top depleted sgRNAs in tumour cells responding to immune pressure in vitro and in vivo (Fig. 1b,c, Extended Data Fig. 1a and Supplementary Table 1a–d), suggesting its role in tumour immune evasion. To validate these findings, we transduced Cas9-expressing B16-OVA tumour cells with two independent sgRNAs targeting *Vdac2* (or non-targeting control, NTC) to mediate *Vdac2* deletion (Extended Data Fig. 1b and Supplementary Table 2). VDAC2-deficient B16-OVA tumour

[1]Department of Immunology, St. Jude Children's Research Hospital, Memphis, TN, USA. [2]Experimental Cellular Therapeutics Laboratory, St. Jude Children's Research Hospital, Memphis, TN, USA. [3]Department of Bone Marrow Transplantation and Cellular Therapy, St. Jude Children's Research Hospital, Memphis, TN, USA. [4]These authors contributed equally: Sujing Yuan, Renqiang Sun. ✉e-mail: hongbo.chi@stjude.org

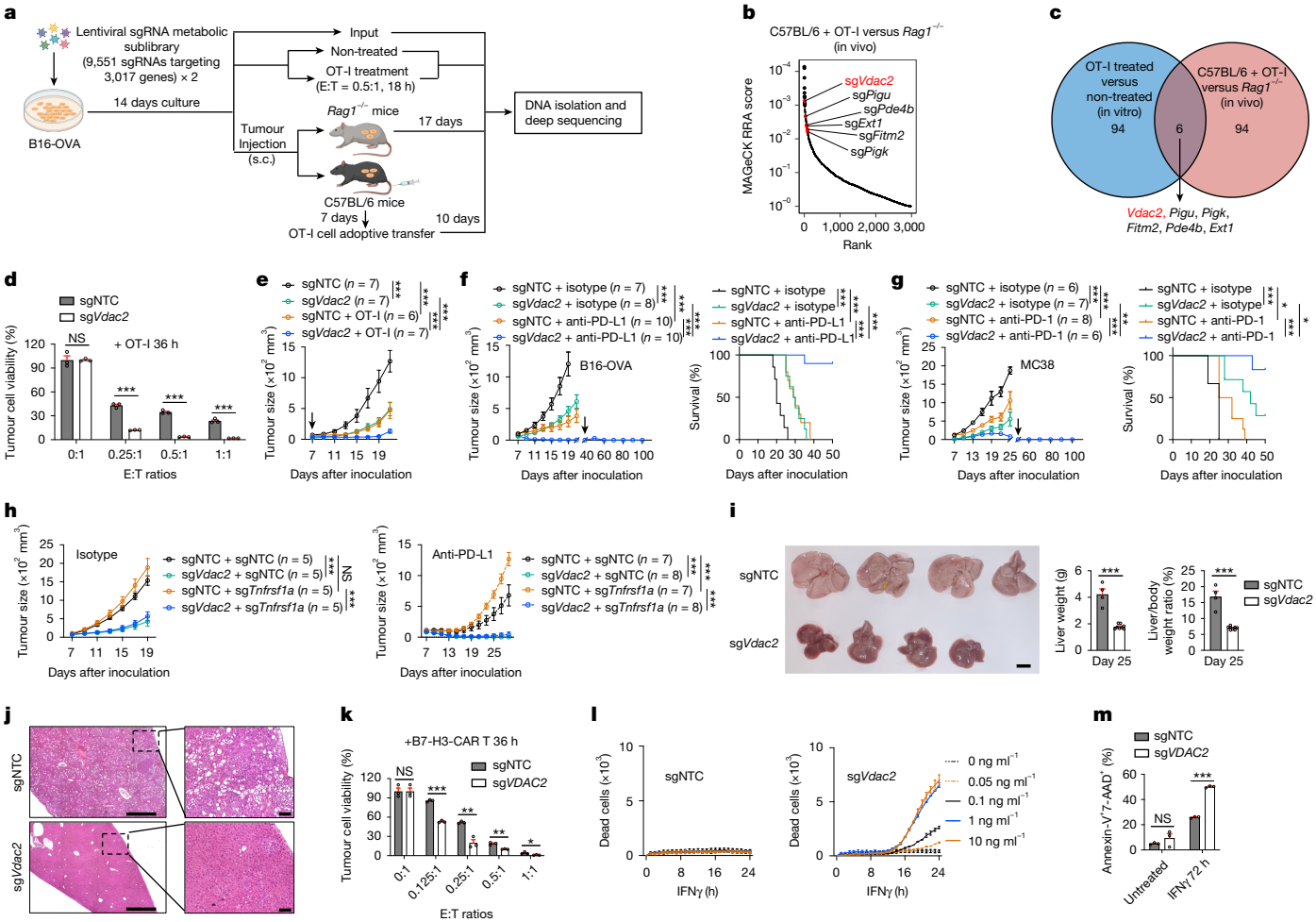

Fig. 1 | VDAC2 deficiency sensitizes tumours to IFNγ-induced cell death and immunotherapy. a, Schematic for CRISPR screening in B16-OVA tumour cells. Created in BioRender. Sun, R. (2025) https://BioRender.com/g06b183. **b**, The top depleted genes in tumour cells from C57BL/6 + OT-I cell versus *Rag1*$^{-/-}$ condition. RRA, robust rank aggregation. **c**, The overlap between the top 100-ranked gene candidates from CRISPR screens. **d**, Control or VDAC2-deficient tumour cell viability after co-culture with OT-I cells. $n = 3$ per group. E:T, effector:target ratio. **e**, Control or VDAC2-deficient B16-OVA tumour growth without or with (indicated by arrow) adoptive transfer of activated OT-I cells. **f**, Control and VDAC2-deficient B16-OVA tumour growth after the indicated treatments. Arrow indicates tumour rechallenge of sg*Vdac2* and anti-PD-L1 group (left). Right, the survival of mice after primary tumour challenge. **g**, Control and VDAC2-deficient MC38 tumour growth after the indicated treatments. Arrow indicates tumour rechallenge of sg*Vdac2* and anti-PD-1 group (left). Right, the survival of mice after primary tumour challenge. **h**, Indicated sgRNA-transduced B16-OVA tumour growth after the indicated treatments. **i**,**j**, Liver tumour burden (**i**) and histological analyses (**j**) at day 25. $n = 4$ (sgNTC) and $n = 8$ (sg*Vdac2*). Scale bars, 1 cm (**i**), 500 µm (**j**, left) and 100 µm (**j**; high-magnification inset, right). **k**, Control or VDAC2-deficient LoVo tumour cell viability after co-culture with B7-H3-CAR T cells. $n = 3$ per group. **l**,**m**, Control or VDAC2-deficient B16-OVA (**l**, $n = 2$ per group) or LoVo (**m**, $n = 3$ per group) tumour cell death after IFNγ treatment. Data are mean ± s.e.m., representative of three (**f**, **i**, **j** and **m**), two (**d**, **e**, **g**, **k** and **l**) or one (**h**) independent experiments. Statistical analysis was performed using two-tailed unpaired Student's *t*-tests (**d**, **i** and **k**), two-way analysis of variance (ANOVA) (**e**; **f** and **g** (tumour size); **h** and **m**) and Mantel–Cox tests (**f** and **g** (survival)); NS, not significant; $^{*}P < 0.05$; $^{**}P < 0.01$; $^{***}P < 0.001$.

cells were more sensitive to OT-I-mediated cytotoxicity (Fig. 1d and Extended Data Fig. 1c) but showed undisturbed in vitro proliferation (Extended Data Fig. 1d). Also, *Vdac2* deletion in MC38-OVA tumour cells increased their sensitivity to OT-I-cell-mediated killing (Extended Data Fig. 1b,e). After transplantation into immunocompetent wild-type mice, VDAC2-deficient tumour cells showed greatly reduced growth, associated with extended mouse survival, while such phenotypes were not observed in immunodeficient *Rag1*$^{-/-}$ mice (Extended Data Fig. 1f,g), suggesting adaptive-immune-dependent effects. Moreover, VDAC2-deficient tumours were markedly sensitized to OT-I-mediated therapeutic effects in an ACT model (Fig. 1e and Extended Data Fig. 1h). Together, these results indicate that VDAC2 targeting sensitizes tumour cells to CD8^{+} T cell-mediated killing in vitro and in vivo.

We next tested whether VDAC2 deficiency influences ICB efficacy. VDAC2 deficiency in tumours greatly improved responsiveness to anti-PD-L1 and anti-PD-1 in B16-OVA and MC38 tumour models, respectively (Fig. 1f,g), and tumour-free mice after ICB therapy were protected against tumour rechallenge (Fig. 1f,g), indicating robust induction of long-term immune memory. In a metastatic tumour model, VDAC2 loss reduced the lung tumour burden and extended mouse survival in an adaptive-immune-dependent manner (Extended Data Fig. 1i–l). Given that unresponsiveness to tumour necrosis factor (TNF) represents a major therapeutic barrier to ICB[20], we generated B16-OVA tumour cells lacking both VDAC2 and TNF receptor (TNFR; encoded by *Tnfrsf1a*) to test whether VDAC2 targeting overcomes ICB resistance in TNF-unresponsive tumours. Although TNFR-deficient tumours were resistant to OT-I-cell- or IFNγ- and TNF-induced killing[21], *Vdac2* co-deletion improved their responsiveness to these treatments (Extended Data Fig. 1m,n). Furthermore, *Vdac2* co-deletion also sensitized TNFR-deficient tumours to anti-PD-L1 ICB therapy (Fig. 1h and

Extended Data Fig. 1o), indicating that VDAC2 loss enhances the therapeutic potential of ICB-resistant tumours. Finally, we targeted VDAC2 in a well-established genetic model of constitutively active AKT and NRAS-driven liver cancer. The liver tumour burden was decreased and mouse survival was extended after VDAC2 targeting (Fig. 1i,j and Extended Data Fig. 1p). Such effects were not observed in *Rag1*$^{-/-}$ mice (Extended Data Fig. 1p–r), suggesting that *Vdac2* deletion also conferred adaptive-immune-dependent protection in this genetic model. Thus, VDAC2 deficiency impedes tumour growth and improves anti-tumour and immunotherapeutic effects in multiple tumour models in vivo.

To expand the physiological and therapeutic relevance, we examined the dependency of human cancer cells for VDAC2 using the Cancer DepMap. *VDAC2* perturbation impaired the fitness of a small subgroup of human tumour cell lines (Extended Data Fig. 1s), suggesting that *VDAC2* is not a common essential gene for tumour fitness. By contrast, *VDAC2* deletion in a patient-derived melanoma cell line modestly sensitized those cells to tumour-infiltrating lymphocyte (TIL) therapy in vitro[22] (Extended Data Fig. 1t). Consistent with this notion, VDAC2-deficient LoVo tumour cells (a human colon cancer cell line that expresses the B7-H3 antigen) were more sensitive to B7-H3 chimeric antigen receptor (CAR)-T cell-mediated killing in vitro (Fig. 1k and Extended Data Fig. 1u). Collectively, targeting VDAC2 in tumour cells represents a powerful means to overcome immune evasion and bolster cancer immunotherapy.

VDAC2 loss enables tumour killing by IFNγ

To determine the mechanisms underlying improved CD8$^+$ T cell-mediated killing of VDAC2-deficient tumour cells, we generated perforin-, IFNγ- or TNF-deficient OT-I cells and cultured them with control or VDAC2-deficient B16-OVA tumour cells. Loss of IFNγ but not perforin or TNF prevented OT-I-cell-mediated killing of VDAC2-deficient tumours (Extended Data Fig. 2a). Similar impairment occurred after IFNγ blockade (Extended Data Fig. 2b). Consistent with this notion, co-deletion of *Ifngr1*, *Ifngr2* or *Jak1* in VDAC2-deficient B16-OVA cells blocked their increased susceptibility to OT-I-cell-mediated killing (Extended Data Fig. 2c). Thus, IFNγ enables increased CD8$^+$ T cell-mediated killing of VDAC2-deficient tumour cells in vitro.

We therefore tested whether VDAC2 deficiency renders tumour cells more sensitive to IFNγ. Whereas control cells were not susceptible to IFNγ-induced cell death, VDAC2-deficient B16-OVA cells showed markedly increased cell death and lactate dehydrogenase (LDH) release after IFNγ (but not TNF) stimulation (Fig. 1l and Extended Data Fig. 2d,e). To validate the cell-intrinsic effects, we used a dual-colour co-culture system (Methods) and found that IFNγ but not TNF treatment impaired the survival of VDAC2-deficient B16-OVA cells compared with the control cells (Extended Data Fig. 2f), indicating that IFNγ mediates the increased death of VDAC2-deficient tumour cells. Mechanistically, VDAC2 deficiency did not affect canonical IFNγ–STAT1 signalling (Extended Data Fig. 2g). Instead, we found increased cleavage of caspase-3, caspase-7 and gasdermin E (GSDME) in VDAC2-deficient cells after IFNγ stimulation (Extended Data Fig. 2g). Such effects on GSDME cleavage were dependent on caspase-3 or caspase-9 (Extended Data Fig. 2h), suggesting activation of secondary necrosis mediated by caspase-3 and GSDME[23–25] in the absence of VDAC2.

To assess the requirement of specific caspases or GSDME in mediating cell death in response to IFNγ treatment, we generated VDAC2-deficient tumours cells lacking caspase-3, caspase-7 or GSDME (Extended Data Fig. 2i). Individual targeting of these molecules showed partial effects in mitigating the increased IFNγ-induced death of VDAC2-deficient cells (Extended Data Fig. 2j,k). Similarly, treatment with the pan-caspase inhibitor emricasan reduced IFNγ-induced cell death of VDAC2-deficient tumour cells, while inhibition of ferroptosis (using ferrostatin-1), necroptosis (using necrostatin-1) and GSDMD-mediated pyroptosis (with disulfiram) had no such effects (Extended Data Fig. 2l). Moreover, there was increased staining of activated caspase-3 and elevated cleavage of caspase-3, caspase-7 and GSDME in VDAC2-deficient tumours, especially in response to anti-PD-L1 treatment, which promoted IFNγ production in the TME (Extended Data Fig. 2m–o). Collectively, VDAC2 loss drives IFNγ-mediated tumour cell death, mediated by apoptosis and secondary necrosis, in vitro and in vivo.

We next analysed the expression of VDAC family members in tumour cells and immune cells from syngeneic mouse tumour (Gene Expression Omnibus (GEO): GSE121861), human melanoma (GEO: GSE215121) and human lung cancer (GEO: GSE148071), and found higher expression in mouse and human tumour cells compared with in various immune cells (Extended Data Fig. 2p,q). However, only tumour cells deficient in VDAC2 but not VDAC1 or VDAC3 showed elevated IFNγ-induced cell death (Extended Data Fig. 2r), indicating the selectivity for VDAC2 deficiency. In human LoVo tumour cells, VDAC2 deficiency also increased IFNγ-induced cell death (Fig. 1m), suggesting conserved effects in mouse and human tumour cell lines.

PTPN2 targeting improves the immunotherapeutic response by enhancing IFNγ signalling[7]. B16-OVA tumour cells lacking VDAC2 or PTPN2 showed comparable sensitivity to CD8$^+$ T cell-mediated killing (Extended Data Fig. 3a), whereas VDAC2-deficient cells showed greater sensitivity to IFNγ-induced cell death (Extended Data Fig. 3b). Moreover, targeting of VDAC2 or PTPN2 in tumour cells showed a similar therapeutic benefit in vivo (Extended Data Fig. 3c). Importantly, *Vdac2* and *Ptpn2* co-deletion further enhanced IFNγ-induced death of VDAC2-deficient tumour cells and impaired their in vivo growth compared with loss of either molecule alone (Extended Data Fig. 3d–f), suggesting that VDAC2 and PTPN2 represent molecular targets for combination therapy.

Loss of VDAC2 inflames the TME

To unbiasedly profile the tumour immune microenvironment, we performed paired single-cell RNA-sequencing (scRNA-seq) with single-cell T cell receptor sequencing (scTCR-seq) analysis of intratumoural immune cells (CD45$^+$) and tumour cells (CD45$^-$) from control and VDAC2-deficient B16-OVA tumour-bearing mice. Unsupervised manifold approximation and projection (UMAP) clustering of intratumoural CD45$^+$ cells identified several major immune cell populations (Fig. 2a). Among them, the CD8$^+$ T cell proportion was increased in VDAC2-deficient tumours (Fig. 2b). Flow cytometry analysis validated the increased proportion and number of CD8$^+$ T cells, as well as the increased cellularity of intratumoural CD45$^+$ cells and CD4$^+$ T cells (Fig. 2c,d and Extended Data Fig. 4a). Furthermore, the ratio of CD8$^+$ T cells to regulatory T (T_{reg}) cells was increased in VDAC2-deficient tumours (Fig. 2e), consistent with improved anti-tumour effects. Moreover, CD8$^+$ T cells had markedly increased clonal expansion in VDAC2-deficient tumours (Fig. 2f). Furthermore, CD8$^+$ T cells from VDAC2-deficient tumours showed increased activity scores of gene signatures related to early activation and effector/cytokine production (Fig. 2g) and augmented expression of *Ifng* and *Prf1* (Extended Data Fig. 4b), indicating enhanced effector function. Accordingly, there was an increased number of IFNγ$^+$TNF$^+$ or granzyme B$^+$ (GZMB$^+$) cells among intratumoural CD8$^+$ T cells, and expression of IFNγ, TNF and IL-2 was also elevated in intratumoural CD8$^+$ T cells (Fig. 2h,i and Extended Data Fig. 4c), suggesting improved quality of CD8$^+$ T cell effector function in the TME.

Additionally, stem-like and terminally differentiated CD8$^+$ T cells showed reduced and increased frequencies in the VDAC2-deficient TME, respectively (Extended Data Fig. 4d–f). Notably, terminally differentiated CD8$^+$ T cells retained high expression of *Prf1*, *Ifng* and *Gzmb* (Extended Data Fig. 4e), suggesting that these cells were not fully exhausted. Moreover, the effector-like CD8$^+$ T cell population[26–29] was increased in VDAC2-deficient tumours (Extended Data Fig. 4f), consistent with their more activated state (Fig. 2g). For further mechanistic insights, we performed assay for transposase-accessible

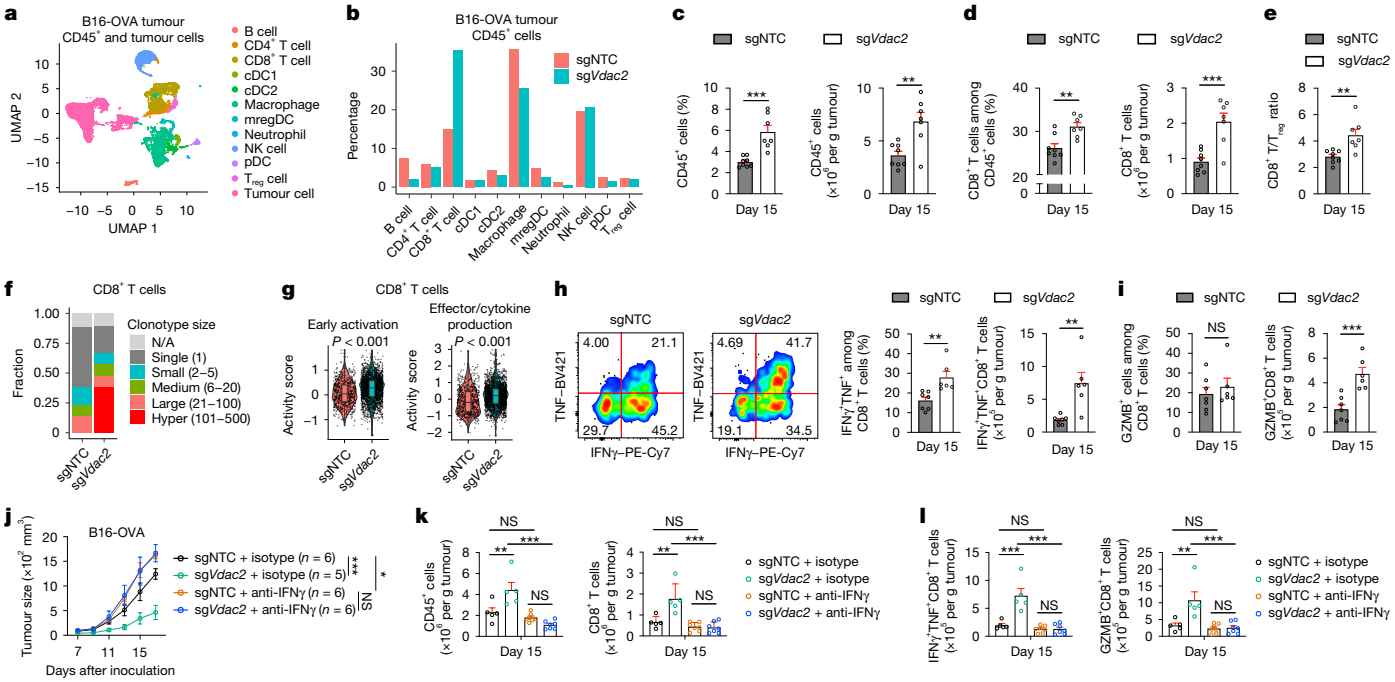

Fig. 2 | VDAC2-deficiency-induced TME inflammatory reprogramming requires IFNγ. a, UMAP plot of the indicated cell clusters from scRNA-seq profiling of control and VDAC2-deficient tumours. $n = 2$ biological replicates per group. cDC, conventional dendritic cell; mregDC, mature dendritic cell enriched in immunoregulatory molecules; pDC, plasmacytoid dendritic cell. **b**, The frequencies of the indicated intratumoural immune cell populations among CD45$^+$ cells in each genotype. **c**–**e**, CD45$^+$ cells (**c**), CD8$^+$ T cells (**d**) and the ratio of CD8$^+$ T cells to T_{reg} cells (**e**) in control ($n = 8$) and VDAC2-deficient ($n = 7$) B16-OVA tumours. **f**, The frequencies of CD8$^+$ T cells grouped by clonotype sizes, as assessed by scTCR-seq. N/A, TCR type not detected. **g**, Activity scores of early activation and effector/cytokine production-related gene signatures in intratumoural CD8$^+$ T cells from control ($n = 710$ cells) and VDAC2-deficient ($n = 2{,}295$ cells) B16-OVA tumours. The box plots show the median (centre line) and the interquartile range (25% to 75%; box limits). **h**,**i**, IFNγ$^+$TNF$^+$ (**h**) and GZMB$^+$ (**i**) CD8$^+$ T cells from B16-OVA tumours. $n = 7$ (sgNTC) and $n = 6$ (sg*Vdac2*). **j**, Control and VDAC2-deficient tumour growth after the indicated treatments. **k**,**l**, CD45$^+$ cells (**k**, left) and CD8$^+$ T cells (**k**, right) or IFNγ$^+$TNF$^+$ (**l**, left) and GZMB$^+$ (**l**, right) CD8$^+$ T cells from the indicated B16-OVA tumours. $n = 5$ (sgNTC + isotype and sg*Vdac2* + isotype) and $n = 7$ (sgNTC + anti-IFNγ and sg*Vdac2* + anti-IFNγ). Data are mean ± s.e.m., representative of three (**c**–**e**, **h** and **i**) or two (**j**–**l**) independent experiments. Statistical analysis was performed using two-tailed unpaired Student's *t*-tests (**c**–**e**, **h** and **i**), one-way ANOVA (**k** and **l**), two-way ANOVA (**j**) and two-tailed Wilcoxon rank-sum tests (**g**).

chromatin using sequencing (ATAC–seq) analysis of PD-1$^-$ and PD-1$^+$CD8$^+$ T cells from control and VDAC2-deficient tumours. Both PD-1$^-$ and PD-1$^+$CD8$^+$ T cells (largely representing non-clonally expanded and clonally expanded cells, respectively; Extended Data Fig. 4d,e) from VDAC2-deficient tumours had increased chromatin accessibility of T cell-activation-associated genes including *Batf*, *Ifng* and *Prkcb* (Extended Data Fig. 4g, Supplementary Table 3). Accordingly, the frequency of effector-like PD-1$^+$Ki67$^+$CD8$^+$ T cells[29] was increased in VDAC2-deficient tumours (Extended Data Fig. 4h), further establishing increased effector function.

Chronic IFNγ stimulation increases the expression of ligands for T cell inhibitory receptors (TCIRs) such as PD-L1 and TNFRSF14[30]. We therefore inoculated wild-type mice with control or VDAC2-deficient B16-OVA tumour cells and analysed the expression of TCIR ligands[30] (Extended Data Fig. 4i). VDAC2 deficiency did not exert major or consistent effects on TCIR ligands at days 15 and 21 after primary tumour inoculation, except for a modest increase in CD86 expression (Extended Data Fig. 4j). We next isolated control or VDAC2-deficient tumour cells on day 21 after primary tumour challenge, and reinoculated these cells into naive recipient mice (Extended Data Fig. 4i). On day 15 after transplantation into new recipients, TCIR ligands were also not upregulated (Extended Data Fig. 4k). Thus, TCIR ligand expression is not increased after long-term loss of VDAC2.

Beyond B16-OVA tumours, MC38-OVA tumours lacking VDAC2 had reduced tumour growth and altered immune cell compositions (Extended Data Fig. 4l–q). Notably, the effects of *Vdac2* deletion in tumour cells on intratumoural CD8$^+$ T cells were similar to those induced by anti-PD-1 treatment in B16-OVA[31] and MC38[32] tumours (Extended Data Fig. 4r,s), suggesting that VDAC2 deficiency in tumour cells reprograms CD8$^+$ T cell activity, potentially through pathways that overlap with PD-1 blockade. Thus, VDAC2 deficiency reshapes the tumour immune compartment, with a particular effect on intratumoural CD8$^+$ T cells.

To establish translational relevance, we examined the correlation between *VDAC2* expression and inflammatory signatures or T cell-related genes in human tumour types (Methods), and found that 9 out of 33 tumour types showed a negative correlation ($P \leq 0.05$) between *VDAC2* expression and a tumour inflammation signature (Extended Data Fig. 4t). Moreover, *VDAC2* expression was often negatively correlated ($P \leq 0.05$) with *CCL5* (13 out of 33 tumour types) or *CD3D* expression (18 out of 33 tumour types) (Extended Data Fig. 4t). Accordingly, melanoma and non-small cell lung cancer with high *VDAC2* expression had reduced CD8$^+$ and CD4$^+$ T cell fractions (Extended Data Fig. 4u,v), suggesting that *VDAC2* expression negatively correlates with inflammatory- and T cell-related signatures and T cell infiltration in human tumours. Finally, high expression of a curated VDAC2-suppressed gene signature was associated with improved overall survival in patients with melanoma, including those treated with anti-PD-1 antibody (Extended Data Fig. 4w,x and Supplementary Table 4). Thus, an increase in VDAC2-suppressed gene signature corresponds to improved disease outcomes and response to ICB in patients with melanoma.

VDAC2 loss improves anti-tumour immunity

To examine the contribution of IFNγ to VDAC2-deficiency-associated effects, we treated VDAC2-deficient B16-OVA tumour-bearing mice

with anti-IFNγ, which enhanced tumour growth to levels comparable to those observed in anti-IFNγ-treated control tumours (Fig. 2j). Blocking IFNγ also reduced intratumoural CD45$^+$ immune cells and the abundance and effector function of CD8$^+$ T cells in VDAC2-deficient tumours (Fig. 2k,l). We next treated mice transiently with anti-IFNγ at early or late time periods after tumour inoculation (Methods) and found that both treatment regimens eliminated the beneficial effects of *Vdac2* deletion (Extended Data Fig. 5a,b). Thus, IFNγ reshapes the tumour immune microenvironment of VDAC2-deficient tumours.

To determine the cellular sources of IFNγ, we compared *Ifng* expression in different immune cell populations and found high expression of *Ifng* in CD8$^+$ T cells and, to a lesser extent, natural killer (NK) cells, in both control and VDAC2-deficient B16-OVA tumours (Extended Data Fig. 5c). Given the pronounced accumulation of CD8$^+$ T cells in VDAC2-deficient tumours, we then depleted CD8$^+$ T cells. We found that VDAC2-deficient tumour growth was increased (Extended Data Fig. 5d,e), suggesting the importance of CD8$^+$ T cells in mediating VDAC2 deficiency-associated effects. To test whether CD8$^+$ T cell-derived IFNγ contributes to these effects, we generated $Cd8^{cre}Ifng^{fl/fl}$ chimeras to deplete *Ifng* specifically in CD8$^+$ T cells (Methods) (Extended Data Fig. 5f). Compared with control tumours, VDAC2-deficient tumours had the expected reduction in tumour growth and enhanced mouse survival in wild-type chimeras, whereas VDAC2-deficient tumours and control tumours had comparable growth in $Cd8^{cre}Ifng^{fl/fl}$ chimeras (Extended Data Fig. 5g). Collectively, these results indicate that intratumoural IFNγ derived from CD8$^+$ T cells has a major role in mediating the impaired growth of VDAC2-deficient tumours.

VDAC2 impedes IFNγ-induced STING signalling

To determine the mechanistic basis, we first analysed the transcriptome profiles of control and VDAC2-deficient tumour cells in the scRNA-seq dataset. Gene set enrichment analysis (GSEA) showed that VDAC2-deficient tumour cells had increased IFNα- and IFNγ-related gene signatures (Fig. 3a). Furthermore, GSEA of tumour cells treated with IFNγ or OT-I cells revealed increased IFNγ and IFNα response signatures in VDAC2-deficient versus control tumour cells, with such signatures representing the only shared Hallmark pathways upregulated in the absence of VDAC2 under conditions of immune pressure (Extended Data Fig. 6a–c and Supplementary Table 5). Accordingly, multiple genes in the IFN-responsive pathways were upregulated in VDAC2-deficient tumours treated with IFNγ or OT-I cells (Fig. 3b,c and Extended Data Fig. 6d). Furthermore, *Ifnb1* and *Ccl5*, which are induced by cGAS–STING[33], were increased in IFNγ-treated VDAC2-deficient tumour cells, with elevated IFNβ protein levels also detected after IFNγ treatment in vitro or in tumour lysates in vivo (Fig. 3d–f and Extended Data Fig. 6e). Thus, IFNγ stimulation aberrantly upregulates the type I IFN response in VDAC2-deficient tumour cells.

Furthermore, Ingenuity pathway analysis (IPA) revealed upregulated activities of STING, IRF3 and IRF7 in VDAC2-deficient tumour cells after IFNγ or OT-I cell treatment (Fig. 3g and Supplementary Table 6). ATAC–seq profiling of VDAC2-deficient versus control tumour cells, followed by motif enrichment analysis of differentially accessible chromatin, revealed that IRF5 and IRF7 (albeit not IRF1) activities were increased in VDAC2-deficient tumour cells (Fig. 3h), indicating enhanced type I IFN-related responses in VDAC2-deficient tumour cells in vitro and in vivo. On the basis of these findings, we examined STING expression and activation, and found that STING expression was upregulated in both control and VDAC2-deficient tumour cells after IFNγ treatment (Fig. 3i and Extended Data Fig. 6f). By contrast, compared with control tumours, the levels of phosphorylated STING (Ser365), TBK1 (Ser172) and IRF3 (Ser396) were increased in VDAC2-deficient tumour cells at ≥12 h of IFNγ stimulation (Fig. 3i and Extended Data Fig. 6f). Thus, VDAC2 restrains IFNγ-induced STING activation.

We next co-targeted cGAS or STING in VDAC2-deficient tumour cells to establish functional effects and found that their targeting largely blocked the capacity of VDAC2-deficient tumour cells to increase TBK1 or IRF3 phosphorylation or IFNβ expression after IFNγ stimulation (Fig. 3j–l). Co-deletion of *Irf3* (albeit not *Mavs*, which induces STING-independent type I IFN response[34]) also rectified such aberrant IFNβ expression (Extended Data Fig. 6g,h). In transcriptome profiling, STING co-deletion largely reversed the increased expression of IFN-response genes induced by VDAC2 deficiency (Fig. 3m). By contrast, co-deletion of *Cgas*, *Sting1* or *Irf3* did not mitigate the excessive cell death of IFNγ-stimulated VDAC2-deficient tumour cells (Extended Data Fig. 6i), suggesting that the effects of STING signalling were specific in mediating the increased type I IFN response, albeit not the cell death phenotypes, induced by *Vdac2* deletion. Likewise, IFNγ-induced cell death of VDAC2-deficient cells was unaltered after IFNαR1 blockade (Extended Data Fig. 6j). Upon in vivo tumour challenge, *Sting1* or *Irf3* co-deletion also partly blocked the therapeutic benefits of *Vdac2* deletion on tumour growth and mouse survival (Fig. 3n and Extended Data Fig. 6k). Together, these results reveal an interplay between IFNγ signalling, VDAC2 and STING activation that dictates type I IFN response and tumour growth.

Ccl5 expression was among the top-most upregulated genes in VDAC2-deficient tumour cells treated with IFNγ or OT-I cells (Fig. 3b and Extended Data Fig. 6d). This increased *Ccl5* expression was rectified after co-deletion of *Cgas*, *Sting1* or *Irf3* (albeit not *Mavs*) and was validated to occur after co-culture with OT-I cells in vitro (Extended Data Fig. 6l–o). Furthermore, VDAC2-deficient tumour cells expressed higher levels of *Ccl5* in vivo, whereas intratumoural CD8$^+$ T cells from such tumours expressed higher levels of *Ccr5* (Extended Data Fig. 6p,q). These results prompted us to test whether CCL5 contributes to the reshaping of the tumour immune landscape after *Vdac2* deletion. *Ccl5* co-deletion impeded the increased accumulation of CD8$^+$ T cells, including those expressing IFNγ and TNF or GZMB, in the VDAC2-deficient TME (Extended Data Fig. 6r). Thus, CCL5 contributes to the robust accumulation of effector CD8$^+$ T cells in VDAC2-deficient tumours.

Cytosolic mitochondrial DNA (mtDNA) release triggers STING activation[35]. As VDAC2 is a mitochondrial protein (Extended Data Fig. 6s), we hypothesized that cytosolic mtDNA release may occur in IFNγ-treated VDAC2-deficient tumour cells. Indeed, immunostaining revealed a decreased abundance of mitochondrially localized double-stranded DNA in VDAC2-deficient tumour cells after IFNγ treatment (Fig. 3o and Extended Data Fig. 6t). Furthermore, VDAC2-deficient tumour cells showed increased abundance of cytosolic mtDNA (Fig. 3p and Extended Data Fig. 6u). We next generated control and VDAC2-deficient tumour cells lacking mtDNA (ρ^0 cells; Methods) and found that mtDNA depletion in IFNγ-stimulated VDAC2-deficient tumour cells rectified the increased levels of phosphorylated TBK1, IFNβ and *Ccl5* (Fig. 3q and Extended Data Fig. 6v–y). Likewise, VDAC2-deficient human LoVo cells had increased inflammatory gene expression and STING activation (Fig. 3r,s, Extended Data Fig. 6z and Supplementary Table 7), thereby establishing that VDAC2 restrains IFNγ-induced STING activation in human tumour cells. Together, aberrant cytosolic mtDNA drives cGAS–STING signalling and type I IFN response in IFNγ-stimulated VDAC2-deficient cells.

VDAC2–BAK axis tunes tumour remodelling

To unbiasedly identify functional genetic interactions for enhanced susceptibility to IFNγ-induced cell death, we performed a genetic interaction screen by co-transducing VDAC2-deficient B16-OVA-Cas9 tumour cells with a genome-scale sgRNA library and, after IFNγ treatment, assessed sgRNA enrichment or depletion among the viable VDAC2-deficient tumour cells to nominate genetic interactions that either alleviate or synergize with VDAC2 deficiency-driven effects on tumour cell death (Fig. 4a). Targeting *Ptpn2* potentiated, and depleting

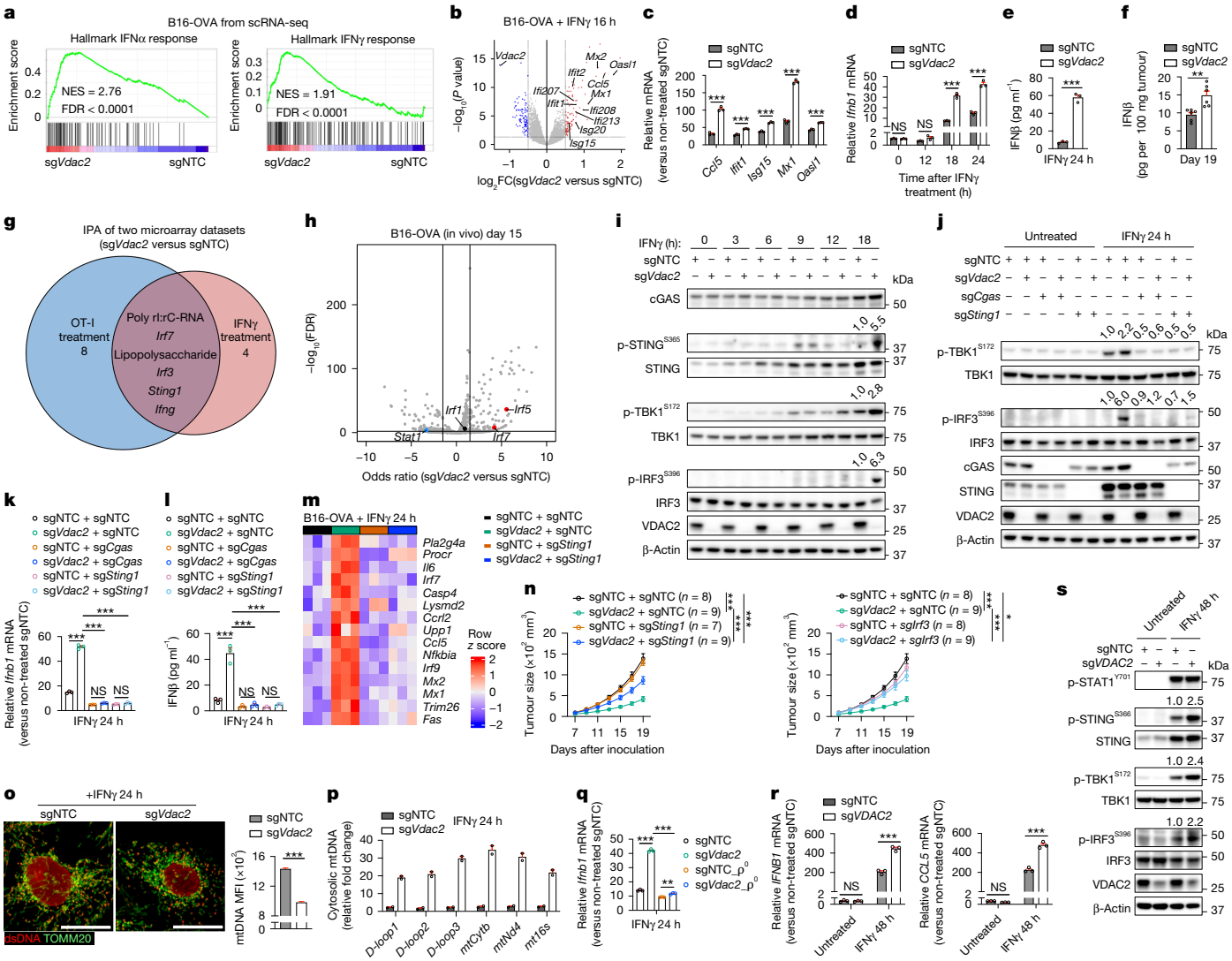

Fig. 3 | VDAC2 loss enables IFNγ-induced mtDNA release and STING activation. a, Hallmark IFNα and IFNγ response signatures. FDR, false-discovery rate; NES, normalized enrichment score. **b**, Gene expression profiles in IFNγ-treated B16-OVA tumour cells, with selective upregulated (red) and downregulated (blue) genes labelled. **c**,**d**, The relative levels of IFN-responsive genes (**c**) or *Ifnb1* (**d**) in IFNγ-treated B16-OVA tumour cells. $n = 3$ per group. **e**,**f**, IFNβ levels in culture supernatants from IFNγ-treated B16-OVA tumour cells (**e**; $n = 3$ per group) or from tumour lysates after inoculation into wild-type mice (**f**; $n = 6$ per group). **g**, Overlap of activated IPA-predicted upstream regulators from transcriptome profiling of OT-I- or IFNγ-treated B16-OVA tumour cells. The numbers indicate uniquely activated regulators. **h**, Motif enrichment analysis of differentially accessible chromatin profiled by ATAC–seq ($n = 4$ per group), with selective upregulated (red) and downregulated (blue) motifs labelled and black-labelled genes being unaltered. **i**,**j**, Immunoblot analysis of B16-OVA tumour cells after IFNγ treatment, with densiometric quantification of phosphorylated STING (p-STING), p-TBK1 or p-IRF3 shown (**i**), and p-TBK1 or p-IRF3 shown (**j**). **k**,**l**, The relative levels of *Ifnb1* in indicated cells (**k**; $n = 3$ per group) and IFNβ in culture supernatants of indicated cells (**l**; $n = 3$ per group). **m**, The relative expression of IFN-responsive genes repressed by VDAC2 in the indicated IFNγ-treated B16-OVA tumour cells. $n = 3$ per group. **n**, The growth of B16-OVA tumours. The same sgNTC and sg*Vdac2* groups are shown on the left and right. **o**, dsDNA and TOMM20 co-localization in IFNγ-treated B16-OVA tumour cells. $n = 4{,}525$ (sgNTC) and 5,948 (sg*Vdac2*). Scale bar, 20 μm. MFI, mean fluorescence intensity. **p**, Relative cytosolic mtDNA levels (versus non-treated control cells) in IFNγ-treated B16-OVA tumour cells. $n = 2$ per group. **q**, Relative *Ifnb1* levels in IFNγ-treated B16-OVA tumour cells that lack (ρ^0 cells) or contain mtDNA ($n = 3$ per group). **r**, The relative *IFNB1* and *CCL5* levels in IFNγ-treated LoVo tumour cells. $n = 3$ per group. **s**, Immunoblot analysis of LoVo tumour cells before and after IFNγ treatment, with densiometric quantification of p-STING, p-TBK1 or p-IRF3 shown. Data are mean ± s.e.m., representative of three (**c**, **d**, **i**, **k** and **l**), two (**e**, **j** and **o**–**s**) or one (**f** and **n**) independent experiments. Statistical analysis was performed using two-tailed unpaired Student's *t*-tests (**c**–**f** and **o**), one-way ANOVA (**k**, **l** and **q**), two-way ANOVA (**n** and **r**) and two-tailed Fisher's exact test (**h**).

IFNγ signalling-associated genes (*Ifngr1*, *Ifngr2*, *Jak1*, *Jak2* and *Stat1*) alleviated, VDAC2 deficiency-mediated cell death after IFNγ treatment (Extended Data Fig. 7a and Supplementary Table 8a,b). Next, we overlaid these genetic interaction screen hits with the MitoCarta 3.0 database, which contains all annotated mitochondria-associated genes[36]. We found that targeting *Casp9* and *Bak1* (encoding BAK) had the most substantial effects on alleviating VDAC2-deficiency-mediated tumour cell death (Fig. 4b and Supplementary Table 8c). BAK and/or the closely related protein BAX orchestrate mitochondria-dependent cell death by promoting mitochondrial outer membrane permeabilization (MOMP), cytochrome c release and initiation of APAF-1- and caspase-9-dependent cell death[25]. We found that co-deletion of *Bak1*, but not *Bax*, blocked IFNγ-induced cell death and LDH release of VDAC2-deficient tumour cells (Extended Data Fig. 7b,c). Furthermore, in the absence of IFNγ treatment, overexpression of *Bak1*, but not *Bax*, promoted cell death of VDAC2-deficient tumour cells (Extended Data Fig. 7d), further

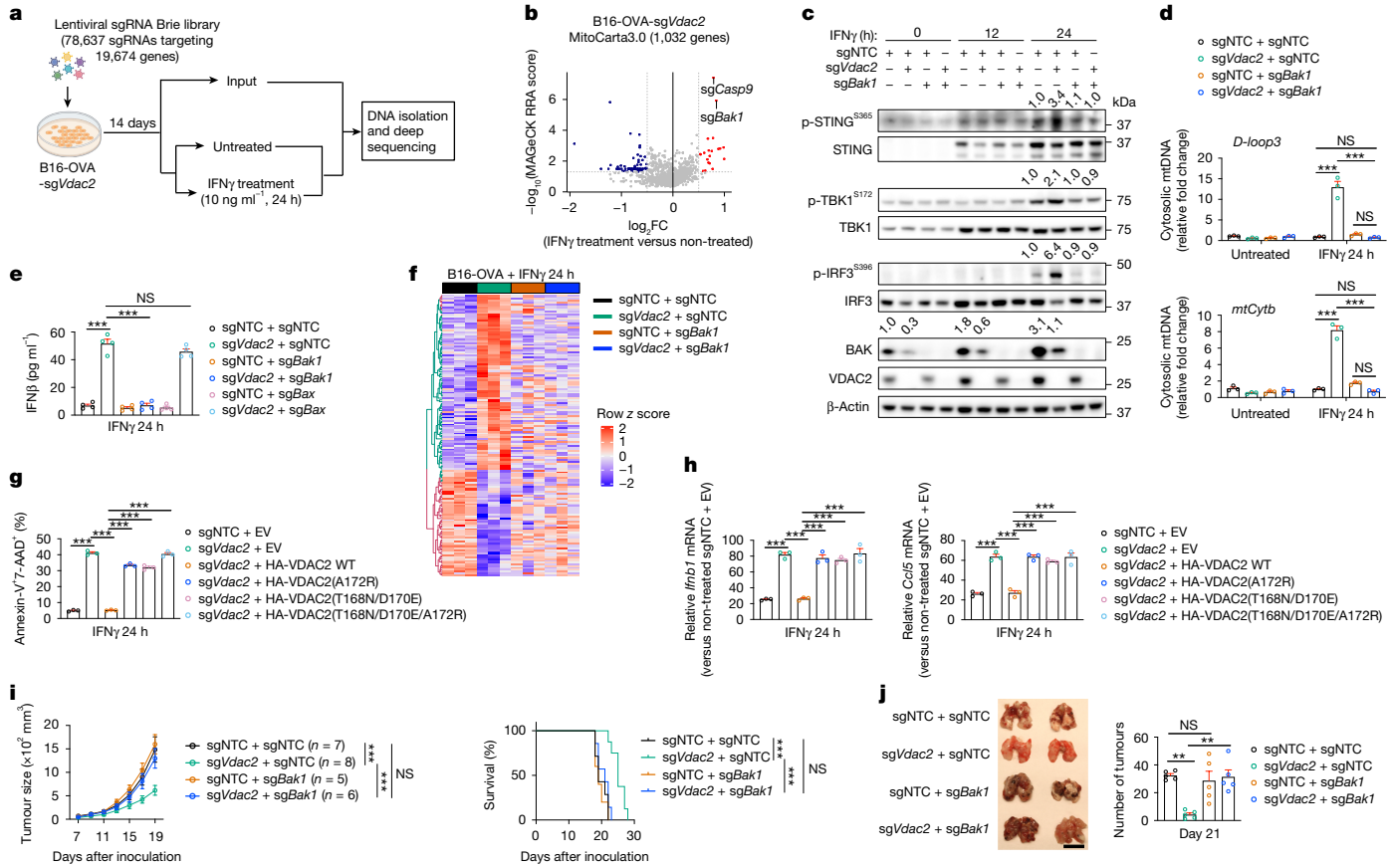

Fig. 4 | BAK mediates VDAC2-deficiency-driven effects in response to IFNγ. a, Schematic of the secondary genome-scale CRISPR screen. Created in BioRender. Sun, R. (2025) https://BioRender.com/g06b183. **b**, Enriched (red) and depleted (blue) sgRNAs targeting mitochondria-associated genes in IFNγ-treated versus non-treated VDAC2-deficient B16-OVA tumour cells. **c**, Immunoblot analysis of the indicated sgRNA-transduced B16-OVA tumour cells after IFNγ treatment for indicated times; densiometric quantification of p-STING, p-TBK1, p-IRF3 or total BAK is shown. **d**, The relative cytosolic mtDNA levels (versus non-treated control cells) in the indicated B16-OVA tumour cells treated with or without IFNγ. $n = 3$ per group. **e**, IFNβ levels in the culture supernatants from the indicated B16-OVA tumour cells after IFNγ treatment. $n = 4$ per group. **f**, The relative gene expression in the indicated B16-OVA tumour cells after IFNγ treatment. $n = 3$ per group. **g**, Cell death of the indicated B16-OVA tumour cells treated with IFNγ. $n = 3$ per group. EV, empty vector. **h**, Relative *Ifnb1* and *Ccl5* levels (versus non-treated control cells) in the indicated B16-OVA tumour cells treated with IFNγ. $n = 3$ per group. **i**, Control, VDAC2-deficient, BAK-deficient, or VDAC2 and BAK co-deficient B16-OVA tumour growth (left) and survival of tumour-bearing mice (right). **j**, Lung tumour burden in mice that received intravenous injection of the indicated B16-OVA tumour cells. $n = 5$ per group. Scale bar, 1 cm. Data are mean ± s.e.m., representative of three (**c** and **i**), two (**d**, **e**, **g**, **h** and **j**) or one (**j**) independent experiments. Statistical analysis was performed using one-way ANOVA (**d**, **e**, **g**, **h** and **j**), two-way ANOVA (**i** (tumour size)) and Mantel–Cox test (**i** (survival)).

supporting an interplay between VDAC2 and BAK in orchestrating tumour cell death.

Next, we examined STING activation in cells lacking VDAC2 and BAK and found that *Bak1* co-deletion blocked the increased phosphorylation of STING, TBK1 and IRF3 in IFNγ-stimulated VDAC2-deficient cells (Fig. 4c). Furthermore, co-deletion of *Bak1* (but not *Bax*) rectified the increased mtDNA release and expression of IFNβ and IFN-responsive genes (Fig. 4d,e and Extended Data Fig. 7e,f). Global transcriptome alterations induced by VDAC2 deficiency were also substantially mitigated by BAK co-deletion (Fig. 4f and Extended Data Fig. 7g). Collectively, *Vdac2* deletion acts through BAK to mediate mtDNA release, STING activation and inflammatory reprogramming.

Mechanistically, VDAC2 interacted with BAK but not BAX in B16-OVA tumour cells, consistent with previous findings[37] (Extended Data Fig. 7h). To determine whether VDAC2 affects BAK or BAX activity, we measured BAK or BAX oligomer formation[38] in mitochondrial fractions of IFNγ-treated control and VDAC2-deficient cells, which revealed increased BAK but not BAX dimer and trimer formation in VDAC2-deficient cells, especially after IFNγ treatment (Extended Data Fig. 7i). Thus, there was aberrant activation of BAK in IFNγ-treated VDAC2-deficient cells, which occurred despite a reduction in total BAK protein abundance (Fig. 4c). Accordingly, downstream events of BAK activation, including MOMP[39] and cytosolic release of cytochrome *c* and SMAC, were increased in VDAC2-deficient tumour cells after IFNγ treatment (Extended Data Fig. 7j,k). Thus, VDAC2 interacts with and suppresses BAK in tumour cells, and IFNγ-stimulated BAK activity is unleashed after *Vdac2* deletion.

To establish the functional importance of the VDAC2–BAK interaction, we generated a wild-type VDAC2 construct or three types of VDAC2 mutants impairing the VDAC2–BAK interaction[40,41]. The interactions between these mutant proteins with BAK were substantially reduced compared with wild-type VDAC2 (Extended Data Fig. 7l). Moreover, only wild-type, but not mutant, VDAC2 largely rectified the phenotypes of VDAC2-deficient cells, including enhanced IFNγ-induced cell death and type I IFN responses (Fig. 4g,h and Extended Data Fig. 7m), thereby establishing the functional importance of the VDAC2–BAK interaction to VDAC2-mediated effects in response to IFNγ.

We next compared the functional effects of VDAC2 with MCL-1 and BCL-2, which are known to inhibit BAK[25,42]. At 24 h of IFNγ treatment, in contrast to VDAC2-deficient cells, MCL-1- or BCL-2-deficient cells showed slightly increased or negligible cell death, respectively (Extended Data Fig. 7n,o), and no major changes in type I IFN responses

(Extended Data Fig. 7n,p). Nonetheless, after extended (48 h) IFNγ treatment, MCL-1-deficient cells and, to a lesser extent, BCL-2-deficient cells, showed increased cell death (albeit less pronounced than VDAC2-deficient cells) (Extended Data Fig. 7o) and *Ifnb1* and/or *Ccl5* expression (Extended Data Fig. 7p). Furthermore, only VDAC2-deficient cells displayed increased BAK activation at 24 h after IFNγ treatment, while both VDAC2- and MCL-1-deficient cells showed enhanced BAK activation at 48 h (Extended Data Fig. 7q). Compared with the pronounced effects of *Vdac2* deletion, loss of MCL-1 or BCL-2 modestly sensitized tumour cells to OT-I-cell-mediated killing (Extended Data Fig. 7r). Thus, VDAC2-deficient B16-OVA cells are more sensitive than MCL-1- and BCL-2-deficient cells to these IFNγ-induced effects of cell death and inflammation.

To mechanistically understand how VDAC2 deficiency unleashes the sensitivity to IFNγ-induced mitochondrial apoptosis, we examined the gene expression of BCL-2-family members in control and VDAC2-deficient B16-OVA tumour cells treated with IFNγ. IFNγ stimulation increased expression of *Bcl2l11* (encoding BIM) and *Bid*, along with their downstream target *Bak1*, with such observations also evident at the protein levels (Extended Data Fig. 8a,b). By contrast, except for BIM, these proteins were not upregulated by anti-cancer apoptosis inducers such as cisplatin and etoposide, which instead promoted expression of PUMA and p53 (Extended Data Fig. 8c). Mechanistically, BID and BAK expression was decreased in STAT1- or IRF1-deficient cells, whereas BIM and STING expression was reduced in STAT1-deficient cells (Extended Data Fig. 8d,e). Furthermore, the protein levels of BIM and BAK (but not BID) (Extended Data Fig. 8f), as well as STING (Fig. 3s), were increased in IFNγ-stimulated human LoVo tumour cells, suggesting conserved effects between human and mouse tumour cells.

To determine the functional contributions of STAT1 and IRF1 signalling, we co-deleted *Stat1* or *Irf1* in VDAC2-deficient tumour cells. Co-deletion of *Stat1* or *Irf1* completely or partially rectified the IFNγ-induced cell death and type I IFN phenotypes of VDAC2-deficient cells, respectively (Extended Data Fig. 8g,h). Thus, STAT1 and, to a lesser extent, IRF1 contribute to the increased sensitivity of VDAC2-deficient cells to IFNγ-induced cell death and inflammatory remodelling. We next co-deleted *Bcl2l11* and *Bid* in VDAC2-deficient tumour cells, which largely rescued IFNγ-induced cell death or $CD8^+$ T cell-mediated killing (Extended Data Fig. 8i,j). Accordingly, compared with VDAC2-deficient tumour cells, VDAC2-deficient tumour cells lacking BIM and BID had reduced BAK oligomerization (Extended Data Fig. 8k) and cytochrome *c* or mtDNA release, as well as decreased STING activation and inflammatory gene expression after IFNγ treatment (Extended Data Fig. 8l–p). Together, IFNγ sensitizes tumour cells by upregulating expression of BIM, BID and BAK, with VDAC2 loss triggering BAK activation and subsequent cell death and cGAS–STING activation.

Our genetic interaction CRISPR screen and validation experiments also revealed that co-deletion of pro-apoptotic APAF-1 or caspase-9[25] rescued the increased cell death and LDH release of IFNγ-stimulated VDAC2-deficient tumour cells (Extended Data Figs. 7a and 9a–c). Similarly, pan-caspase inhibitor treatment led to a greater than 90% reduction in IFNγ-induced cell death in VDAC2-deficient cells (Extended Data Fig. 9d). Notably, inhibition of apoptosis through pharmacological or genetic approaches only delayed cell death of VDAC2-deficient tumour cells, as extensive cell death was still observed after 72 h of IFNγ stimulation (Extended Data Fig. 9e–g). Furthermore, co-deletion of *Apaf1* or *Casp9* in VDAC2-deficient tumour cells led to further enhanced IFNγ-induced STING signalling and expression of downstream inflammatory genes (Extended Data Fig. 9h–k), in contrast to *Bak1* co-deletion, which blocked both the increased cell death and cGAS–STING activation. Similar effects were observed in VDAC2-deficient cells with *Casp3* or *Casp7* co-deletion and those that were treated with the pan-caspase inhibitor Q-VD-OPh or emricasan (Extended Data Fig. 9l,m), consistent with the notion that apoptotic caspases inhibit the type I IFN response[43–46]. Accordingly, GSEA revealed upregulation of the IFNα signature in IFNγ-stimulated VDAC2 and APAF-1 co-deficient tumour cells compared with that in VDAC2-deficient tumour cells (Extended Data Fig. 9n and Supplementary Table 9). Moreover, co-deletion of *Apaf1* or *Casp9*, or treatment with emricasan, further reduced the growth of VDAC2-deficient tumours in vivo, corresponding to increased mouse survival (Extended Data Fig. 9o,p), suggesting that inhibition of apoptosis modestly boosts the therapeutic effects of VDAC2 deficiency. Together, these data reveal that VDAC2 deficiency overrides the inhibitory effects of apoptotic caspases on cGAS–STING activation to enable BAK-dependent caspase and STING activation after IFNγ stimulation.

To establish the physiological relevance of VDAC2–BAK axis in vivo, we challenged wild-type mice with control B16-OVA tumours or those lacking VDAC2 and/or BAK. *Bak1* co-deletion reversed the reduced growth of VDAC2-deficient tumours in both subcutaneous (s.c.) and lung metastasis models (Fig. 4i,j). Moreover, *Bak1* co-deletion largely blocked the increased accumulation and effector-like features of $CD8^+$ T cells (Extended Data Fig. 9q,r). *Bak1* co-deletion also blocked the enhanced therapeutic benefit of combining anti-PD-L1 treatment with VDAC2 deficiency in tumour cells (Extended Data Fig. 9s,t). Thus, the VDAC2–BAK axis tunes anti-tumour and ICB responses in vivo.

To further explore the potential widespread effects of targeting VDAC2, we examined whether VDAC2 limits IFNγ-induced cell death of non-tumorigenic cells. IFNγ stimulation did not cause marked cell death of VDAC2-deficient mouse embryonic fibroblasts (MEFs), in contrast to treatment with etoposide or TNF plus cycloheximide[37] (Extended Data Fig. 10a). IFNγ also did not induce substantial cell death of control or VDAC2-deficient OT-I cells in vitro (Extended Data Fig. 10b) and, accordingly, VDAC2-deficient OT-I cells retained potent anti-tumour function in vivo (Extended Data Fig. 10c). Similarly, VDAC2 deficiency did not alter cell death of T helper type 1 (T_H1) and in vitro-derived T_{reg} (iT_{reg}) cells (Extended Data Fig. 10d). We also found that only BAK (but not BIM or BID) was upregulated by IFNγ in control and VDAC2-deficient MEFs, whereas BID expression was modestly downregulated in IFNγ-treated OT-I cells (Extended Data Fig. 10e,f). These results suggest that IFNγ stimulation coordinately upregulates BIM, BID and BAK selectively in tumour cells, associated with their increased sensitivity to VDAC2-deficiency-driven cell death.

Finally, tumour cells are in a more primed state compared with normal cells for apoptosis, with such effects associated with their more abundant expression of certain apoptotic molecules[42,47]. Given that VDAC2-deficient B16-OVA cells but not MEFs are sensitive to IFNγ-induced cell death, we compared the expression of BCL-2-family proteins in these cell types in the absence or presence of IFNγ. Without IFNγ stimulation, B16-OVA tumour cells and MEFs showed comparable BIM, BID, BAK, MCL-1 and BCL-xL expression, while BAX, PUMA and BCL-2 levels were highly expressed in B16-OVA tumour cells (Extended Data Fig. 10g). These results suggest that B16-OVA cells probably exist in a partly primed state for apoptosis compared with MEFs. After IFNγ treatment, BIM, BID and BAK expression was upregulated to considerably higher levels in B16-OVA cells compared with in MEFs (Extended Data Fig. 10g). Thus, IFNγ differentially regulates the expression of BIM, BID and BAK in tumour cells compared with in MEFs, which probably underlies the capacity of IFNγ to selectively sensitize tumour cells to cell death after *Vdac2* deletion (Extended Data Fig. 10h).

Discussion

Tumour immune evasion and resistance to T cell-mediated killing represent barriers to effective immune-mediated cancer therapies. Besides directly killing tumour cells, T cells produce cytokines such as IFNγ that remodel the inflammatory status of the TME[48]. Mechanisms mediating tumour cell responsiveness to IFNγ-mediated cytotoxicity are underexplored. Here we identified *Vdac2* as a potent immune evasion gene, and the deletion of *Vdac2* induced IFNγ-mediated destruction of tumour cells in vivo. Notably, although IFNγ signalling in tumours cells may

favour tumour immune evasion by epigenome remodelling to induce expression of TCIR ligands[30], VDAC2-deficient tumour cells showed no such effects. Furthermore, VDAC2 deficiency promoted mitochondrial damage, suggesting that targeting VDAC2 may override the metabolic advantage enabled by IFNγ signalling for immune evasion[49]. Notably, co-deletion of *Vdac2* and *Ptpn2* further boosted anti-tumour immunity, probably through combined effects at potentiating IFNγ-induced canonical JAK–STAT signalling[7] (through *Ptpn2* deletion) together with activating *Vdac2*-deletion-associated downstream events, including induction of pronounced cell death phenotypes that were stronger than *Ptpn2* deletion. Mechanistically, IFNγ stimulation increased the expression of BIM, BID and BAK in tumour cells, while VDAC2 counterbalances BAK activation downstream of IFNγ priming and protects tumour cells from IFNγ-induced MOMP and mitochondrial disruption to inhibit cell death and inflammatory remodelling. Overall, our study broadens our understanding of IFNγ signalling in mediating T cell-dependent cytotoxicity against tumours and cancer immunotherapy.

Although cGAS–STING signalling contributes to tumour immune surveillance, cancers often silence STING activity to mediate immune evasion[50] by maintaining genome stability[51] or clearing cytosolic DNA[52]. However, whether STING activity and mtDNA release in tumour cells are shaped by adaptive immunity remains unclear. We establish targeting VDAC2 as an effective means to overcome immune evasion by sensitizing tumour cells to IFNγ-induced mtDNA release and cGAS–STING activation, highlighting the role of VDAC2 as a gatekeeper for such non-canonical IFNγ signalling events. Consequently, VDAC2-deficient tumours showed increased $CD8^+$ T cell accumulation and anti-tumour responses. Therefore, VDAC2 targeting links $CD8^+$ T cell-mediated IFNγ production and adaptive immune responses to tumour-intrinsic activation of innate immune machinery as well as eliciting excessive tumour cell death, which mechanistically distinguishes VDAC2 from other targets that mediate tumour immune evasion[7,31,53–55]. Although BAK mediates both effects of VDAC2 targeting, our data reveal that cell death and STING-mediated inflammatory signals become divergent downstream of BAK, further highlighting the role of VDAC2 in coordinately orchestrating these two events.

From a therapeutic perspective, our study highlights the importance of the dual effects of destructing and inflaming tumours to induce effective tumour immunity and immunotherapy, thereby advancing our knowledge on cancer–immunity cycle[3]. Notably, many clinical trials combining ICB with other anti-tumour drugs are underway to explore possible combinatorial effects[56]. Targeting VDAC2 may provide opportunities to improve ICB therapies, and may be further leveraged in combination with ACT or with small-molecule inhibitors such as those targeting PTPN2[57]. It will be important to determine the therapeutic window and/or specific targeting strategies to minimize potential deleterious effects. Although *Vdac2* deletion impairs the development and survival of thymocytes[58], we showed that mature $CD8^+$ T cells retained their anti-tumour effects in the absence of VDAC2, highlighting discrete functional effects of VDAC2 in different T cell populations. Thus, selective targeting of VDAC2 or the VDAC2–BAK axis may be permissive to facilitate IFNγ- and $CD8^+$ T cell-mediated killing and inflammatory rewiring of tumour cells. Collectively, our study establishes the targeting of VDAC2 in tumour cells as a potent strategy for cancer therapy, by enforcing IFNγ-dependent apoptotic cell death and an inflammation feedforward loop (Extended Data Fig. 10h), namely the induction of 'inflammatory apoptosis' by partially overriding caspase-mediated inhibition of STING activation. While innate control of adaptive immunity is a fundamental immunological principle[59,60], our study provides insights into how adaptive immunity instructs innate immune-like reprogramming in tumour cells. Whether *Vdac2* deletion effects and coordination of adaptive and innate responses and cell death are functionally conserved in additional contexts that require IFNγ signalling and type 1 immunity, such as infectious, inflammatory and autoimmune diseases, warrants further investigation.

Online content

Any methods, additional references, Nature Portfolio reporting summaries, source data, extended data, supplementary information, acknowledgements, peer review information; details of author contributions and competing interests; and statements of data and code availability are available at https://doi.org/10.1038/s41586-025-08732-6.

1. Waldman, A. D., Fritz, J. M. & Lenardo, M. J. A guide to cancer immunotherapy: from T cell basic science to clinical practice. *Nat. Rev. Immunol.* **20**, 651–668 (2020).
2. Sharma, P. et al. Immune checkpoint therapy-current perspectives and future directions. *Cell* **186**, 1652–1669 (2023).
3. Mellman, I., Chen, D. S., Powles, T. & Turley, S. J. The cancer-immunity cycle: indication, genotype, and immunotype. *Immunity* **56**, 2188–2205 (2023).
4. Golstein, P. & Griffiths, G. M. An early history of T cell-mediated cytotoxicity. *Nat. Rev. Immunol.* **18**, 527–535 (2018).
5. Wang, W. et al. $CD8^+$ T cells regulate tumour ferroptosis during cancer immunotherapy. *Nature* **569**, 270–274 (2019).
6. Larson, R. C. et al. CAR T cell killing requires the IFNγR pathway in solid but not liquid tumours. *Nature* **604**, 563–570 (2022).
7. Manguso, R. T. et al. In vivo CRISPR screening identifies Ptpn2 as a cancer immunotherapy target. *Nature* **547**, 413–418 (2017).
8. Finck, A. V., Blanchard, T., Roselle, C. P., Golinelli, G. & June, C. H. Engineered cellular immunotherapies in cancer and beyond. *Nat. Med.* **28**, 678–689 (2022).
9. Gao, J. et al. Loss of IFN-γ pathway genes in tumor cells as a mechanism of resistance to Anti-CTLA-4 therapy. *Cell* **167**, 397–404 (2016).
10. Zaretsky, J. M. et al. Mutations associated with acquired resistance to PD-1 blockade in melanoma. *N. Engl. J. Med.* **375**, 819–829 (2016).
11. Sharma, P., Hu-Lieskovan, S., Wargo, J. A. & Ribas, A. Primary, adaptive, and acquired resistance to cancer immunotherapy. *Cell* **168**, 707–723 (2017).
12. Chapman, N. M. & Chi, H. Metabolic adaptation of lymphocytes in immunity and disease. *Immunity* **55**, 14–30 (2022).
13. Park, J., Hsueh, P. C., Li, Z. & Ho, P. C. Microenvironment-driven metabolic adaptations guiding $CD8^+$ T cell anti-tumor immunity. *Immunity* **56**, 32–42 (2023).
14. Raynor, J. L. & Chi, H. Nutrients: signal 4 in T cell immunity. *J. Exp. Med.* **221**, e20221839 (2024).
15. Chapman, N. M. & Chi, H. Metabolic rewiring and communication in cancer immunity. *Cell Chem. Biol.* **31**, 862–883 (2024).
16. Mangalhara, K. C. et al. Manipulating mitochondrial electron flow enhances tumor immunogenicity. *Science* **381**, 1316–1323 (2023).
17. Lawson, K. A. et al. Functional genomic landscape of cancer-intrinsic evasion of killing by T cells. *Nature* **586**, 120–126 (2020).
18. Wei, J. et al. Targeting REGNASE-1 programs long-lived effector T cells for cancer therapy. *Nature* **576**, 471–476 (2019).
19. Shi, H., Doench, J. G. & Chi, H. CRISPR screens for functional interrogation of immunity. *Nat. Rev. Immunol.* **23**, 363–380 (2023).
20. Vredevoogd, D. W. et al. Augmenting immunotherapy impact by lowering tumor TNF cytotoxicity threshold. *Cell* **178**, 585–599 (2019).
21. Kearney, C. J. et al. Tumor immune evasion arises through loss of TNF sensitivity. *Sci. Immunol.* **3**, eaar3451 (2018).
22. Frangieh, C. J. et al. Multimodal pooled Perturb-CITE-seq screens in patient models define mechanisms of cancer immune evasion. *Nat. Genet.* **53**, 332–341 (2021).
23. Wang, Y. et al. Chemotherapy drugs induce pyroptosis through caspase-3 cleavage of a gasdermin. *Nature* **547**, 99–103 (2017).
24. Rogers, C. et al. Cleavage of DFNA5 by caspase-3 during apoptosis mediates progression to secondary necrotic/pyroptotic cell death. *Nat. Commun.* **8**, 14128 (2017).
25. Newton, K., Strasser, A., Kayagaki, N. & Dixit, V. M. Cell death. *Cell* **187**, 235–256 (2024).
26. Beltra, J. C. et al. Developmental relationships of four exhausted $CD8^+$ T cell subsets reveals underlying transcriptional and epigenetic landscape control mechanisms. *Immunity* **52**, 825–841 (2020).
27. Hudson, W. H. et al. Proliferating transitory T cells with an effector-like transcriptional signature emerge from $PD\text{-}1^+$ stem-like $CD8^+$ T cells during chronic infection. *Immunity* **51**, 1043–1058 (2019).
28. Zander, R. et al. $CD4^+$ T cell help is required for the formation of a cytolytic $CD8^+$ T cell subset that protects against chronic infection and cancer. *Immunity* **51**, 1028–1042 (2019).
29. Zhou, P. et al. Single-cell CRISPR screens in vivo map T cell fate regulomes in cancer. *Nature* **624**, 154–163 (2023).
30. Benci, J. L. et al. Tumor interferon signaling regulates a multigenic resistance program to immune checkpoint blockade. *Cell* **167**, 1540–1554 (2016).
31. Sun, Y. et al. Targeting TBK1 to overcome resistance to cancer immunotherapy. *Nature* **615**, 158–167 (2023).
32. Arlauckas, S. P. et al. Arg1 expression defines immunosuppressive subsets of tumor-associated macrophages. *Theranostics* **8**, 5842–5854 (2018).
33. Mowat, C., Mosley, S. R., Namdar, A., Schiller, D. & Baker, K. Anti-tumor immunity in mismatch repair-deficient colorectal cancers requires type I IFN-driven CCL5 and CXCL10. *J. Exp. Med.* **218**, e20210108 (2021).
34. Liu, S. et al. Phosphorylation of innate immune adaptor proteins MAVS, STING, and TRIF induces IRF3 activation. *Science* **347**, aaa2630 (2015).
35. West, A. P. et al. Mitochondrial DNA stress primes the antiviral innate immune response. *Nature* **520**, 553–557 (2015).
36. Rath, S. et al. MitoCarta3.0: an updated mitochondrial proteome now with sub-organelle localization and pathway annotations. *Nucleic Acids Res.* **49**, D1541–D1547 (2021).
37. Cheng, E. H., Sheiko, T. V., Fisher, J. K., Craigen, W. J. & Korsmeyer, S. J. VDAC2 inhibits BAK activation and mitochondrial apoptosis. *Science* **301**, 513–517 (2003).

38. Dewson, G. et al. To trigger apoptosis, Bak exposes its BH3 domain and homodimerizes via BH3:groove interactions. *Mol. Cell* **30**, 369–380 (2008).
39. Tait, S. W. et al. Resistance to caspase-independent cell death requires persistence of intact mitochondria. *Dev. Cell* **18**, 802–813 (2010).
40. Yuan, Z. et al. Key residues in the VDAC2-BAK complex can be targeted to modulate apoptosis. *PLoS Biol.* **22**, e3002617 (2024).
41. Naghdi, S., Varnai, P. & Hajnoczky, G. Motifs of VDAC2 required for mitochondrial Bak import and tBid-induced apoptosis. *Proc. Natl Acad. Sci. USA* **112**, E5590–E5599 (2015).
42. Singh, R., Letai, A. & Sarosiek, K. Regulation of apoptosis in health and disease: the balancing act of BCL-2 family proteins. *Nat. Rev. Mol. Cell Biol.* **20**, 175–193 (2019).
43. Han, C. et al. Tumor cells suppress radiation-induced immunity by hijacking caspase 9 signaling. *Nat. Immunol.* **21**, 546–554 (2020).
44. Rongvaux, A. et al. Apoptotic caspases prevent the induction of type I interferons by mitochondrial DNA. *Cell* **159**, 1563–1577 (2014).
45. White, M. J. et al. Apoptotic caspases suppress mtDNA-induced STING-mediated type I IFN production. *Cell* **159**, 1549–1562 (2014).
46. Ning, X. et al. Apoptotic caspases suppress type I interferon production via the cleavage of cGAS, MAVS, and IRF3. *Mol. Cell* **74**, 19–31 (2019).
47. Ni Chonghaile, T. et al. Pretreatment mitochondrial priming correlates with clinical response to cytotoxic chemotherapy. *Science* **334**, 1129–1133 (2011).
48. Hoekstra, M. E. et al. Distinct spatiotemporal dynamics of $CD8^+$ T cell-derived cytokines in the tumor microenvironment. *Cancer Cell* **42**, 157–167 (2024).
49. Tsai, C. H. et al. Immunoediting instructs tumor metabolic reprogramming to support immune evasion. *Cell Metab.* **35**, 118–133 (2023).
50. Ablasser, A. & Chen, Z. J. cGAS in action: expanding roles in immunity and inflammation. *Science* **363**, eaat8657 (2019).
51. Lu, C. et al. DNA sensing in mismatch repair-deficient tumor cells is essential for anti-tumor immunity. *Cancer Cell* **39**, 96–108 (2021).
52. Tani, T. et al. TREX1 inactivation unleashes cancer cell STING-interferon signaling and promotes antitumor immunity. *Cancer Discov.* **14**, 752–765 (2024).
53. Ishizuka, J. J. et al. Loss of ADAR1 in tumours overcomes resistance to immune checkpoint blockade. *Nature* **565**, 43–48 (2019).
54. Pan, D. et al. A major chromatin regulator determines resistance of tumor cells to T cell-mediated killing. *Science* **359**, 770–775 (2018).
55. Patel, S. J. et al. Identification of essential genes for cancer immunotherapy. *Nature* **548**, 537–542 (2017).
56. Kim, T. K., Vandsemb, E. N., Herbst, R. S. & Chen, L. Adaptive immune resistance at the tumour site: mechanisms and therapeutic opportunities. *Nat. Rev. Drug Discov.* **21**, 529–540 (2022).
57. Baumgartner, C. K. et al. The PTPN2/PTPN1 inhibitor ABBV-CLS-484 unleashes potent anti-tumour immunity. *Nature* **622**, 850–862 (2023).
58. Ren, D. et al. The VDAC2-BAK rheostat controls thymocyte survival. *Sci. Signal.* **2**, ra48 (2009).
59. Iwasaki, A. & Medzhitov, R. Control of adaptive immunity by the innate immune system. *Nat. Immunol.* **16**, 343–353 (2015).
60. Chi, H., Pepper, M. & Thomas, P. G. Principles and therapeutic applications of adaptive immunity. *Cell* **187**, 2052–2078 (2024).

Methods

Mice

C57BL/6 (000664), OT-I (003831), SMARTA (030450), Rosa26-Cas9 knock-in (026179), *Cd8*^{Cre} (008766) and *Rag1*$^{-/-}$ (002216) mice (all on the C57BL/6 background) were purchased from the Jackson Laboratory. OT-I mice were crossed with Rosa26-Cas9 knock-in mice to generate OT-I-Cas9 mice. To generate *Ifng*$^{fl/fl}$ mice, *loxP* sites were inserted into intron 1 and the 3′ UTR of the *Ifng* gene, resulting in Cre-mediated deletion of exons 2–4, which were then bred with *Cd8*^{cre} mice to generate *Cd8*^{Cre}*Ifng*$^{fl/fl}$ mice. Sex- and age-matched (6–10-week-old) mice with predetermined genotypes (not blinded to investigators) were randomly assigned to control and experimental groups throughout the study, and both male and female mice were used. To generate complete bone marrow chimeras, bone marrow cells from *Cd8*^{Cre}*Ifng*$^{fl/fl}$ or control *Ifng*$^{fl/fl}$ mice were flushed from mouse tibias and femurs, and red blood cells were lysed using ACK lysis buffer, followed by intravenous injection into sublethally (5.5 Gy) irradiated *Rag1*$^{-/-}$ recipient mice. Mice were inoculated with the indicated tumours at 8 weeks after bone marrow reconstitution. All of the mice were maintained under specific-pathogen-free conditions in the Animal Resource Center at St. Jude Children's Research Hospital. The animals were housed under 12 h–12 h light–dark cycles coinciding with daylight in Memphis, TN, USA (light on at 06:00 and off at 18:00). Food and water were provided ad libitum. The St. Jude Children's Research Hospital Animal Resource Center was maintained at 20–25 °C and 30–70% humidity. The research conducted in this study complied with all of the relevant ethical regulations. Experiments and procedures were approved by and performed in accordance with the Institutional Animal Care and Use Committee (IACUC) of St. Jude Children's Research Hospital. The number of mice per group were selected based on previous publications[29,49,61].

Cell lines

B16-OVA, MC38-OVA and MC38 cell lines were provided by D. Vignali. The HEK293T and LoVo cell lines were purchased from the American Type Culture Collection (ATCC). The Plat-E cell line was provided by Y.-C. Liu. All cell lines were cultured in Dulbecco's modified Eagle's medium (DMEM) (Gibco) or RPMI-1640 medium (Gibco) supplemented with 10% (v/v) FBS and 1% (v/v) penicillin–streptomycin at 37 °C with 5% CO_2. No commonly misidentified cell lines (International Cell Line Authentication Committee) were used in this study. Cell lines were tested and determined to be free of mycoplasma contamination. The aforementioned cell lines were not independently authenticated.

Plasmid and stable cell line generation

The sgRNAs targeting *Vdac2*, *Casp3*, *Casp7*, *Gsdme*, *Ifng*, *Tnf*, *Tnfrsf1a*, *Prf1*, *Ifngr1*, *Ifngr2*, *Jak1*, *Ptpn2*, *Vdac1*, *Vdac3*, *Cgas*, *Sting1*, *Mavs*, *Irf3*, *Ccl5*, *Bak1*, *Bax*, *Apaf1* and *Casp9* or non-targeting control were synthesized, annealed and ligated into BbsI-HF-digested (R3539L, NEB) retroviral sgRNA vectors (LMA or pSIR-DsRed (BbsI), with Ametrine or DsRed as a selection marker, respectively)[18,62]. A list of the sgRNA sequences is provided in Supplementary Table 10. For the mouse liver tumour model, pX330-sgNTC and pX330-sg*Vdac2* plasmids were generated from pX330 (42230, Addgene) according to the established protocol[63]. To generate Cas9-expressing tumour cell lines (B16-OVA-Cas9, MC38-OVA-Cas9 and MC38-Cas9), lentivirus was produced by co-transfecting Lenti-Cas9-GFP (86145, Addgene) plasmid with psPAX2 (12260, Addgene) and pMD2.G (12259, Addgene) packing plasmids into HEK293T cells. The supernatant containing viral particles was collected at 48 h after transfection. B16-OVA, MC38-OVA and MC38 cells were transduced with viral supernatant for 48 h in RPMI-1640 (for B16-OVA) or DMEM (for MC38-OVA and MC38) + 10% (*v*/*v*) FBS supplemented with 10 μg ml^{-1} polybrene (Sigma-Aldrich), followed by sorting of transduced (GFP$^+$) into single clones, followed by expansion. Cas9 expression was verified by immunoblot analysis[61]. To generate tumour cells deficient for the indicated genes using CRISPR–Cas9, retrovirus was produced by co-transfecting the indicated LMA or pSIR-DsRed (BbsI) vector(s) with pCL-Eco (12371, Addgene) and VSV.G (14888, Addgene) packing plasmids into Plat-E cells. The supernatant containing viral particles was collected 48 h after transfection. B16-OVA-Cas9, MC38-OVA-Cas9 or MC38-Cas9 cells were transduced with viral supernatant for 48 h in RPMI 1640 (for B16-OVA) or DMEM (for MC38-OVA and MC38) + 10% (v/v) FBS supplemented with 10 μg ml^{-1} polybrene (Sigma-Aldrich), followed by sorting Ametrine$^+$ or Ametrine$^+$DsRed$^+$ (for dual targeting) cells. Cells were cultured for another 14 days for genome editing and expansion. Unless otherwise noted, Cas9-expressing tumour cells were used for all of the experiments described in this study.

To generate the pMIG-II-HA-VDAC2 plasmid used for VDAC2–BAK interaction analysis in B16-OVA cells that did not express Cas9 (see the 'Immunoprecipitation and immunoblot analysis' section below), the *Vdac2* coding sequence was PCR-amplified from B16-OVA cDNA and cloned into the pcDNA3.1-HA vector (128034, Addgene). The *HA-Vdac2* coding sequence was amplified and cloned into the pMIG-II (52107, Addgene) retroviral vector. To generate the pMIA-Flag-BAK and pMIA-Flag-BAX plasmids, *Flag-Bak1* and *Flag-Bax* coding sequences were PCR-amplified from pcDNA-Flag-BAK or pMIG-BAX (8788, Addgene) and cloned into pMIA (52113, Addgene). To generate wide-type HA-VDAC2 plasmid, the *HA-Vdac2* sequence with 6 amino acid synonymous mutation at sg*Vdac2* targeting sequence (to circumvent CRISPR–Cas9-mediated cleavage; ATCCATGGGTCAGCTGTCTTTGGT changed (bold bases) to AT**A**CA**C**GG**A**TC**G**GC**A**GT**A**TTTGGT) was first synthesized by Integrated DNA Technologies (IDT). On the basis of this CRISPR–Cas9-resistant VDAC2 construct, we designed three VDAC2 mutants to alter specific sequences (A172R, T168N and D170E (T168N/D170E) or T168N, D170E and A172R (T168N/D170E/A172R) reported to have reduced ability to bind BAK[40,41], and these were synthesized by IDT. The following sequences were used for introducing such mutations: (1) A172R (GCC > **CG**C); (2) T168N/D170E (ACCTTTGAC > A**A**CTTTGA**A**); (3) T168N/D170E/A172R (ACCTTTGACAGTGCC > A**A**CTTTGA**A**AG T**CG**C). All of the plasmids were cloned using the NEBuilder HiFi DNA Assembly Cloning Kit (E5520S, NEB). To generate stable B16-OVA cells with Omi-mCherry (for imaging analysis), HA-VDAC2 and/or Flag-BAK/BAX overexpression (for immunoprecipitation), retrovirus was produced by co-transfecting pBabe(puro)-Omi-mCherry (48685, Addgene), pMIG-II-HA-VDAC2 or pMIA-Flag-BAK/BAX plasmid with pCL-Eco (12371, Addgene) and VSV.G (14888, Addgene) packing plasmids into plat-E cells. Omi-mCherry-, HA-VDAC2-, Flag-BAK- or Flag-BAX-expressing cells were sorted based on the fluorescence reporter mCherry (for Omi-mCherry), GFP (for HA-VDAC2) or Ametrine (for Flag-BAK or Flag-BAX).

T cell-mediated tumour cell killing assay in vitro

In total, 1×10^5 tumour cells were seeded into a 12-well plate for the timepoints indicated in the figures and their legends. Naive OT-I CD8$^+$ T cells were isolated from the spleen and peripheral lymph nodes of OT-I mice and activated using 10 μg ml^{-1} anti-CD3 (2C11, Bio X Cell, BE0001-1) and 5 μg ml^{-1} anti-CD28 (37.51, Bio X Cell, BE0015-1) antibodies as previously described[18]. Activated OT-I cells were then expanded in Click's medium (Irvine Scientific) containing 10% dialysed FBS supplemented with glutamine in the presence of human recombinant IL-2 (20 IU ml^{-1}; PeproTech), mouse IL-7 (12.5 ng ml^{-1}; PeproTech) and IL-15 (25 ng ml^{-1}; PeproTech) for 2–3 days. Preactivated OT-I CD8$^+$ T cells were then cocultured with tumour cells at the indicated effector:tumour target ratios. The live tumour cell number was calculated, and the mean value of E:T = 0:1 group was set equal to 100%. Fresh human leukapheresis products were purchased from Charles River. These leukapheresis products were obtained from three de-identified healthy donors (donor numbers ECT026, ECT028 and ECT031) and were used to generate human CAR T cells (ECT24-PD030) by St. Jude Experimental Cellular Therapeutics Laboratory (ECTL), using an established protocol and a previously

described lentiviral vector that encodes a B7-H3-CAR with a CD28ζ signalling domain[64]. Generated CAR T cells were cryopreserved at the end of production. As de-identified leukapheresis products were used, CAR T cell generation and experiments with these cells are considered non-human subject research. This determination was confirmed by the Institutional Review Board (IRB) at St. Jude Children's Research Hospital. Before conducting cytotoxicity assays, CAR T cells were thawed and cultured in X-VIVO-15 medium (BEBP04-744Q, Lonza) containing 5% human serum (H4522, Sigma-Aldrich) in the presence of human recombinant IL-7 (10 ng ml^{-1}, 130-093-764, Miltenyi) and human recombinant IL-15 (10 ng ml^{-1}, 130-095-362, Miltenyi) for 24 h. Recovered CAR T cells were then co-cultured with sgNTC- or sg*VDAC2*-transduced LoVo cells[65] at the indicated B7-H3-CAR T effector:tumour target ratios. At the indicated timepoints of co-culture, the number of live tumour cells were counted by flow cytometry using CountBright Absolute Counting Beads (C36950, Invitrogen).

T cell purification, differentiation and viral transduction for in vitro assays and adoptive transfer into tumour-bearing mice

Naive Cas9-expressing OT-I CD8$^+$ T cells were isolated as mentioned above. Purified naive OT-I cells were activated in vitro for 18–20 h with 10 μg ml^{-1} anti-CD3 (2C11, Bio-X-Cell), 5 μg ml^{-1} anti-CD28 (37.51; Bio-X-Cell) before viral transduction. Viral transduction was performed by spin-infection at 900*g* at 25 °C for 3 h with 10 mg ml^{-1} polybrene (Sigma-Aldrich). After transduction, cells were cultured in T cell medium containing human recombinant IL-2 (20 IU ml^{-1}; PeproTech), mouse recombinant IL-7 (12.5 ng ml^{-1}; PeproTech) and mouse recombinant IL-15 (25 ng ml^{-1}; PeproTech) for 4 days. Naive Cas9-expressing CD4$^+$ T cells were isolated from the spleen and peripheral lymph nodes of Cas9-SMARTA mice as previously described[66]. Viral transduction was performed by spin-infection at 900*g* at 25 °C for 3 h with 10 mg ml^{-1} polybrene (Sigma-Aldrich). After transduction, cells were cultured for iT$_{reg}$ or T$_H$1 differentiation: naive CD4$^+$ T cells were stimulated with 5 μg ml^{-1} anti-CD3 (2C11; Bio-X-Cell), 5 μg ml^{-1} anti-CD28 (37.51; Bio-X-Cell) in the presence of human IL-2 (100 U ml^{-1}) plus human TGFβ (0.5 ng ml^{-1}; PeproTech) for iT$_{reg}$ polarization; or human recombinant IL-2 (100 U ml^{-1}) plus mouse recombinant IL-12 p40 (0.5 ng ml^{-1}; BD Biosciences) for T$_H$1 polarization for 5.5 days. Transduced cells were sort-purified based on the expression of Ametrine.

For assays involving IFNγ or anti-IFNγ treatments of sgNTC- or sg*Vdac2*-transduced OT-I, iT$_{reg}$ or T$_H$1 cells, Ametrine$^+$ sorted cells were incubated with IFNγ (10 ng ml^{-1}) or anti-IFNγ (10 μg ml^{-1}) for 12–24 h as indicated in the figure legends. Cells were collected for flow cytometry, immunoblotting or quantitative PCR with reverse transcription (RT–qPCR) analysis as indicated in the figure legends. For adoptive transfer of sgNTC- or sg*Vdac2*-transduced OT-I cells into B16-OVA tumour-bearing mice, C57BL/6 mice were s.c. injected with 3×10^5 B16-OVA melanoma cells on day 0. At day 12 after tumour inoculation, a total of 4×10^6 sgNTC-transduced (labelled with Ametrine) and sg*Vdac2*-transduced (labelled with Ametrine) OT-I cells were injected intravenously into separate B16-OVA tumour-bearing mice. Tumour growth and mouse survival were monitored.

Cas9$^+$ MEF isolation, transduction and treatment

Cas9-expressing mouse embryos were isolated from Cas9-transgenic mice on E14.5. The embryos were euthanized by decapitation, and the fetal liver and heart were removed with forceps, followed by rinsing of the embryos with ice-cold PBS. The embryos were incubated with 3–5 ml ice-cold Trypsin-EDTA (25200-56, Gibco) overnight on ice in a 50 ml conical tube (Falcon). The trypsin-EDTA was aspirated off the embryos, followed by resuspension in 2 ml of pre-warmed (37 °C) trypsin-EDTA and incubation for 5–7 min in a 37 °C water bath. The digestion reaction was stopped by addition of 10 ml of MEF medium (DMEM + 10% FBS) followed by pipetting without introduction of air bubbles. After resting for 5 min at room temperature, the embryo suspension was transferred to a new 50 ml conical tube and centrifuged at 1,500 rpm for 5 min. The cell pellet was resuspended in MEF medium and filtered through a 70 μm cell strainer to remove debris. The cells from each embryo were plated into one T-160 plates or three T-75 (or 10 cm plates), reaching around 70% confluency within approximately 2 days. MEFs were transduced with sgNTC- or sg*Vdac2*-expressing retrovirus for 48 h in MEF medium containing 10 μg ml^{-1} polybrene (Sigma-Aldrich), followed by sorting Ametrine$^+$ MEFs. Ametrine$^+$ transduced MEFs were cultured for another 14 days for genome editing and expansion. For assays involving IFNγ (10 ng ml^{-1}, 24 h), TNF (10 ng ml^{-1}) plus cycloheximide (5 μg ml^{-1}, 4 h), or etoposide (20 μM, 24 h) treatments, sgNTC- or sg*Vdac2*-transduced MEFs were treated for the indicated times listed above, followed by flow cytometry, immunoblotting or RT–qPCR analysis, as indicated in the figure legends.

Tumour models and immunotherapeutic treatments

Mice (C57BL/6 mice, Cas9$^+$ transgenic mice, *Rag1*$^{-/-}$ mice or complete bone marrow chimeras) were injected s.c. with 1×10^6 B16-OVA-Cas9, MC38-OVA-Cas9 or MC38-Cas9 cells expressing the indicated sgRNAs in the right flank. For the lung metastasis model, 1×10^6 B16-OVA-Cas9 cells transduced with the indicated sgRNAs were resuspended in 100 μl phosphate-buffered saline (PBS, Gibco) and injected into Cas9$^+$ transgenic mice through the tail vein. After tumour inoculation, mice were randomly assigned to different groups for ICB and/or ACT treatments. For tumour models with OT-I T cell transfer, preactivated OT-I cells (the details are provided above) were transferred intravenously into tumour-bearing mice at day 7 after tumour inoculation (1×10^7 OT-I cells per mouse). Anti-PD-L1 antibody (10 F.9G2, Bio X Cell) or IgG isotype control (LTF-2, Bio X Cell) was injected intraperitoneally three times at a dose of 100 μg in 100 μl PBS on days 7, 10 and 13 after inoculation of B16-OVA-Cas9 cells transduced with the indicated sgRNAs, as described previously[61]. Anti-PD-1 antibody (J43, Bio X Cell) or rat IgG isotype control (LTF-2, Bio X Cell) was injected intraperitoneally three times at a dose of 100 μg in 100 μl PBS on days 7, 9 and 11 after inoculation of MC38-Cas9 cells expressing the indicated sgRNAs, as described previously[61]. Mice that completely rejected tumours were rechallenged with 1×10^6 B16-OVA-Cas9-sgNTC or MC38-Cas9-sgNTC cells on day 40 or day 50. Anti-CD8α antibody (2.43, Bio X Cell) or rat IgG isotype control (LTF-2, Bio X Cell) was injected intraperitoneally at a dose of 200 μg in 100 μl PBS on days −1, 2, 5, 8 and 11. Anti-IFNγ antibody (XMG1.2, Bio X Cell) or IgG isotype control (HRPN, Bio X Cell) was injected intraperitoneally at a dose of 200 μg in 100 μl PBS on days −1, 3, 7, 11 and 15 or the timepoints as indicated in the figures and their legends. Emricasan was dissolved in PBS and tumour-bearing mice were treated with emricasan (or PBS vehicle) intraperitoneally at 20 mg kg^{-1}, twice a day for 3 days[43]. To establish the constitutively active AKT and NRAS-driven liver tumour mouse model, 6-week-old male mice were injected with 5 μg pT3-EF1a-myrAKT1-HA (31789, Addgene), 5 μg pT-Caggs-NRAS^{G12V} (20205, Addgene) and 2.5 μg pCMV(CAT)T7-SB100 (34879, Addgene) as previously described[67]. To target *Vdac2* in vivo, 50 μg pX330-sgNTC or pX330-sg*Vdac2* was mixed together with the above oncogenic vectors and injected into mice. A volume of plasmid solution equal to 10% of the body weight in sterile Ringer's solution was injected through the tail vein within 5–7 s[67]. s.c. B16-OVA, MC38-OVA and MC38 tumours were measured every 2 days with digital callipers and the tumour volumes were calculated using the formula: length × width × width × π/6. To isolate intratumoural lymphocytes, s.c. tumours were collected on the indicated days after inoculation, excised, minced and digested with 1 mg ml^{-1} collagenase IV (LS004188, Worthington Biochemicals) and 200 U ml^{-1} DNase I (DN25-1G, Sigma-Aldrich) for 1 h at 37 °C and passed through 70-μm filters to remove undigested tumour tissues. TILs from MC38-OVA tumours were further isolated by density-gradient centrifugation over Percoll (17089101, Cytiva). Tumour size limits were approved to reach a maximum of 3,000 mm^3 or ≤20% of body weight

(whichever was lower) by the IACUC of St. Jude Children's Research Hospital.

CRISPR–Cas9 mutagenesis screening using the lentiviral metabolic library

Lentiviral sgRNA metabolic library construction. The mouse metabolic library containing 3,017 genes was synthesized based on the gene list from reported human metabolic-associated genes, and library synthesis, purification and quality control were described previously[18]. In brief, 6 sgRNAs were designed for each gene and were split into two sub-libraries (AAAQ05 and AAAQ07), with each containing 3 sgRNAs targeting one gene and 500 non-targeting controls.

In vitro and in vivo screens. Lentivirus was produced by co-transfecting HEK293T cells with the two lentiviral metabolic sublibrary plasmids, psPAX2 (12260, Addgene) and pCAG4-Eco (35617, Addgene). Then, 48 h after transfection, the supernatant containing viral particles was collected and frozen at −80 °C. A single clone of B16-OVA-Cas9 cells with high Cas9-editing activity was expanded and transduced with the two sub-pools at a multiplicity of infection (MOI) of 0.2–0.3 to achieve 20–30% transduction efficiency. The sublibrary-transduced B16-OVA-Cas9 cells were purified by sorting of Ametrine$^+$ cells and then mixed at 1:1 ratio. Cells were cultured in vitro for another 14 days for genome editing and expansion. An aliquot of 5×10^6 transduced B16-OVA-Cas9 cells (about 250× cell coverage per sgRNA) was saved as the input. For in vitro screening, transduced B16-OVA-Cas9 cells were co-cultured with preactivated OT-I CD8$^+$ T cells (see details above) for 18 h. The remaining tumour cells (5×10^6, about 250× cell coverage per sgRNA) were sorted and used for deep sequencing analysis. For in vivo screening, 1×10^6 transduced B16-OVA cells were inoculated into *Rag1*$^{-/-}$ mice or Cas9$^+$ transgenic mice (10 mice each group, 2 replicates). Preactivated OT-I cells (the details are provided above) were transferred intravenously into B16-OVA tumour-bearing mice at day 7 after tumour inoculation (1×10^7 OT-I cells per mouse). At day 17 after tumour challenge, Ametrine$^+$ tumour cells were collected from the pooled tumour tissues using a cell sorter. At least 5×10^6 sorted B16-OVA cells (>250× cell coverage per sgRNA) were used for deep sequencing analysis.

Sequencing library preparation. Genomic DNA was extracted by using the DNeasy Blood & Tissue Kits (69506, Qiagen). Primary PCR was performed using the KOD Hot Start DNA Polymerase (71086, Millipore) and the following pair of Nextera next-generation sequencing (NGS) primers: (Nextera NGS forward (-F): TCGTCGGCAGCGTCAG ATGTGTATAAGAGACAGTTGTGGAAAGGACGAAACACCG; Nextera NGS reverse (-R): GTCTCGTGGGCTCGGAGATGTGTATAAGAGACAGCC ACTTTTTCAAGTTGATAACGG). Primary PCR products were purified using the AMPure XP beads (A63881, Beckman). A second PCR reaction was performed to attach Illumina adaptors and indexes to barcode each sample. Hi-seq 50-bp single-end sequencing (Illumina) was performed for library sequencing.

Secondary genome-scale CRISPR–Cas9 mutagenesis screening in VDAC2-deficient tumour cells

In vitro screening after IFNγ treatment. Lentivirus was produced by co-transfecting HEK293T cells with lentiviral genome-scale Brie library plasmids with the puromycin-resistance gene[68], psPAX2 (12260, Addgene) and pCAG4-Eco (35617, Addgene). Then, 48 h after transfection, the supernatant containing viral particles was collected and frozen at −80 °C. VDAC2-deficient B16-OVA-Cas9 cells (transduction efficiency, ~5%) were subsequently transduced with the Brie library at an MOI of 0.2–0.3. Brie-library-transduced VDAC2-deficient B16-OVA-Cas9 cells were then cultured with 4 μg ml^{-1} puromycin for another 14 days to select for transduced cells. An aliquot of 8×10^6 transduced VDAC2-deficient B16-OVA-Cas9 cells (about 100× cell coverage per sgRNA) were saved as input. In total, 5×10^7 transduced VDAC2-deficient B16-OVA-Cas9 cells were treated with IFNγ (554587, BD) at 10 ng ml^{-1} for 24 h, resulting in more than 50% tumour cell death (2 replicates). Transduced VDAC2-deficient B16-OVA-Cas9 cells without IFNγ treatment were used as control. A total of 8×10^6 transduced VDAC2-deficient tumour cells (about 100× cell coverage per sgRNA) was collected and used for deep sequencing. DNA exaction and sequencing library preparation were as described in the 'Sequencing library preparation' section using Q5 enzyme (M0541L, NEB) for PCR reactions.

Data processing. For data analysis, FASTQ read files obtained after sequencing were demultiplexed using the Hi-Seq analysis software (Illumina) and processed using MAGeCK (v.0.5.9.4)[69]. Raw counts for each sgRNA were generated with MAGeCK 'count' module by mapping reads to the mouse metabolic library or the Brie library with non-targeting sgRNAs as the control. The MAGeCK 'test' function was used to identify screen hits. For the initial in vitro and in vivo screens, we were able to detect the majority (~99.9% and ~98.8%, respectively) of genes contained in the library from tumour cells (Supplementary Table 1). Total read counts were used for raw count normalization and the secondbest method was used for $\log_2$FC quantification. The effects of screen hits were ranked by MAGeCK RRA score.neg (in vitro OT-I treated versus non-treated or C57BL/6 mice + OT-I versus *Rag1*$^{-/-}$ mice). For the genome-scale secondary genetic interaction screen using the Brie library[68], median read counts across all samples were used for normalization, and the 'mean' method was used for $\log_2$FC quantification and --gene-test-fdr-threshold was set to 1. The significantly enriched or depleted screen hits in sg*Vdac2*-transduced B16-OVA tumour cells were defined as $|\log_2 FC| > 0.5$ and MAGeCK RRA score < 0.05 (Extended Data Fig. 7a). The targeted genes in the Brie library were further overlapped with genes included in the MitoCarta 3.0 database[36] (1,140 for total) to generate a list of 1,032 mitochondria-associated genes (Fig. 4b). The $\log_2$FC values and MAGeCK RRA scores of the mitochondria-associated genes in this secondary genetic interaction screen were visualized as a volcano plot by ggplot2 R package (v.3.3.5), with the top 1 and 2 significantly enriched (based on MAGeCK RRA score) mitochondria-associated gene candidates (*Casp9* and *Bak1*) annotated.

Flow cytometry

For analysis of surface markers, cells were first incubated with Fc block (2.4G2, Bio X Cell) for 10 min in PBS containing 2% (w/v) FBS, and then stained with the appropriate antibodies on ice for 30 min. For intracellular cytokine detection, cells were stimulated for 4 h with phorbol 12-myristate-13-acetate (Sigma-Aldrich) plus ionomycin (Sigma-Aldrich) in the presence of monensin (GolgiStop, 554724, BD Biosciences) and stained for surface markers. The cells were fixed and permeabilized using the CytoFix/CytoPerm fixation/permeabilization kit (554774, BD Biosciences) according to the manufacturer's instructions followed by intracellular cytokine staining using the appropriate antibodies on ice for 30 min. For transcription factor staining, cells were stained for surface markers, followed by fixation and permeabilization using FOXP3/transcription factor staining buffer set (00-5523-00, eBioscience) according to the manufacturer's instructions and intracellular staining with the appropriate antibodies on ice for 30 min. 7-AAD (A9400, 1:200, Sigma-Aldrich) or fixable viability dye (65-0865-18, 1:1,000, eBioscience) was used for dead cell exclusion. Active caspase-3 staining of control and VDAC2-deficient tumour cells was performed using instructions and reagents from an active caspase-3 apoptosis kit (BD Biosciences). The following antibodies were used: PE–anti-CD45 (1:400, 30-F11, 12-0451-83, eBioscience), FITC–anti-CD45.2 (1:400, 104, 109806, BioLegend), Brilliant Violet 785–anti-CD45.2 (1:400, 104, 109839, BioLegend), Alexa Fluor 700–anti-CD8α (1:400, 53-6.7, 100730, BioLegend), Brilliant Violet 605–anti-CD8α (1:400, 53-6.7, 100743, BioLegend), Alexa Fluor 650–anti-CD4 (1:400, GK1.5, 100469, BioLegend), Brilliant Violet 785–anti-TCRβ (1:400, H57-597,

109249, BioLegend), PE/Dazzle 594–anti-PD-1 (1:400, 29F.1A12, Biolegend,135228), Brilliant Violet 711–anti-B220 (1:400, RA3-6B2, 103255, BioLegend), FITC–anti-CD19 (1:400, eBio1D3, 11-0193-85, eBioscience), PE/Cyanine7–anti-IFNγ (1:200, XMG1.2, 505826, BioLegend), Brilliant Violet 421–anti-TNF (1:200, MP6-XT22, 506328, BioLegend), Alexa Fluor 647–anti-GZMB (1:100, GB11, 515406, BioLegend), FITC–anti-FOXP3 (1:200, FJK-16s, 11-5773-82, eBioscience), BV650–anti-Ki-67 (1:100, B56, 563757, BD Biosciences), Alexa Fluor 647–anti-active caspase-3 (1:100, C92-605, 560626, BD Biosciences), PE–anti-IL-2 (1:200, JES6-5H4, 554428, BD Biosciences). Intratumoural $CD8^+$ T cells were gated as $CD45^+CD8^+TCR\beta^+$; $CD4^+FOXP3^-$ T cells were gated as $CD45^+CD4^+TCR\beta^+FOXP3^-$; $CD4^+FOXP3^+$ T_{reg} cells were gated as $CD45^+CD4^+TCR\beta^+FOXP3^+$; B cells were gated as $CD45^+B220^+CD19^+$. Tumour cells were gated as $Ametrine^+CD45^-$ cells. BD FACSDIva software (v.8) was used to collect flow cytometry data on LSRII, Fortessa or Symphony A3 cytometers (BD Biosciences).

Cytokine-induced cell death assays in vitro

To analyse cytokine-induced cell death, the indicated concentration of IFNγ and/or TNF (554589, BD) or human IFNγ (554616, BD) was added. For cell death inhibition assays, pan-caspase inhibitor emricasan[43] (20 μM), ferroptosis inhibitor ferrostatin-1[70] (Fer-1, 10 μM), necroptosis inhibitor necrostatin-1[71] (Nec-1, 20 μM) and GSDMD-mediated pyroptosis inhibitor disulfiram[72] (20 μM) were used. Tumour cell numbers were quantified at the indicated timepoints by flow cytometry using the cell counting beads. Alternatively, cell death was detected and quantified in real-time using the IncuCyte S3 or IncuCyte SX5 imaging system (Sartorius). In brief, 2×10^4 B16-OVA cells per well were plated into a 48-well plate in RPMI-1640 medium containing 10% FBS, 500 nM propidium iodide (P3566, Invitrogen) or 100 nM SYTOX Deep Red (S11381, Invitrogen) and the indicated concentration of IFNγ (details are provided in the associated figures). Cells were imaged every 1 or 2 h and the PI^+ or SYTOX Deep Red^+ cells (counted as dead cells) were quantified using the IncuCyte FLR or Zoom software (http://www.essenbioscience.com/en/products/software/) as described previously[73]. For the LDH-release assay, the cell culture medium was collected at the indicated timepoints and centrifuged at 2,000*g* for 5 min to obtain the supernatant. LDH release was detected using the CytoTox 96 Non-Radioactive Cytotoxicity Assay Kit (G1780, Promega) according to the manufacturer's instructions. The absorbance was measured on the VERSAmax Tunable Microplate Reader (Molecular Devices). For annexin-V and 7-AAD staining, tumour cells (including both the adherent and suspension fractions) were washed and resuspended with annexin V binding buffer (00-0055-56, eBioscience) and then stained with APC–anti-annexin V (1:50, BMS306APC-100, Invitrogen) in annexin V binding buffer for 15 min at room temperature. After washing with annexin V binding buffer, the cells were resuspended with 7-AAD working solution (51-65875X, BD) and analysed using flow cytometry.

Cytosolic mtDNA extraction and quantification

B16-OVA cells were cultured in a 10 cm dish and treated with 10 ng ml^{-1} IFNγ plus pan-caspase inhibitor Q-VD-OPh (40 μM, HY-12305, MedChemExpress) for 24 h, followed by extraction and detection of total DNA and cytosolic DNA as described previously[35]. In brief, 1×10^7 B16-OVA cells were divided into two equal aliquots. One aliquot was resuspended in 300 μl of 50 mM NaOH and boiled for 60 min to solubilize DNA. Then, 10% volume of 1 M Tris-HCl (pH 7.5) was added to neutralize the pH and then centrifuged at 12,000*g* for 10 min to pellet intact cells. Moreover, these extracts served as normalization controls for total genomic DNA and mtDNA. The second equal aliquots were resuspended in 300 μl of buffer containing 150 mM NaCl, 50 mM HEPES (pH 7.4), and 20 mg ml^{-1} digitonin (D141, Sigma-Aldrich). The homogenates were incubated for 15 min on ice to allow selective plasma membrane permeabilization and then sequentially centrifuged at 980*g* for 3 min for a total of three times to pellet intact cells. Finally, the cytosolic supernatants were transferred to fresh tubes and centrifuged at 16,000*g* for 10 min to pellet any remaining cellular debris. The cytosolic DNA and total cellular DNA (from whole-cell extracts) were purified using the DNeasy Blood & Tissue Kit (69506, Qiagen). RT–qPCR was performed on both whole-cell extracts and cytosolic fractions using mtDNA primers (*mtCytb*, *mtNd4*, *mt16S*, *D-loop1*, *D-loop2* and *D-loop3*), and the C_T values of whole-cell extracts served as normalization controls for the values of cytosolic fractions ($FC = \log_2^{-\Delta\Delta CT}$). A list of the primers used for qPCR analysis is provided in Supplementary Table 11.

Generation of mtDNA-depleted cells

B16-OVA cells were cultured in the presence or absence of 200 ng ml^{-1} ethidium bromide (EtBr, E7637, Sigma-Aldrich), as described previously[44,45], for 6 days. Before IFNγ treatment, the culture medium was replaced, and cells were cultured overnight in the absence of EtBr. To measure the efficiency of mtDNA depletion, total extracts were prepared by resuspending the cells in NaOH 50 mM, incubating at 95 °C for 1 h and neutralizing by adding 10% volume 1 M Tris (pH 7.5). The ratio of mtDNA versus genomic DNA was measured using qPCR .

Immunoprecipitation, subcellular fractionation and immunoblot analysis

For immunoprecipitation, 2×10^6 cells expressing HA-VDAC2 and/or Flag-BAK or Flag-BAX were lysed in ice-cold Pierce IP lysis buffer (87787, Thermo Fisher Scientific) containing protease and phosphatase inhibitor cocktail (78442, Thermo Fisher Scientific) and 1% digitonin (D141, Sigma-Aldrich) with rotation at 4 °C for 30 min. The cell lysate was centrifuged at 13,000*g* for 10 min at 4 °C, and the supernatant was incubated with anti-Flag (M8823, Sigma-Aldrich) or anti-HA (88836, Thermo Fisher Scientific) magnetic beads at 4 °C for 2 h. The beads were washed three times with ice-cold IP lysis buffer (87787, Thermo Fisher Scientific) and resuspended with 1× complete Laemmle sample buffer (1610747, Bio-Rad).

To detect cytochrome *c* and SMAC in the subcellular fractions, the mitochondrial and cytosolic fractions were isolated using the Mitochondrial Fractionation Kit (Active Motif) according to the manufacturer's instructions. In brief, cells were treated with 10 ng ml^{-1} IFNγ plus 40 μM pan-caspase inhibitor Q-VD-OPh for 24 h and then washed using pre-chilled 1× PBS and centrifuged at 600*g* for 5 min at 4 °C. The cell pellet was resuspended in 1 ml ice-cold cytosolic buffer and incubated on ice for 15 min, then transferred to a pre-chilled pestle homogenizer. Cells were homogenized using 30–50 strokes with the homogenizer and centrifuged at 800*g* for 20 min at 4 °C. After centrifugation, the supernatant was transferred to a fresh pre-chilled microcentrifuge tube and centrifuged at 10,000*g* for 20 min at 4 °C to pellet the mitochondria; the supernatant contained the cytosolic fraction. The mitochondrial pellet was washed once with 100 μl 1× cytosolic buffer and lysed with 100 μl complete mitochondrial buffer on ice for 15 min to obtain the mitochondrial fraction. The cytosolic fraction was transferred to a fresh pre-chilled microcentrifuge tube and centrifuged at 16,000*g* for 20 min at 4 °C to remove any residual mitochondria.

For chemical cross-linking of cysteines, cells were treated with IFNγ (10 ng ml^{-1}) plus Q-VD-OPh[74] (40 μM) for 24 h or ABT-737 (5 mM) + S63845 (5 mM) + Q-VD-OPh[75] (40 μM) for 6 h. The mitochondrial fraction was obtained as mentioned before and resuspended in cross-linking buffer (20 mM HEPES/KOH (pH 7.5), 100 mM sucrose, 2.5 mM $MgCl_2$ and 50 mM KCl) containing the fresh added 1,6-bis-maleimidohexane (BMH, 0.5 mM, 13.0 A° linker, Thermo Fisher Scientific) and incubated for 30 min at room temperature. Cross-linking was quenched by addition of reducing buffer (1× complete Laemmle sample buffer with 10% 2-mercaptoethanol, M6250, Sigma-Aldrich), and the samples were analysed by SDS–PAGE.

For immunoblot analysis of tumours treated with isotype or anti-PD-L1 in vivo (as described above), B16-OVA tumour tissues (~100 mg) from tumour-bearing mice were homogenized in 1 ml

ice-cold RIPA buffer (89900, Thermo Fisher Scientific) containing protease and phosphatase inhibitor cocktail and homogenized using the Bead Ruptor Elite (OMNI). The lysate was centrifuged at 13,000*g* for 10 min at 4 °C, and the supernatant was mixed with 4× complete Laemmli Sample Buffer (1610747, Bio-Rad). For immunoblot analysis of cells treated with IFNγ, cisplatin (HY-17394, MCE) or etoposide (HY-13629, MCE) in vitro, cultured cells were directly lysed with 1× complete Laemmli sample buffer. In Extended Data Figs. 8c and 10g, IFNγ-induced expression of BCL-2 family members was analysed in B16-OVA cells without Cas9 expression. All of the protein samples were boiled at 95 °C for 10 min, separated using 4–12% Criterion XT Bis-Tris Protein Gel (3450125, Bio-Rad) and transferred to a PVDF membrane (1620177, Bio-Rad). The membranes were blocked using 5% BSA for 1 h and then incubated overnight with primary antibodies (see below). The membranes were then washed with TBST and then incubated with secondary antibodies for 2 h. After antibody incubation, HRP was activated with Supersignal West Dura Extended Duration Substrate (34075, Thermo Fisher Scientific) and visualized with a chemiluminscent detection system using Amersham Imager 600 (GE Healthcare Life Sciences). The blots were then processed and analysed using Image J. Primary antibodies and dilutions were as follows: anti-VDAC2 (1:1,000, PA5-28106, Invitrogen), anti-BCL-2 (1:1,000, sc-7382, Santa Cruz), anti-MCL-1 (1:1,000, ab32087, Abcam), anti-GSDME (1:1,000, ab215191, Abcam), anti-Flag (1:5,000, F1804, Sigma-Aldrich), anti-BIM (1:1,000, B7929, Sigma-Aldrich); anti-Cas9 (1:5,000, 14697), anti-β-actin (1:5,000, 4970), anti-p-STAT1^{Y701} (1:1,000, 9167), anti-STAT1 (1:1,000, 14994), anti-caspase-3 (1:1,000, 9662), anti-cleaved caspase-3 (1:1,000, 9661), anti-caspase-7 (1:1,000, 9492), anti-cleaved caspase-7 (1:1,000, 9491), anti-caspase-9 (1:1,000, 9504), anti-APAF-1 (1:1,000, 8969), anti-cGAS (1:1,000, 31659), anti-STING (1:1,000, 13647), anti-p-STING^{S365} for mouse cells (1:1,000, 72971), anti-p-STING^{S366} for human cells (1:1,000, 19781), anti-TBK1 (1:1,000, 38066), anti-p-TBK1^{S172} (1:1,000, 5483), anti-IRF3 (1:1,000, 4302), anti-p-IRF3^{S396} (1:1,000, 29047), anti-MAVS (1:1,000, 4983), anti-BAK (1:1,000, 12105), anti-BAX (1:1,000, 2772), anti-BCL-xL (1:1,000, 2764), anti-BID for mouse cells (1:1,000, 2003), anti-BID for human cells (1:1,000, 2002), anti-PUMA (1:1,000, 98672), anti-HA (1:5,000, 3724), anti-SMAC (1:1,000; 15108), anti-cytochrome *c* (1:1,000, 4280) and anti-TOMM20 (1:1,000, 42406) (all from Cell Signaling Technology). Secondary antibodies and dilutions were as follows: HRP-conjugated anti-mouse IgG (1:3,000; W4021; Promega) or HRP-conjugated anti-rabbit IgG (1:3,000, W4011, Promega). Densiometric quantification of phosphorylated protein levels was normalized relative to the corresponding total protein, and densiometric quantification of total protein expression was normalized relative to the loading control β-actin or TOMM20 (specifically for Extended Data Fig. 7k). All densiometric quantifications depict the fold changes compared with the relative control (set equal to 1.0) and are shown above the immunoblot image.

MTT assay

To assess tumour cell expansion in vitro, the MTT cell proliferation assay was performed using a commercial kit (30-1010K, ATCC). In brief, 1,000 cells per well B16-OVA-Cas9-sgNTC or B16-OVA-Cas9-sg*Vdac2* cells were plated onto the 96-well plate on day 0, and the cell number was detected every 24 h according to the manual. Absorbance was measured on the VERSAmax Tunable Microplate Reader (Molecular Devices).

ELISA

For in vivo IFNγ and IFNβ detection, B16-OVA tumour tissues (~200 mg) from tumour-bearing mice were homogenized in 500 µl ice-cold RIPA buffer (89900, Thermo Fisher Scientific) containing protease and phosphatase inhibitor cocktail using Bead Ruptor Elite device (OMNI). The lysate was centrifuged at 13,000*g* for 10 min at 4 °C, and the supernatant was used for IFNγ and IFNβ enzyme-linked immunosorbent assay (ELISA). For in vitro cultured cells, the culture medium was collected at the indicated timepoints and centrifuged at 13,000*g* for 10 min at 4 °C to obtain the supernatant. IFNγ and IFNβ was measured by ELISA using the Mouse IFNγ Quantikine ELISA Kit (MIF00-1, R&D systems) or Mouse IFNβ Quantikine ELISA Kit (MIFNB0, R&D systems) according to the manufacturer's instructions. Absorbance was measured on a VERSAmax Tunable Microplate Reader (Molecular Devices).

Immunostaining and histology analyses

Live-cell imaging was performed using B16-OVA-Cas9-sgNTC or B16-OVA-Cas9-sg*Vdac2* cells, which were cultured in chambered coverslips (80426, Ibidi). Tumour cells expressing Omi-mCherry were used for determination of MOMP (the pBabe(puro)-Omi-mCherry plasmid expresses fusion protein in the mitochondria intermembrane space, and is released on MOMP[39]). Time-lapse imaging was performed using the A1RHD25 (Nikon Instruments) resonant scanning confocal equipped with heat and CO_2 incubation, and NIS Elements software (64 bit, v.5.30.03). Images were collected with either a ×40/1.3 NA Plan Fluor or 60× 1.3 NA Plan Apo oil objective and 561 nm laser excitation, and acquired with 1,024 × 1,024 with 0.1 µm px^{-1} resolution.

mtDNA imaging was performed using control (sgNTC) and VDAC2-deficient B16-OVA cells with or without 10 ng ml^{-1} IFNγ plus 40 µM pan-caspase inhibitor Q-VD-OPh treatment for 0 to 24 h as indicated in figures. All of the cells were cultured in chambered coverslips (80426, Ibidi), fixed with 2% paraformaldehyde for 10 min at room temperature, and then treated with 0.1% Triton-100 for permeabilization. Cells were blocked with PBS containing 1% bovine serum albumin and 5% normal goat serum before addition of anti-dsDNA (1 µg ml^{-1}; MAB030, Millipore-Sigma), anti-TOMM20 (1 µg ml^{-1}; 186735, Abcam) or anti-HA (1 µg ml^{-1}; 2367, Cell Signaling Technology) antibodies, followed by detection with donkey anti-mouse (1:500, A32773, Thermo Fisher Scientific) and donkey anti-rabbit (1:500, A32795, Thermo Fisher Scientific) secondary antibodies. Images were acquired using the A1RHD25 (Nikon Instruments) resonance scanning confocal microscope using a ×40/1.3 NA Plan Fluor oil objective, 1,024 × 1,024 and 0.1 µm px^{-1} resolution, 561 nm and 640 nm laser lines. Images were deconvolved using NIS Elements (64 bit, v.5.30.03) and analysed using Imaris software (Bitplane, v.9.5.1×64). For histology analyses, mouse tissues were fixed by 10% (v/v) neutral buffered formalin solution, embedded in paraffin, sectioned and stained with haematoxylin and eosin.

RNA isolation and gene expression profiling

Cells were lysed with Buffer RLT in the RNeasy Micro Kit (74004, Qiagen), and total RNA was extracted according to the manufacturer's instructions. Then, 1 µg total RNA was reverse transcribed using the High-Capacity cDNA Reverse Transcription Kit (4368814, Applied Biosystems). Diluted cDNA was subjected to RT–qPCR reactions containing Power SYBR Green PCR Master Mix (4367659, Applied Biosystems) and gene-specific primers. The reactions were performed in a QuantStudio7 Flex Real-Time PCR System (Applied Biosystems). *Actb* was used as the housekeeping control. A list of the primers is provided in Supplementary Table 11.

Microarray transcriptome analyses

For microarray analysis, to analyse the gene expression of tumour cells after treatment with OT-I cells, control or VDAC2-deficient B16-OVA tumour cells were treated with OT-I cells for 24 h, and the remaining tumour cells were sorted for RNA extraction ($n = 4$ replicates each group). To compare the differently expressed genes in various groups (control, VDAC2-deficient; BAK-deficient; VDAC2 and BAK co-deficient; STING-deficient; VDAC2 and STING co-deficient; APAF-1-deficient; VDAC2 and APAF-1 co-deficient; BIM and BID co-deficient; or VDAC2, BIM and BID co-deficient) of B16-OVA tumour cells, tumour cells were treated with or without IFNγ at 10 ng ml^{-1} for 24 h in vitro, and the adherent tumour cell fraction was collected for RNA extraction (3 or 4 replicates for each group). To analyse the gene expression of

LoVo cells after treatment with IFNγ, control or VDAC2-deficient LoVo tumour cells were treated with human IFNγ for 48 h, and the remaining tumour cells were collected for RNA extraction ($n = 3$ replicates each group). After RNA extraction and purification, 125 ng RNA was used to profile with Affymetrix mouse or human Clariom S assay. The expression signals were analysed using Affymetrix Expression Console (v.1.4.1), followed by differential expression analysis performed using R package limma (v.3.34.9). All of the plots were generated using R packages ggplot2 and ComplexHeatmap (v.2.6.2). Volcano plots depicting $\log_2$FC and $-\log_{10}$(*P* value) were plotted, differentially expressed genes were defined by $|\log_2(FC)| > 0.5$; $P < 0.05$, and the top enriched genes were highlighted.

For GSEA, the preprocessed expression dataset and gene sets were input into GSEA (v.4.3.2), and gene sets were ranked based on their enrichment scores calculated using the two-tailed Kolmogorov–Smirnov test. A ranked GSEA was conducted using the default settings except for 'Permutation type', which was set to 'gene_set'. Hallmark signatures from the Molecular Signatures Database were used (MSigDB; https://www.broadinstitute.org/gsea/msigdb/; v.7.4). For IPA analysis, we used the commercial QIAGEN's Ingenuity Pathway Analysis (IPA, QIAGEN; www.qiagen.com/ingenuity, v.01-23-01) software for upstream regulatory analysis of differentially expressed genes identified in VDAC2-deficient versus WT B16-OVA cells at 16 h after IFNγ treatment, or at 24 h after OT-I cell treatment. For upstream regulatory analysis, we used $|\log_2FC| > 0.4$ as the threshold to select 249 upregulated genes and 262 downregulated genes as the input. In the microarray dataset profiling tumour cells with single deletion or co-deletion of VDAC2 and STING treated with IFNγ for 24 h, differentially expressed genes (sg*Vdac2* versus sgNTC tumour cells, $\log_2FC > 0.5$, $P < 0.05$) were first intersected with genes in Hallmark IFNα and IFNγ response pathways to obtain a list of 15 IFN-response genes. The relative expression of these 15 IFN-response genes were then visualized by heat map in the four genotypes (sgNTC + sgNTC, sg*Vdac2* + sgNTC, sgNTC + sg*Sting1* and sg*Vdac2* + sg*Sting1*).

scRNA-seq and data analysis

Library preparation. For scRNA-seq analysis, wild-type mice were challenged with control or VDAC2-deficient B16-OVA tumour cells. $CD45^+$ immune cells and Ametrine$^+$ $CD45^-$ tumour cells in the tumour tissues were sorted on day 14 after tumour inoculation and mixed at a 3:1 ratio ($n = 2$ biological replicates per genotype). The cell mixture was centrifuged at 2,000 rpm for 5 min and then resuspended in 1× PBS (Thermo Fisher Scientific) plus 0.04% BSA (Amresco) with a final concentration of 1×10^6 cells per ml. The single-cell suspensions were loaded onto the Chromium Controller and encapsulated into droplets. The Chromium Next GEM Single Cell 5′ (version 2) and Gel Bead Kit (10x Genomics) was used for the library preparation according to the manufacturer's instructions. The final libraries were quality-checked using the 2100 Bioanalyzer (Agilent Technologies). The resulting libraries were sequenced on the NovaSeq (Illumina) system with paired-end reads of 26 cycles for read 1 and 90 cycles for read 2 and 10 cycles for index 1 and 2 separately). An average of 500 million reads per sample was obtained.

Data processing and quality control. The Cell Ranger (v.6.0.0) Single-Cell software suite (10x Genomics) was used to process the scRNA-seq FASTQ files. The 'cellranger count' command was performed to align the raw FASTQ files to the mm10 mouse reference genome and summarize the data into matrices that describe gene read counts per cell. For the datasets with matched TCR-seq data, the '.vdj' command was used to generate a count matrix, which, after filtering, was used for downstream analyses.

For gene expression sequencing, the filtered count matrices were read into the R package Seurat (v.4.1). The samples (control and VDAC2-deficient tumours with corresponding $CD45^+$ immune cells) were merged into a single Seurat object for consistent filtering, and features detected in fewer than three cells were removed from the dataset. Cells with abnormally low features or unique molecular identifier (UMI) counts or high mitochondrial read percentages (potentially dead or damaged cells) were removed. Cells with abnormally high UMI counts (potentially multiple cells in a single droplet) were also removed. Finally, any remaining multiplets expressing mutually exclusive marker genes were removed. After filtering, 17,344 cells were retained with an average of 4,064 genes per cell (UMI median: 11,006; range: 500–149,945). After quality control, libraries were normalized with the NormalizeData function (scale.factor = 1×10^6) in the Seurat R package.

Cluster annotation and data visualization. Normalized and filtered data were processed using the standard Seurat pipeline. UMAP dimensionality reduction was used for visualization, and Seurat's FindClusters function was used to separate cells into unsupervised clusters. Cell types in clusters were defined using the following marker genes: B cells (*Cd19*$^+$), $CD8^+$ T cells (*Cd3d*$^+$*Cd8a*$^+$), $CD4^+$ T cells (*Cd3d*$^+$*Cd4*$^+$*Foxp3*$^-$), cDC1 (*Xcr1*$^+$), cDC2 (*Cd209a*$^+$), macrophages (*Adgre1*$^+$), mregDC (*Ccr7*$^+$, *Cd200*$^+$, *Fscn1*$^+$), neutrophils (*Hdc*$^+$), NK cells (*Ncr1*$^+$), pDC (*Siglech*$^+$), T_{reg} cells (*Foxp3*$^+$) and tumour cells ($Cd45^-$). Tumour cells were further verified based on the inferred presence of somatic copy-number alterations using inferCNV (v.1.3.5). For the CreateInfercnvObject() function, we used $CD8^+$ T cells as a negative control group. For the run() function, we used the following parameter values: cutoff=0.1, cluster_by_groups=TRUE, denoise=TRUE, HMM=TRUE. $CD8^+$ T cells were further clustered into stem-like (*Tcf7*$^+$*Havcr2*$^-$), effector-like (*Tcf7*$^-$*Havcr2*$^+$*Pdcd1*$^+$*Tox*^{int}*Mki67*$^+$) and terminally differentiated (*Tcf7*$^-$*Havcr2*$^+$*Pdcd1*$^+$*Tox*^{high}*Cd38*$^+$*Cd101*$^+$*Mki67*$^-$) $CD8^+$ T cells based on the expression of the indicated markers.

TCR data analysis and visualization. For TCR-seq, filtered contig annotation matrices from the Cell Ranger output were loaded into R. Annotation and quantification of TCR clonotypes were processed with the scRepertoire package (v.1.3.5). Clonal frequencies in $CD8^+$ T cells (*Cd3d*$^+$*Cd8a*$^+$) were categorized as follows: NA (0), single (1), small (2–5), medium (6–20), large (21–100) and hyper (101–500). Clonal expansion bar plots were generated using the ggplot2 R package. The clonotypic information was integrated to the Seurat object using the combineExpression() function, with the cloneTypes variable set to cloneTypes=c((Single=1, Small=5, Medium=20, Large=100, Hyper-expanded=500). The cell frequencies of different clonetype sizes were further plotted as a stacked bar plot by ggplot2 R package. Cells were considered clonally expanded if the clonotype size was greater than 1 and non-expanded if the clonotype size was equal to 1.

GSEA and signature curation. For scRNA-seq analysis, nonparametric Wilcoxon rank-sum tests were used to compare the gene expression of cells between two genotypes (sg*Vdac2* versus sgNTC) and then genes in each comparison were ranked on the basis of their $\log_2$FC. To identify the enriched pathways, pre-ranked GSEA (an analysis of GSEA against a user-supplied, ranked list of genes) was then performed as previously described[76] against gene sets from the Hallmark collection from the Molecular Signatures Database (mSigDB) (https://www.broadinstitute.org/gsea/msigdb/, v.7.4). For $CD8^+$ T cells, gene signatures of 'early activation' and 'effector/cytokine' were curated using a previous publication[77], with their activity scores calculated using the AddModuleScore() function in Seurat R package. The VDAC2-suppressed gene signature was generated by defining the upregulated genes ($\log_2FC > 0.7$, FDR < 0.05) in VDAC2-deficient versus control tumour cells based on the scRNA-seq data. A total of 26 human homologues of genes included in the list of VDAC2-suppressed genes was used for TGCA analysis (Supplementary Table 4). Specifically, to assess whether expression of VDAC2-suppressed genes is associated with the survival outcome of

patients with cancer, we assigned patients with cutaneous melanoma from the TCGA SKCM cohort to high or low groups based on the median value of expression of VDAC2-suppressed genes and performed overall survival analysis using the interactive web-based tool GEPIA v.2 (http://gepia2.cancer-pku.cn/#survival)[78]. The survival results were displayed using Kaplan–Meier curves. P value = 0.05 was used as the threshold of statistical significance. The dotted lines in Extended Data Fig. 4w indicate the 95% confidence interval. To assess whether the expression of VDAC2-suppressed genes is associated with the survival of patients with cancer with anti-PD-1 therapy, the association between expression of VDAC2-suppressed genes and the overall survival in patients treated with anti-PD-1 were tested using Cox proportional hazards regression analysis in melanoma using TIDE (http://tide.dfci.harvard.edu/login/)[79,80]. The P values were generated using the two-sided Wald test in the Cox proportional hazards regression. Patient groups with high or low expression of VDAC2-suppressed genes were stratified by the median value of the signature expressing.

ATAC–seq sample preparation and analysis

C57BL/6 mice were s.c. implanted with 1×10^6 control or VDAC2-deficient or control B16-OVA cells. At day 15 after tumour inoculation, control or VDAC2-deficient B16-OVA cells were sort-purified for ATAC–seq analysis ($n = 4$ biological replicates per group). For ATAC–seq profiling of $CD8^+$ T cells from tumours, $PD\text{-}1^-CD8^+$ T cells and $PD\text{-}1^+CD8^+$ T cells were sorted from control or VDAC2-deficient B16-OVA tumours at day 14 after tumour inoculation ($n = 4$ biological replicates per group). Sorted cells were incubated in 50 µl ATAC–seq lysis buffer (10 mM Tris-HCl, pH 7.4, 10 mM NaCl, 3 mM $MgCl_2$ and 0.1% IGEPAL CA-630) for 10 min on ice. The resulting nuclei were pelleted at 500g at 4 °C for 10 min. The supernatant was discarded. The pellet was resuspended in 50 µl transposase reaction mix (25 µl 2× TD buffer, 22.5 µl nuclease-free water and 2.5 µl transposase) and incubated at 37 °C for 30 min to allow tagmentation. The DNA was cleaned up using a Qiagen MinElute kit. The barcoding reaction of the tagmented DNA was run by a NEBNext HiFi kit and amplified for five cycles as previously described using the same primers. The optimal cycle numbers were determined from 5 µl (of 50 µl) from the previous reaction mix using KAPA SYBRFast (Kapa Biosystems) and a 20-cycle amplification on the Applied Biosystems 7900HT system. The remaining 45 µl of PCR reaction was amplified in the same reaction mix using the optimal cycle number.

ATAC–seq data analysis

Paired-end reads (2 × 50 bp) generated from NovaSeq were trimmed to remove Nextera adaptors using trimmomatic (v.0.36) in paired-end mode with the parameters LEADING:10, TRAILING:10, SLIDINGWINDOW:4:18 and MINLEN:25. These reads were then aligned to the mm10 mouse genome by BWA (v.0.7.16, default settings). Duplicated reads were flagged using Picard (v.2.9.4) and only unique, properly paired reads were retained using SAMtools (with the parameters '-q 1 -F 1804'; v.1.9). After adjustment of Tn5 transposase shift (with reads shifted +4 bp on the sense strand and −5 bp on the antisense strand), the fragments were divided into nucleosome-free, mononucleosome, dinucleosome and trinucleosome categories based on size as previously described[29]. Bigwig files were created using the centre 80 bp of each fragment, normalized to 30×10^6 nucleosome-free reads. All of the samples contained approximately 2×10^8 nucleosome-free reads, reflecting high data quality. Next, peaks in nucleosome-free regions were identified using MACS2 (v.2.1.1.20160309, with the default parameters with '--extsize 200--nomodel'). To enhance the reproducibility, peaks were retained only if they passed a stricter threshold (MACS2 --q 0.05). Group consensus peaks were formed by retaining peaks present in at least 50% of replicates and discarding the rest. The reproducible peaks were further merged between samples if they overlapped by at least 100 bp and nucleosome-free reads from each sample were counted using bedtools (v.2.25.0).

To identify the differentially accessible open chromatin regions, the raw nucleosome-free read was first normalized as counts per million followed by differential accessibility analysis by implementation of the negative binomial model in the DESeq2 R package (v.1.43.5). $P < 0.05$, $|\log_2(FC)| > 0.4$ were used as cut-off values for more-accessible or less-accessible regions in B16-OVA tumour cells. $P < 0.05$, $|\log_2 FC| > 0.5$ were used as cut-off values for more-accessible or less-accessible regions in $CD8^+$ T cells from tumours. Principal component analysis (PCA) was performed using the function prcomp in R. Functional peak set enrichment was then performed using MSigDB, Hallmark, C2 and C5 collection for those differentially accessible genes. For motif enrichment analysis, 1,000 unchanged regions ($\log_2 FC < 0.05$ and $P > 0.5$) were selected as control regions for each comparison. FIMO from MEME suite (v.4.11.3, '--thresh 1e-4--motif-pseudo 0.0001') was used for scanning motifs (TRANSFAC database release 2019, only included Vertebrata) matches in the nucleosome-free regions, and two-tailed Fisher's exact tests were used to determine whether a motif was significantly enriched in differentially accessible regions compared with the control regions.

Analysis of public transcriptomics datasets

To examine the expression of *VDAC1*, *VDAC2* and *VDAC3* in tumour cells and other immune cells from the TME, the human melanoma (GEO: GSE215121)[81], human non-small cell lung cancer (NSCLC) (GEO: GSE148071)[82] and mouse tumour scRNA-seq (GEO: GSE121861)[83] datasets were analysed using Seurat. For the analysis of the human melanoma dataset, we used the provided read count matrix in GSE215121. After creating the Seurat object, we pooled the 11 samples using the merge() function. Cells were initially quality filtered based on the percentage of mitochondrial reads < 10% (to remove dead cells) and the number of detected RNA features (gene number <5,000 and UMI < 40,000 to remove potential doublets), and then the data were processed using the standard Seurat pipeline. Cell types were determined based on the indicated markers: T cells (*CD3D*$^+$*CD3E*$^+$), B cells (*MS4A1*$^+$*CD79A*$^+$), NK cells (*FGFBP2*$^+$*KLRD1*$^+$), combined monocytes and macrophages (*LYZ*$^+$*CD68*$^+$*CD14*$^+$), melanoma cells (*MLANA*$^+$*PMEL*$^+$*MITF*$^+$*DCT*$^+$), endothelial cells (*VWF*$^+$*PECAM1*$^+$) and fibroblasts (*COL1A1*$^+$*COL3A1*$^+$). For the analysis of the human NSCLC dataset, we used the prefiltered read count matrix provided in GSE148071. After creating the Seurat object, we pooled the 42 samples using the merge() function. The data were then processed using the standard Seurat pipeline. Cell types were defined using the marker provided in the paper[82]: endothelial cells (*CLDN5*$^+$*VWF*$^+$*PECAM1*$^+$), epithelial cells (*CAPS*$^+$*SNTN*$^+$), alveolar cells, (*CLDN18*$^+$*AQP4*$^+$*FLOR1*$^+$), fibroblasts (*COL1A1*$^+$*COL1A2*$^+$*DCN*$^+$), T cells (*CD2*$^+$*CD3D*$^+$*CD3E*$^+$*CD3G*$^+$), B cells (*CD79A*$^+$*CD79B*$^+$), myeloid cells (*CD14*$^+$*LYZ*$^+$), neutrophils (*CSF3R*$^+$*S100A8*$^+$*S100A9*$^+$), follicular dendritic cells (*FDCSP*$^+$), mast cells (*GATA2*$^+$*TPSAB1*$^+$*TPSB2*$^+$) and cancer cells (*EPCAM*$^+$). For both the human melanoma and NSCLC tumour datasets, the expression of *VDAC1*, *VDAC2* and *VDAC3* in different cell types was visualized by DotPlot() function from the Seurat package. For the mouse tumour scRNA-seq dataset, the expression of *Vdac1*, *Vdac2* and *Vdac3* in the indicated cell types from GSE121861 was also visualized using the DotPlot() function from the Seurat package.

The perturbation effects of *VDAC2* among tumour lines in DepMap were visualized by Chronos dependency scores. The perturbation effects of *VDAC2* in human melanoma cells treated with TILs was visualized by comparing 'neg | score' and 'neg | rank' columns in the comparison of cells treated with TILs at 1:1 ratio versus control cells on day 17[22]. The Pearson correlation between the *VDAC2* gene and the 18-gene tumour inflammation signature (including *HLA-E*, *NKG7*, *CD8A*, *PSMB10*, *HLA-DQA1*, *HLA-DRB1*, *CMKLR1*, *CCL5*, *CXCL9*, *CD27*, *CXCR6*, *IDO1*, *STAT1*, *TIGIT*, *LAG3*, *CD274*, *PDCD1LG2* and *CD276*)[84], *CCL5* or *CD3D*[85] was calculated in each tumour type from TCGA database. Skin cutaneous melanoma and NSCLC tumour RNA-seq data from TCGA were deconvoluted by CIBERSORTx (v.1.05)[86] to determine the fraction of $CD4^+$ and $CD8^+$ T cells.

Statistical analysis for biological experiments

For biological experiment (non-omics) analyses, data were analysed by Prism v.10 software (GraphPad) using two-tailed unpaired Student's *t*-tests, one-way ANOVA or two-way ANOVA, as indicated in the figure legends. The Mantel–Cox test was used for comparing mouse survival curves. Two-tailed Wilcoxon rank-sum tests were applied for activity score or expression analysis of scRNA-seq data. $P < 0.05$ was considered statistically significant, with the exact *P* values provided in the source data that accompany this Article. In all bar plots, data are mean ± s.e.m.

Reporting summary

Further information on research design is available in the Nature Portfolio Reporting Summary linked to this article.

Data availability

The data supporting the findings of this study are available within the Article and its Supplementary Information. All microarray, scRNA-seq and ATAC–seq data described in the Article have been deposited in the NCBI GEO database and are accessible through the GEO SuperSeries access number GSE261554. Public scRNA-seq datasets are available through GSE217160, GSE112865, GSE121861, GSE215121 and GSE148071. Hallmark, C2 and C5 collections were from the MSigDB (https://www.broadinstitute.org/gsea/msigdb/). The perturbation effects of VDAC2 (indicated by Public 24Q4+ Chronos dependency score) in different cancer cell lines (https://depmap.org/portal/gene/VDAC2?tab=dependency) in Cancer DepMap portal and TCGA database (https://www.cancer.gov/ccg/research/genome-sequencing/tcga) are publicly available. Source data are provided with this paper.

Code availability

The original code for bioinformatics analyses has been deposited in Zenodo (available at https://doi.org/10.5281/zenodo.14791554)[87].

61. Guo, C. et al. SLC38A2 and glutamine signalling in cDC1s dictate anti-tumour immunity. *Nature* **620**, 200–208 (2023).
62. Li, J. et al. Control of Foxp3 induction and maintenance by sequential histone acetylation and DNA demethylation. *Cell Rep.* **37**, 110124 (2021).
63. Cong, L. et al. Multiplex genome engineering using CRISPR/Cas systems. *Science* **339**, 819–823 (2013).
64. Nguyen, P. et al. Route of 41BB/41BBL costimulation determines effector function of B7-H3-CAR.CD28ζ T cells. *Mol. Ther. Oncolyt.* **18**, 202–214 (2020).
65. Zhang, C. et al. B7-H3 is spliced by SRSF3 in colorectal cancer. *Cancer Immunol. Immunother.* **70**, 311–321 (2021).
66. Long, L. et al. CRISPR screens unveil signal hubs for nutrient licensing of T cell immunity. *Nature* **600**, 308–313 (2021).
67. Ho, C. et al. AKT (v-akt murine thymoma viral oncogene homolog 1) and N-Ras (neuroblastoma ras viral oncogene homolog) coactivation in the mouse liver promotes rapid carcinogenesis by way of mTOR (mammalian target of rapamycin complex 1), FOXM1 (forkhead box M1)/SKP2, and c-Myc pathways. *Hepatology* **55**, 833–845 (2012).
68. Doench, J. G. et al. Optimized sgRNA design to maximize activity and minimize off-target effects of CRISPR-Cas9. *Nat. Biotechnol.* **34**, 184–191 (2016).
69. Li, W. et al. MAGeCK enables robust identification of essential genes from genome-scale CRISPR/Cas9 knockout screens. *Genome Biol.* **15**, 554 (2014).
70. Dixon, S. J. et al. Ferroptosis: an iron-dependent form of nonapoptotic cell death. *Cell* **149**, 1060–1072 (2012).
71. Degterev, A. et al. Identification of RIP1 kinase as a specific cellular target of necrostatins. *Nat. Chem. Biol.* **4**, 313–321 (2008).
72. Hu, J. J. et al. FDA-approved disulfiram inhibits pyroptosis by blocking gasdermin D pore formation. *Nat. Immunol.* **21**, 736–745 (2020).
73. Gong, Y. N. et al. ESCRT-III acts downstream of MLKL to regulate necroptotic cell death and its consequences. *Cell* **169**, 286–300 (2017).
74. McArthur, K. et al. BAK/BAX macropores facilitate mitochondrial herniation and mtDNA efflux during apoptosis. *Science* **359**, eaao6047 (2018).
75. Riley, J. S. et al. Mitochondrial inner membrane permeabilisation enables mtDNA release during apoptosis. *EMBO J.* **37**, e99238 (2018).
76. Reimand, J. et al. Pathway enrichment analysis and visualization of omics data using g:Profiler, GSEA, Cytoscape and EnrichmentMap. *Nat. Protoc.* **14**, 482–517 (2019).
77. Dixon, K. O. et al. TIM-3 restrains anti-tumour immunity by regulating inflammasome activation. *Nature* **595**, 101–106 (2021).
78. Tang, Z., Kang, B., Li, C., Chen, T. & Zhang, Z. GEPIA2: an enhanced web server for large-scale expression profiling and interactive analysis. *Nucleic Acids Res.* **47**, W556–W560 (2019).
79. Jiang, P. et al. Signatures of T cell dysfunction and exclusion predict cancer immunotherapy response. *Nat. Med.* **24**, 1550–1558 (2018).
80. Fu, J. et al. Large-scale public data reuse to model immunotherapy response and resistance. *Genome Med.* **12**, 21 (2020).
81. Zhang, C. et al. A single-cell analysis reveals tumor heterogeneity and immune environment of acral melanoma. *Nat. Commun.* **13**, 7250 (2022).
82. Wu, F. et al. Single-cell profiling of tumor heterogeneity and the microenvironment in advanced non-small cell lung cancer. *Nat. Commun.* **12**, 2540 (2021).
83. Kumar, M. P. et al. Analysis of single-cell RNA-seq identifies cell-cell communication associated with tumor characteristics. *Cell Rep.* **25**, 1458–1468 (2018).
84. Ayers, M. et al. IFN-γ-related mRNA profile predicts clinical response to PD-1 blockade. *J. Clin. Invest.* **127**, 2930–2940 (2017).
85. Zheng, C. et al. Landscape of infiltrating T cells in liver cancer revealed by single-cell sequencing. *Cell* **169**, 1342–1356 (2017).
86. Newman, A. M. et al. Determining cell type abundance and expression from bulk tissues with digital cytometry. *Nat. Biotechnol.* **37**, 773–782 (2019).
87. Shi, H. & Chi, H. VDAC Nature Code 02-03-25. *Zenodo* https://doi.org/10.5281/zenodo.14791554 (2025).

Acknowledgements We acknowledge D. R. Green for the pcDNA3.1-Flag-BAK plasmid; Y. Feng for the pSIR-DsRed (BbsI) vector; J. Shaw for cell death analysis by IncuCyte system; Y. Sun for bioinformatic analysis; F. Zheng and S. Zhou for technical assistance with human CAR T cell assays; Z. You, J. L. Raynor and J. Saravia for scientific discussions; M. Hendren and R. Walton for animal colony management and technical support; the staff at St. Jude Immunology flow cytometry core facility for cell sorting; the members of the Hartwell Center for microarray and scRNA-seq profiling; the members of Center for Advanced Genome Engineering for CRISPR library expansion and deletional analysis; and the members of Genetically Engineered Mouse Models Shared Resource for mouse line development. Parts of the figures were created using BioRender. This work was supported by ALSAC (to S.G. and H.C.) and National Institutes of Health (NIH) grants CA253188, CA281868, AI105887, AI131703, AI140761, AI150241 and AI150514 (to H.C.). The Hartwell Center, Center for Advanced Genome Engineering, and Genetically Engineered Mouse Models Shared Resource are funded by the Cancer Center Support Grant (P30 CA021765). The content is solely the responsibility of the authors and does not necessarily represent the official views of the NIH.

Author contributions S.Y. and R.S. conceived, designed and performed cellular and molecular experiments, analysed data and co-wrote the manuscript. H.S., H.H. and X.M. performed bioinformatic analysis. N.M.C. co-wrote the manuscript. C.G. and S.R. performed imaging experiments. A.K. and G.P. performed omics profiling. X.S. performed OT-I cell adoptive transfer assays. P.Z. prepared tumour cell lines. X.Y. and S.G. generated the human CAR T cells and provided scientific inputs, respectively. H.C. helped to conceive and design experiments, co-wrote the manuscript and provided overall direction.

Competing interests S.G. is a member of the Scientific Advisory Board of Be Biopharma and CARGO and the Data and Safety Monitoring Board (DSMB) of Immatics, and is a co-inventor on patents/patent applications in the fields of immunotherapy and gene therapy. H.C. consults for Kumquat Biosciences and TCura Bioscience, and is a co-inventor on patents/patent applications in the field of immunotherapy. The remaining authors declare no competing interests.

Additional information

Supplementary information The online version contains supplementary material available at https://doi.org/10.1038/s41586-025-08732-6.

Correspondence and requests for materials should be addressed to Hongbo Chi.

Peer review information *Nature* thanks Ping-Chih Ho, Ana J. Garcia-Saez and the other, anonymous, reviewer(s) for their contribution to the peer review of this work.

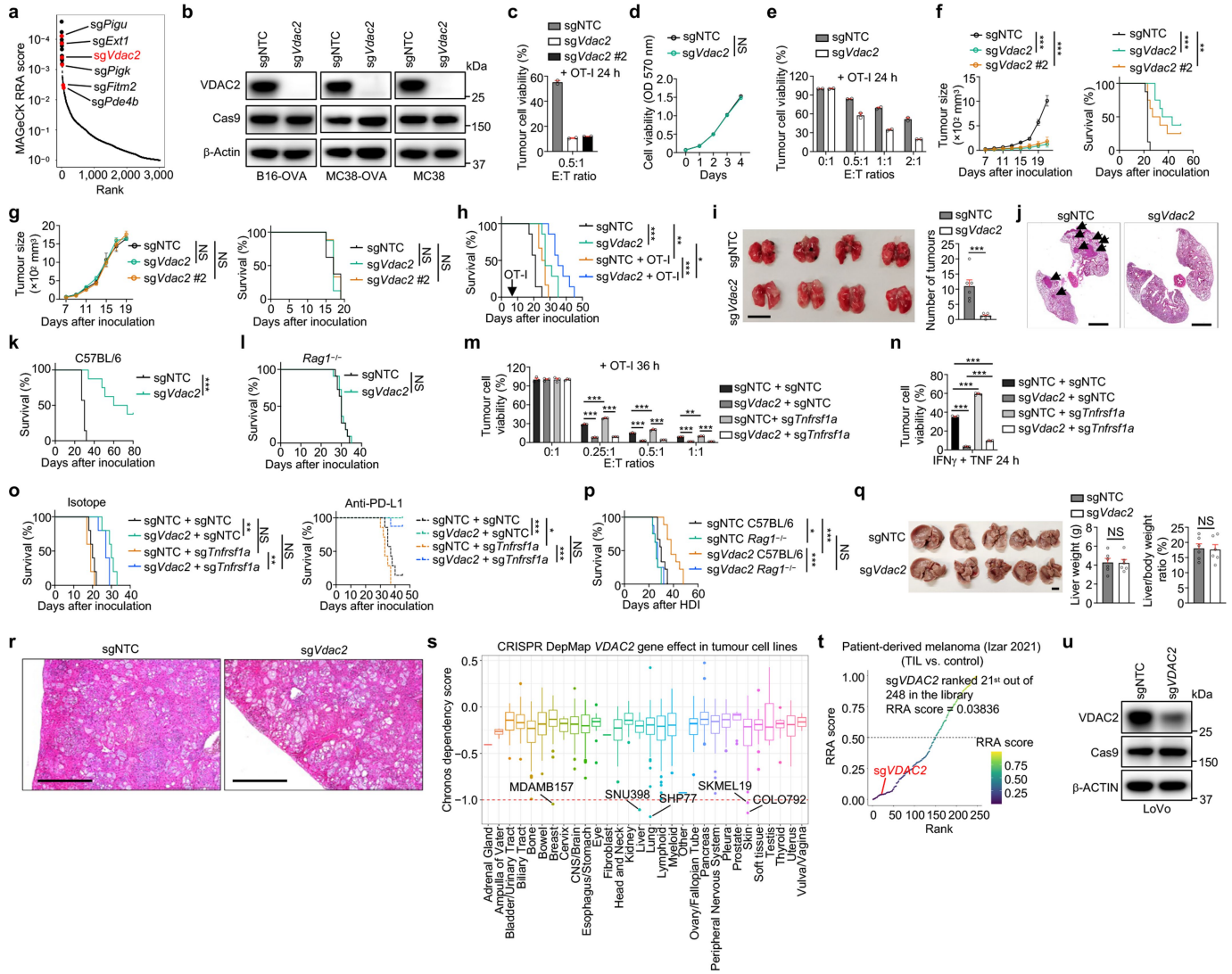

Extended Data Fig. 1 | (related to Fig. 1). VDAC2 targeting overcomes tumour immune evasion and enhances ICB effectiveness in a TNFR-deficient melanoma model. a, MAGeCK analysis of top depleted genes (ranked by RRA score) in tumour cells with OT-I cell treatment versus those without OT-I cell treatment in the in vitro CRISPR screen (depicted in Fig. 1a). **b**, Immunoblot analysis of VDAC2 expression in control and VDAC2-deficient B16-OVA, MC38-OVA, and MC38 tumour cells. **c**, Control or VDAC2-deficient (two different sgRNAs were used to target *Vdac2;* sg*Vdac2* and sg*Vdac2* #2) B16-OVA tumour cell viability after co-culture with OT-I cells for 24 h (n = 2 per group). **d**, Control and VDAC2-deficient B16-OVA tumour cell viability at indicated timepoints, as assessed by MTT assay (n = 6 per group). **e**, Control and VDAC2-deficient MC38-OVA tumour cell viability after co-culture with OT-I cells for 24 h (n = 2 per group). **f**, Control or VDAC2-deficient B16-OVA tumour cell growth in C57BL/6 mice (left). Survival of tumour-bearing C57BL/6 mice (right) (n = 8 per group). **g**, Control or VDAC2-deficient B16-OVA tumour growth in *Rag1*$^{-/-}$ mice (left). Survival of tumour-bearing *Rag1*$^{-/-}$ mice (right) (n = 8 for sgNTC and sg*Vdac2*; 9 for sg*Vdac2* #2). Experiments described in (**f**) and (**g**) were performed in parallel. **h**, C57BL/6 mice were inoculated with control or VDAC2-deficient B16-OVA tumour cells. On day 7 after tumour inoculation, cohorts of these mice received adoptive transfer of activated OT-I cells (indicated by arrow) or PBS. Mouse survival was monitored (n = 7 for PBS treated groups; 6 for sgNTC + OT-I; 7 for sg*Vdac2* + OT-I). **i**, **j**, Cas9^{+} transgenic mice received control or VDAC2-deficient B16-OVA tumour cells by tail vein injection to induce lung metastasis (n = 6 mice per group). Tumour burden (**i**) and histological analyses (**j**) in lung on day 21 after injection. Scale bar, 1 cm in (**i**) or 2 mm in (**j**). **k**, **l**, Survival of Cas9^{+} transgenic mice (n = 7 for sgNTC; 8 for sg*Vdac2*) (**k**) or *Rag1*$^{-/-}$ mice (n = 11 per group) (**l**) that received i.v. injection of control and VDAC2-deficient B16-OVA tumour cells. **m**, Control, VDAC2-deficient, TNFR-deficient, or VDAC2 and TNFR co-deficient B16-OVA tumour cell viability after co-culture with OT-I cells for 36 h (n = 3 per group). **n**, Indicated B16-OVA tumour cell viability after treatment with IFNγ (10 ng ml^{-1}) plus TNF (10 ng ml^{-1}) for 24 h (n = 4 per group). **o**, Survival of C57BL/6 mice inoculated with indicated B16-OVA tumour cells, followed by injection with anti-PD-L1 (or isotype) on days 7, 10, and 13 after tumour inoculation. See also Fig. 1h (n = 5 for isotype treated groups; 7 for sgNTC + sgNTC + anti-PD-L1 and sgNTC + sg*Tnfrsf1a* + anti-PD-L1; 8 for sg*Vdac2* + sgNTC + anti-PD-L1 and sg*Vdac2* + sg*Tnfrsf1a* + anti-PD-L1). **p**, C57BL/6 or *Rag1*$^{-/-}$ mice received AKT and NRAS^{G12V} oncogenic vectors in combination with Cas9- and sgNTC- or sg*Vdac2*-expressing plasmids via hydrodynamic injection (HDI) to induce liver tumorigenesis. Survival of tumour-bearing C57BL/6 mice (see also Fig. 1i,j) and *Rag1*$^{-/-}$ mice (see also Extended Data Fig. 1q,r) were monitored (n = 9 per group for C57BL/6 mice; n = 8 per group for *Rag1*$^{-/-}$ mice). **q**, *Rag1*$^{-/-}$ mice received AKT and NRAS^{G12V} oncogenic vectors in combination with Cas9- and sgNTC- (n = 6) or sg*Vdac2*- (n = 6) expressing plasmids via HDI to induce liver tumorigenesis. Mice were euthanized for analysis of liver tumour burden on day 21 after HDI. Scale bar, 1 cm. **r**, H&E staining of livers from mice (described in **q**) to detect liver tumour burden. Scale bar, 500 µm. **s**, Perturbation effects of *VDAC2* among tumour lines in DepMap were visualized by Chronos dependency scores. **t**, Analysis of public CRISPR screen dataset of human melanoma cells treated with TILs in vitro. sg*VDAC2* ranks in the top 10% (at the gene level) among a sgRNA library targeting 248 genes to deplete tumour cells in TIL versus control (culture medium alone) treatment groups. **u**, Immunoblot analysis of VDAC2 expression in control and VDAC2-deficient LoVo cells. Data are representative of two (**b**–**f**, **h**–**k**, **m**, **n**, **p**, **q**, **u**, **r**) or one (**g**, **l**, **o**) independent experiments and are mean ± s.e.m. Two-tailed unpaired Student's *t*-test (**i**, **q**). One-way ANOVA (**m**, **n**). Two-way ANOVA (**d**, tumour size of **f**, **g**). Mantel–Cox test (survival of **f**, **g**; **h**, **k**, **l**, **o**, **p**).

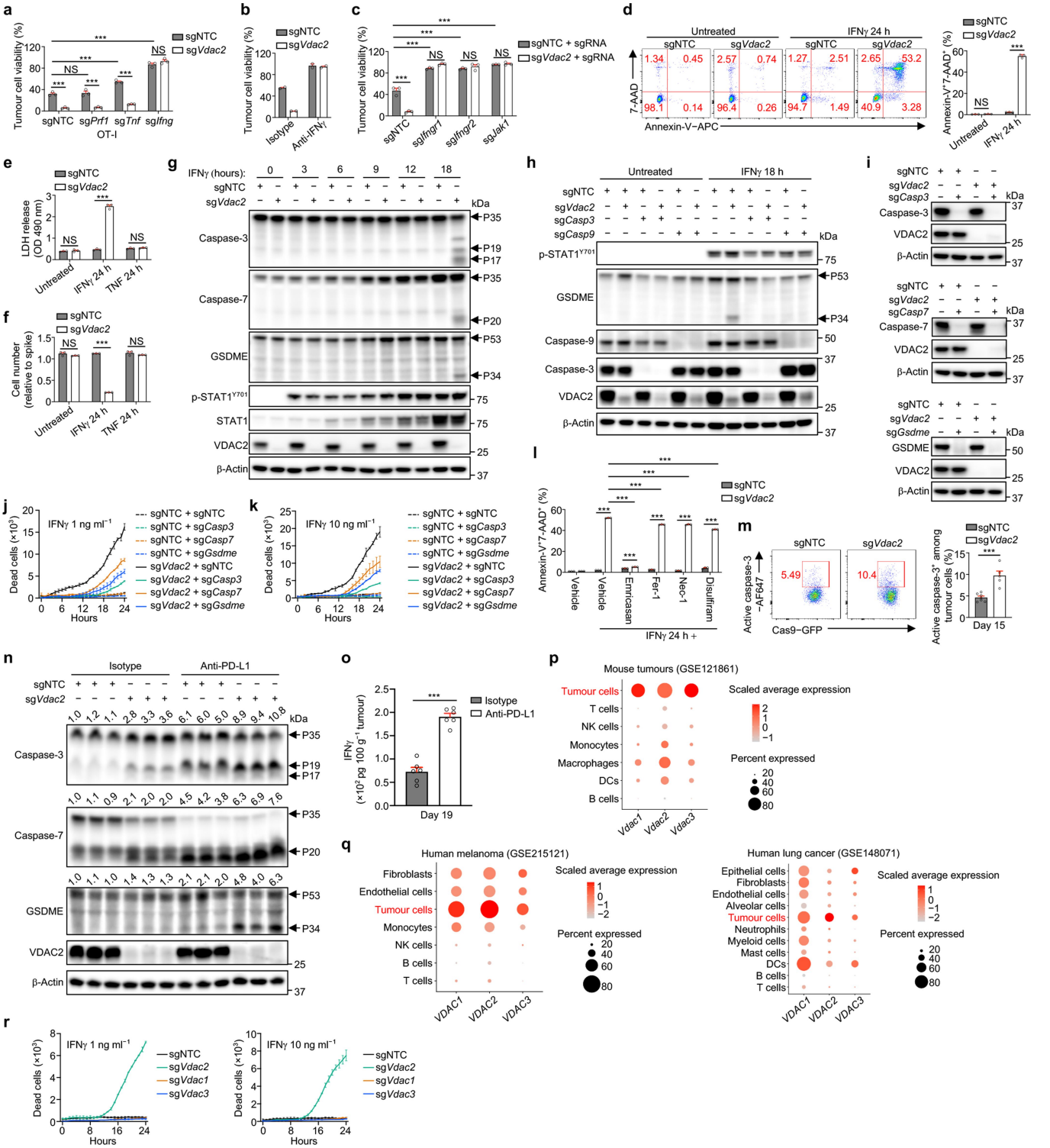

Extended Data Fig. 2 | See next page for caption.

Extended Data Fig. 2 | (related to Fig. 1). VDAC2 deficiency sensitizes tumour cells to IFNγ-induced cell death. a, Control or VDAC2-deficient tumour cell viability after co-culture with sgNTC-, sg*Ifng*-, sg*Tnf*- or sg*Prf1*-transduced OT-I cells at E:T ratio of 0.5:1 for 24 h (n = 3 per group). **b**, Control or VDAC2-deficient B16-OVA tumour cell viability after co-culture with OT-I cells (at E:T ratio of 0.5:1) and anti-IFNγ blocking antibody (or isotype; 10 μg ml^{-1}) for 24 h (n = 2 per group). **c**, Indicated B16-OVA tumour cell viability after co-culture with OT-I cells at E:T ratio of 0.5:1 for 24 h (n = 3 per group). **d**, Control and VDAC2-deficient B16-OVA tumour cell death after treatment with or without IFNγ (10 ng ml^{-1}) for 24 h (n = 3 per group). **e**, LDH release from control and VDAC2-deficient B16-OVA tumour cells treated with or without IFNγ (10 ng ml^{-1}) or TNF (10 ng ml^{-1}) for 24 h (n = 3 per group). **f**, Ametrine$^+$ control or VDAC2-deficient B16-OVA tumour cells were mixed at a 1:1 ratio with mCherry$^+$ spike B16-OVA cells and treated with or without indicated cytokines for 24 h. The relative number of control or VDAC2-deficient cells compared with internal spike cell control is shown (n = 3 per group). **g**, Immunoblot analysis of pro- (P35) and cleaved (P19 and P17) caspase-3; pro- (P35) and cleaved (P20) caspase-7; or pro- (P53) and activated (P34) GSDME in control or VDAC2-deficient B16-OVA tumour cells treated with IFNγ for indicated timepoints. **h**, Immunoblot analysis of pro- (P53) and activated (P34) GSDME in indicated B16-OVA tumour cells treated with or without IFNγ for 18 h. **i**, Expression of caspase-3, caspase-7 and GSDME in indicated B16-OVA tumour cells. **j**, **k**, Real-time survival analysis of indicated B16-OVA tumour cells after treatment with 1 ng ml^{-1} (**j**) or 10 ng ml^{-1} (**k**) of IFNγ (n = 2 per group). **l**, Control and VDAC2-deficient B16-OVA tumour cell death before or after treatment with IFNγ (10 ng ml^{-1}) plus pan-caspase inhibitor emricasan, ferroptosis inhibitor ferrostatin-1 (Fer-1), necroptosis inhibitor necrostatin-1 (Nec-1) or GSDMD-mediated pyroptosis inhibitor disulfiram for 24 h (n = 3 per group). **m**, Activated caspase-3$^+$ cells among control (n = 7) and VDAC2-deficient (n = 5) B16-OVA tumours. **n**, Immunoblot analysis of indicated proteins in control or VDAC2-deficient B16-OVA tumour lysates at day 19 after tumour inoculation. Tumour-bearing mice were treated with isotype IgG or anti-PD-L1 antibody at days 7, 10 and 13 after tumour inoculation (n = 3 per group). Densiometric quantification of cleaved (P19) caspase-3, cleaved (P20) caspase-7 and activated (P34) GSDME is shown. **o**, IFNγ levels in B16-OVA tumour lysates at day 19 after tumour inoculation. Tumour-bearing mice were treated with isotype IgG or anti-PD-L1 antibody at days 7, 10 and 13 after tumour inoculation (n = 6 per group). **p**, Relative expression of *Vdac1*, *Vdac2* and *Vdac3* in indicated mouse cells from publicly available scRNA-seq dataset (GSE121861), which profiled six syngeneic tumour models including B16-F10 melanoma, EMT6 breast mammary carcinoma, LL2 Lewis lung carcinoma, CT26 colon carcinoma, MC38 colon carcinoma and Sa1N fibrosarcoma. **q**, Relative expression of *VDAC1*, *VDAC2* and *VDAC3* in indicated human cell populations (from melanoma (GSE215121, left) and lung cancer (GSE148071, right) datasets). **r**, Real-time survival analysis of indicated B16-OVA tumour cells after treatment with 1 ng ml^{-1} (left; n = 2 per group) or 10 ng ml^{-1} (right; n = 2 per group) of IFNγ. The same control and VDAC2-deficient B16-OVA tumour cells are presented in Fig. 1l. Data are representative of three (**d**, **m**), two (**a**, **c**, **f**–**l**, **n**) or one (**b**, **e**, **o**, **r**) independent experiments and are mean ± s.e.m. Two-tailed unpaired Student's *t*-test (**m, o**). Two-way ANOVA (**a**, **c**–**f, l**).

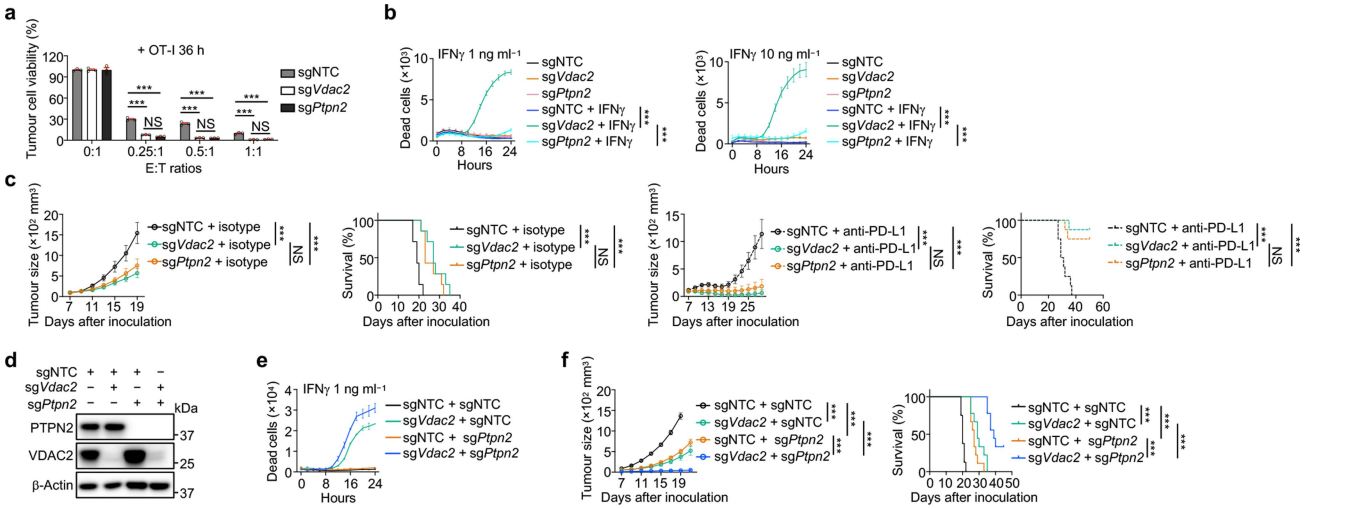

Extended Data Fig. 3 | (related to Fig. 1). Targeting PTPN2 in VDAC2-deficient tumour cells enhanced anti-tumour immunity. a, Control, VDAC2-deficient or PTPN2-deficient B16-OVA tumour cell viability after co-culture with OT-I cells at indicated E:T ratios for 36 h (n = 3 per group). **b**, Real-time survival analysis of indicated B16-OVA tumour cells after treatment with 1 ng ml^{-1} (left) or 10 ng ml^{-1} (right) of IFNγ (n = 5 for sgNTC in 1 ng ml^{-1} treatment group; n = 6 for other groups for both panels). **c**, C57BL6 mice were inoculated with indicated B16-OVA tumour cells, followed by treatment of tumour-bearing mice with isotype control (left panels) or anti-PD-L1 antibody (right panels) at days 7, 10, and 13 after tumour inoculation (n = 7 for isotype-treated groups; n = 8 for anti-PD-L1-treated groups). Tumour growth (first and third panels) and mouse survival (second and fourth panels) were monitored. **d**, Immunoblot analysis of VDAC2 and PTPN2 expression in control, VDAC2-deficient, PTPN2-deficient or VDAC2 and PTPN2 co-deficient B16-OVA tumour cells. **e**, Real-time survival analysis of indicated B16-OVA tumour cells after treatment with 1 ng ml^{-1} of IFNγ (n = 2 per group). **f**, C57BL/6 mice were inoculated with indicated B16-OVA tumour cells (n = 8 for sgNTC + sgNTC; 9 for all other groups). Tumour growth (left) and mouse survival (right) were monitored. Data are representative of three (**a**), two (**b**, **e**, **f**) or one (**c**, **d**) independent experiments and are mean ± s.e.m. One-way ANOVA (**a**). Two-way ANOVA (**b**; tumour size of **c**, **f**). Mantel–Cox test (survival of **c**, **f**).

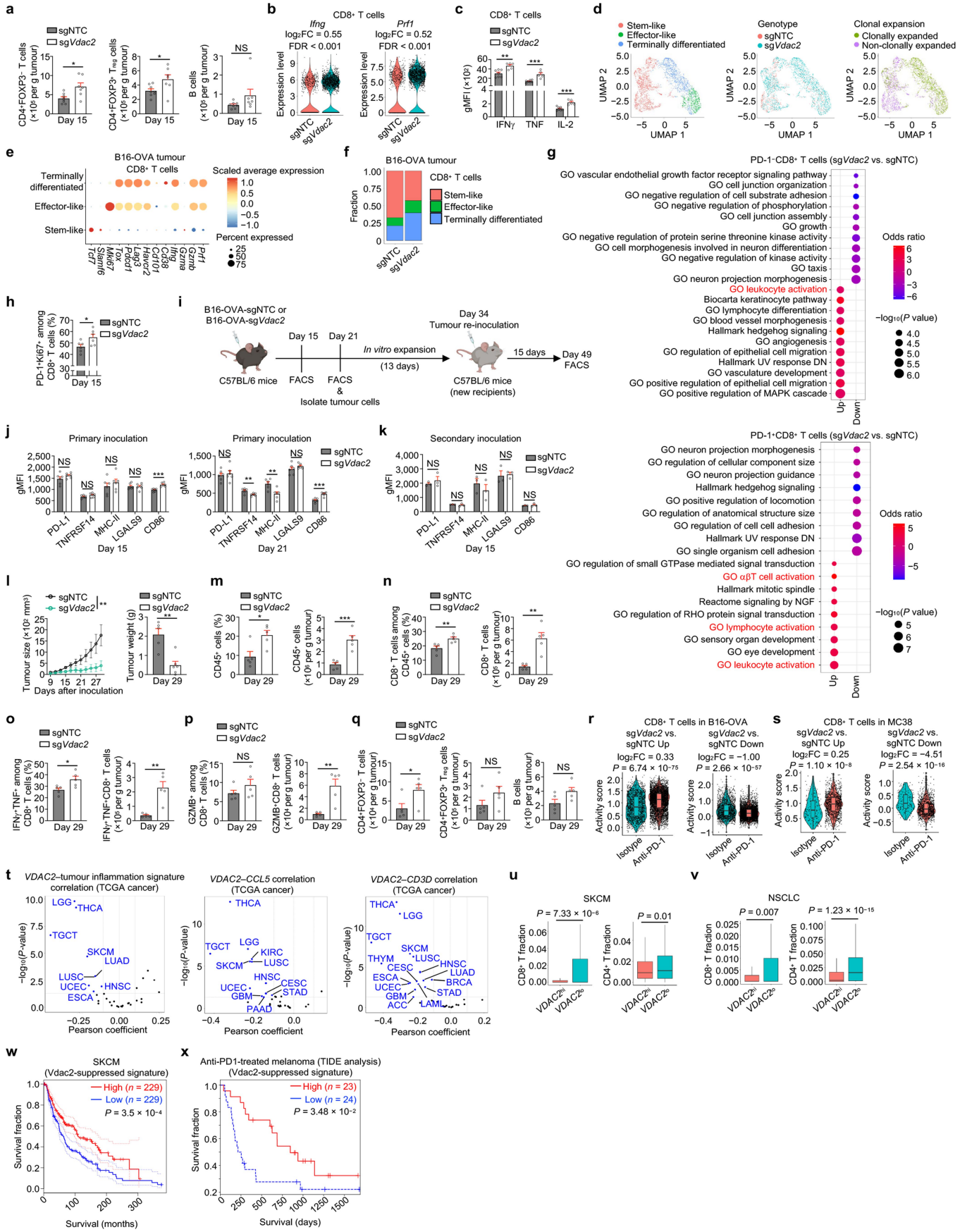

Extended Data Fig. 4 | See next page for caption.

Extended Data Fig. 4 | (related to Fig. 2). VDAC2 deficiency reshapes TME and improves anti-tumour responses. a, Numbers of conventional $CD4^+FOXP3^-$ T cells, $CD4^+FOXP3^+$ T_{reg} cells and B cells in control (n = 8) or VDAC2-deficient (n = 7) B16-OVA tumours on day 15 after tumour inoculation into C57BL/6 mice. **b**, Expression of *Ifng* and *Prf1* in intratumoral $CD8^+$ T cells from control (n = 710 cells) or VDAC2-deficient (n = 2,295 cells) B16-OVA tumours, from scRNA-seq profiling described in Fig. 2a. **c**, Quantification of the geometric mean fluorescence intensities (gMFIs) of IFNγ, TNF and IL-2 in intratumoral $CD8^+$ T cells from control (n = 7) or VDAC2-deficient (n = 5) B16-OVA tumour-bearing C57BL/6 mice on day 15 after tumour inoculation. **d**–**f**, Intratumoral $CD8^+$ T cells from control and VDAC2-deficient B16-OVA tumours were profiled by scRNA-seq plus scTCR-seq as described in Fig. 2a (n = 2 biological replicates per group). UMAP plots coloured based on stem-like, effector-like and terminally differentiated $CD8^+$ T cells among intratumoral $CD8^+$ T cells (left), genotype (middle), or clonal expansion (right) (**d**). Relative expression of stem-like, effector-like and terminally differentiated $CD8^+$ T cell-associated genes used to annotate the populations described in **d** (**e**). Frequencies of stem-like, effector-like and terminally differentiated $CD8^+$ T cells from control and VDAC2-deficient B16-OVA tumours as described in **d** (**f**). **g**, $PD\text{-}1^-$ or $PD\text{-}1^+$ $CD8^+$ T cells were sort-purified from control and VDAC2-deficient B16-OVA tumours at day 14 after tumour inoculation and profiled by ATAC-seq (n = 4 each group). Bubble plot showing the top upregulated (Up) and downregulated (Down) pathways enriched in intratumoral $PD\text{-}1^-$ (upper) or $PD\text{-}1^+$ (lower) $CD8^+$ T cells from VDAC2-deficient versus control tumours. **h**, Frequencies of effector-like $PD\text{-}1^+Ki67^+CD8^+$ T cells in control or VDAC2-deficient B16-OVA tumours as described in **a** (n = 6 per group). **i**, Schematic for long-term VDAC2 deficiency analysis (primary inoculation) and tumour re-inoculation (secondary inoculation) assay. Created in BioRender. Sun, R. (2025) https://BioRender.com/g06b183. **j**, Expression (based on gMFIs) of PD-L1, TNFRSF14, MHC-II, LGALS9 and CD86 on control (n = 6) or VDAC2-deficient (n = 6) B16-OVA tumour cells on day 15 (left) or 21 (right) after tumour inoculation as described in **i**. **k**, Expression (based on gMFIs) of PD-L1, TNFRSF14, MHC-II, LGALS9 and CD86 on control (n = 3) or VDAC2-deficient (n = 3) B16-OVA tumours on day 15 after tumour re-inoculation in secondary hosts as described in **i**. **l**, C57BL/6 mice were inoculated with control (n = 5) or VDAC2-deficient (n = 6) MC38-OVA tumours. Tumour growth (left) and endpoint tumour weight (on day 29, right) were monitored. **m**–**q**, Control or VDAC2-deficient MC38-OVA tumours were isolated as described in **l** (n = 5 per group). Frequencies and numbers of $CD45^+$ cells (**m**), total $CD8^+$ T cells (**n**), $IFN\gamma^+TNF^+$ $CD8^+$ T cells (**o**), or $GZMB^+$ $CD8^+$ T cells (**p**) in tumours. Numbers of conventional $CD4^+FOXP3^-$ T cells, $CD4^+FOXP3^+$ T_{reg} cells and B cells (**q**). **r**, **s**, Activity scores of upregulated (first and third panels) or downregulated (second and fourth panels) gene signatures in intratumoral $CD8^+$ T cells from VDAC2-deficient versus control B16-OVA tumours. Signatures were derived from published datasets of $CD8^+$ T cells from anti-PD-1-treated versus isotype control-treated B16-OVA[31] (**r**) or anti-PD-1-treated versus isotype control-treated MC38[32] (**s**) tumours. Box plots show the median with interquartile range of 25% to 75%. **t**, Correlation between *VDAC2* expression with tumour inflammation signature (left), *CCL5* expression (middle), or *CD3D* expression (right) in 33 cancer types from the TCGA database. *P* values were obtained by comparing the *t*-statistic to the *t*-distribution with n−2 degrees of freedom. **u**, **v**, Box plots showing the median with interquartile range of 25% to 75% of CIBERSORTx-inferred frequencies of infiltrated $CD8^+$ T cells (left) and $CD4^+$ T cells (left) in the RNA-seq analysis of skin cutaneous melanoma (SKCM) (**u**), and non-small cell lung cancer (NSCLC) (**v**) stratified by high (≥ median) or low (<median) *VDAC2* expression. **w**, The overall survival of individuals with SKCM (from the TCGA database) stratified by high and low VDAC2-suppressed gene signature (see Methods). **x**, Survival of melanoma patients treated with anti-PD-1 ICB therapy stratified by high and low activity of VDAC2-suppressed gene signature (see Methods). Data are representative of three (**a**, **c**, **h**), two (**j**, **l**–**q**) or one (**k**) independent experiments and are mean ± s.e.m. Two-tailed unpaired Student's *t*-test (**a**, **c**, **h**, **j**, **k**; tumour weight of **l**; **m**–**q**). Two-way ANOVA (tumour size of **l**). Two-tailed Wilcoxon rank sum test (**b, r, s**, **u**, **v**). Fisher's exact test (**g**). Mantel–Cox test (**w**). Two-sided Wald test (**x**).

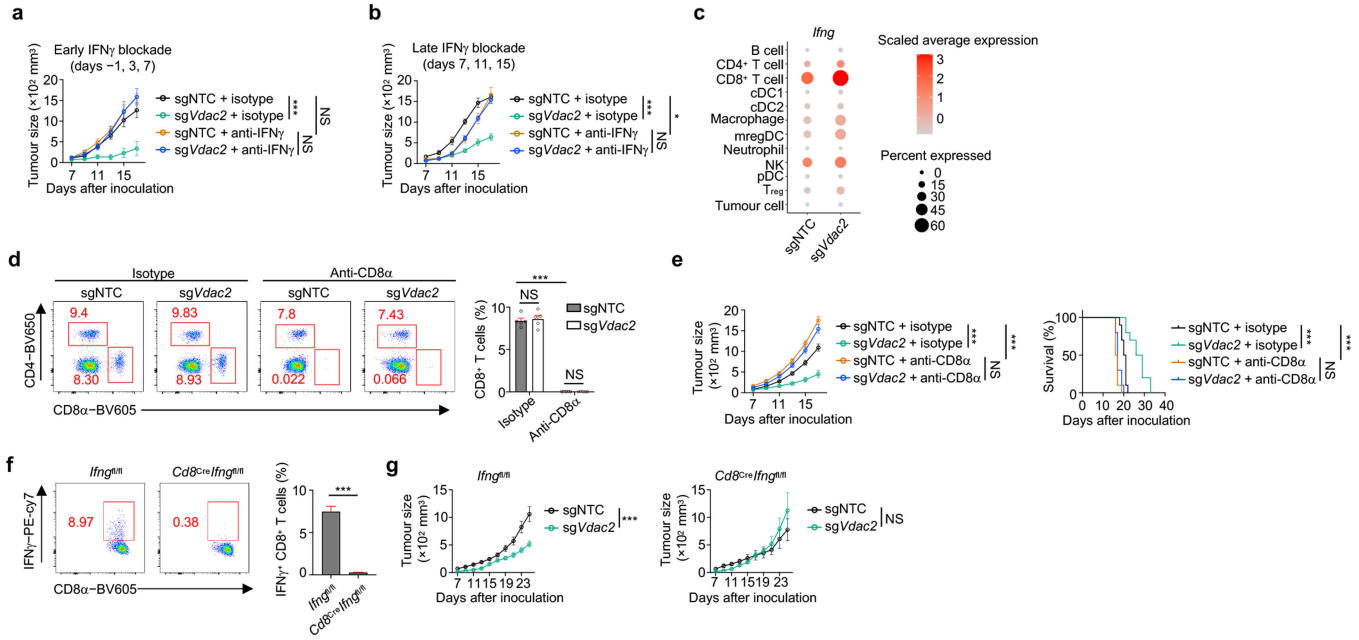

Extended Data Fig. 5 | (related to Fig. 2). VDAC2 deficiency-associated improvement of anti-tumour immunity depends on CD8⁺ T cell-derived IFNγ. **a**, **b**, C57BL/6 mice inoculated with control or VDAC2-deficient B16-OVA tumours were treated with anti-IFNγ (or isotype) on days −1, 3, 7 after tumour challenge (**a**, n = 6 for isotype-treated groups; 6 for sgNTC + anti-IFNγ; 5 for sg*Vdac2* + anti-IFNγ), or on days 7, 11, 15 after tumour challenge (**b**, n = 6 for isotype-treated groups; 6 for sg*Vdac2* + anti-IFNγ; 5 for sgNTC + anti-IFNγ). Tumour growth was monitored. **c**, Relative expression of *Ifng* in indicated cell populations from control or VDAC2-deficient B16-OVA tumours from scRNA-seq profiling described in Fig. 2a. **d**, Frequency of CD8⁺ T cells in peripheral blood of mice receiving anti-CD8α depleting antibody (or isotype control) on days −1, 2, 5, 8 and 11 after tumour inoculation (n = 5 per group). **e**, C57BL/6 mice were inoculated with control or VDAC2-deficient B16-OVA tumours, followed by treatment with anti-CD8α (or isotype control) as described in **d**. Tumour growth (left) and mouse survival (right) were monitored (n = 10 per group). **f**, Frequencies of IFNγ⁺ CD8⁺ T cells in the peripheral blood of B16-OVA tumour-bearing control *Ifng*$^{fl/fl}$ or *Cd8*^{Cre}*Ifng*$^{fl/fl}$ chimeras (n = 13 per group). **g**, Control and VDAC2-deficient B16-OVA tumour growth in *Ifng*$^{fl/fl}$ (n = 10 per group) and *Cd8*^{Cre}*Ifng*$^{fl/fl}$ (n = 5 for sgNTC; 7 for sg*Vdac2*) chimeras. Data are representative of two (**f**, **g**) or one (**a**, **b**, **d**, **e**) independent experiments and are mean ± s.e.m. Two-tailed unpaired Student's *t*-test (**f**). Two-way ANOVA (**a**, **b**, **d**; tumour size of **e**; **g**). Mantel–Cox test (survival of **e**).

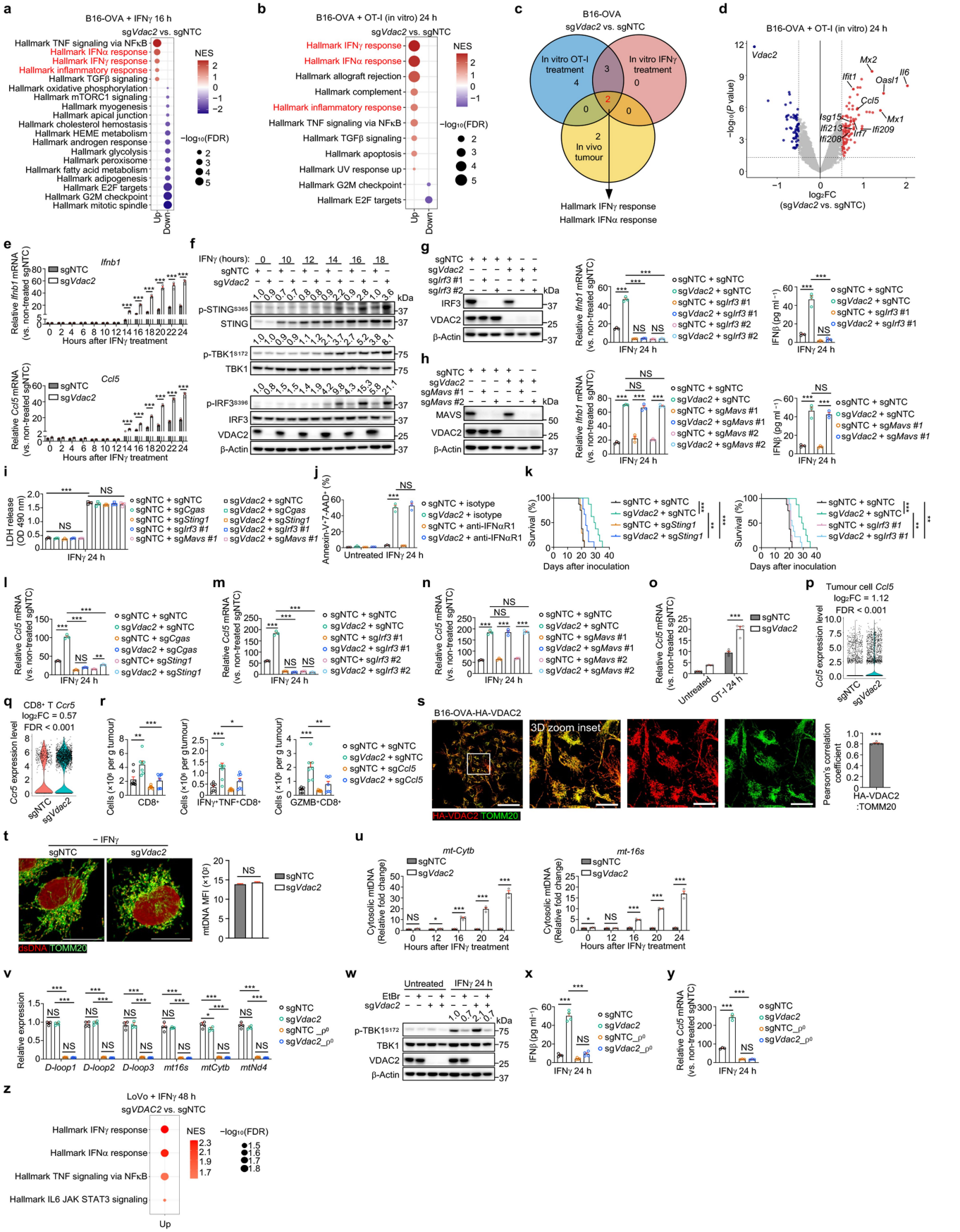

Extended Data Fig. 6 | See next page for caption.

Extended Data Fig. 6 | (related to Fig. 3). VDAC2 loss boosts IFNγ-triggered STING activation and type-I IFN response. a, **b**, Bubble plots depicting upregulated (Up; red) and downregulated (Down; blue) pathways in VDAC2-deficient versus control B16-OVA tumour cells after treatment with IFNγ for 16 h (**a**) or OT-I cells for 24 h (**b**) (n = 4 samples per group). Pathways of interest are labelled in red. **c**, Overlapping upregulated Hallmark pathways in VDAC2-deficient versus control B16-OVA tumour cells from the indicated transcriptome profiling datasets. In vivo tumour denotes the scRNA-seq profiling data from Fig. 2a. **d**, Differential gene expression profiles in OT-I-treated VDAC2-deficient versus OT-I-treated control B16-OVA tumour cells (as described in **b**; n = 4 per group). Selective upregulated (red) and downregulated (blue) genes are annotated. **e**, Relative *Ifnb1* and *Ccl5* levels (versus non-treated control cells) in control or VDAC2-deficient B16-OVA tumour cells treated with IFNγ for indicated timepoints (n = 3 per group). **f**, Immunoblot analysis of indicated proteins in control and VDAC2-deficient B16-OVA tumour cells treated with or without IFNγ for indicated timepoints. Densiometric quantification of p-STING, p-TBK1 or p-IRF3 is shown. **g**, Immunoblot analysis of IRF3 and VDAC2 expression in control, VDAC2-deficient, IRF3-deficient or VDAC2 and IRF3 co-deficient B16-OVA tumour cells (left). Relative *Ifnb1* levels (versus non-treated control cells; middle) and IFNβ levels (right) in culture supernatants of indicated B16-OVA tumour cells treated with IFNγ for 24 h (n = 3 per group). **h**, Immunoblot analysis MAVS and VDAC2 expression in control, VDAC2-deficient, MAVS-deficient or VDAC2 and MAVS co-deficient B16-OVA tumour cells (left). Relative *Ifnb1* levels (versus non-treated control cells; middle) and IFNβ levels (right) in culture supernatants of indicated B16-OVA tumour cells treated with IFNγ for 24 h (n = 3 per group). The same control and VDAC2-deficient samples are presented in right panels of **g** and **h**. **i**, LDH release from control, VDAC2-deficient, cGAS-deficient, STING-deficient, IRF3-deficient, MAVS-deficient, VDAC2 and cGAS co-deficient, VDAC2 and STING co-deficient, VDAC2 and IRF3 co-deficient or VDAC2 and MAVS co-deficient B16-OVA tumour cells treated with IFNγ for 24 h (n = 3 per group). NS indicates no statistical differences in all groups versus sgNTC + sgNTC (left) or sg*Vdac2* + sgNTC (right). **j**, Cell death analysis of control or VDAC2-deficient B16-OVA tumour cells treated with or without IFNγ (10 ng ml^{-1}) in the presence of anti-IFNαR1 antibody (or isotype control; 20 μg ml^{-1}) for 24 h (n = 3 per group). **k**, Control (n = 8), VDAC2-deficient (n = 8), STING-deficient (n = 7), IRF3-deficient (n = 8), VDAC2 and STING co-deficient (n = 9), or VDAC2 and IRF3 co-deficient (n = 9) B16-OVA tumour cells were inoculated into C57BL/6 mice. Mouse survival was monitored. The same sgNTC and sg*Vdac2* groups are shown in left and right panels. **l**–**n**, Relative *Ccl5* levels (versus non-treated control cells) in indicated B16-OVA tumour cells treated with IFNγ for 24 h (n = 3 per group). The same control and VDAC2-deficient B16-OVA tumour cells are shown in **m** and **n**. **o**, Relative *Ccl5* levels (versus non-treated control cells) in control or VDAC2-deficient B16-OVA tumour cells co-cultured with or without OT-I cells for 24 h (n = 4 per group). **p**, **q**, *Ccl5* expression in control (n = 3,264 cells) or VDAC2-deficient (n = 3,290 cells) B16-OVA tumour cells (**p**) and *Ccr5* expression in intratumoral CD8$^+$ T cells from control (n = 710 cells) or VDAC2-deficient (n = 2,295 cells) B16-OVA tumours (**q**), as profiled by scRNA-seq as described in Fig. 2a. **r**, Numbers of total (left), IFNγ$^+$TNF$^+$ (middle), or GZMB$^+$ (right) CD8$^+$ T cells in control (n = 8 for total number; 7 for IFNγ$^+$TNF$^+$ and GZMB$^+$ cell number), VDAC2-deficient (n = 7), CCL5-deficient (n = 8 for total number; 7 for IFNγ$^+$TNF$^+$ and GZMB$^+$ cell number) or VDAC2 and CCL5 co-deficient (n = 8 for total number; 7 for IFNγ$^+$TNF$^+$ or GZMB$^+$ cell number) B16-OVA tumours on day 14 after tumour inoculation. **s**, Representative images and Pearson's correlation coefficient of HA-VDAC2 (based on HA staining; red) co-localization with mitochondria (based on TOMM20 staining; green). Scale bar, 100 μm (wide field) and 25 μm (3D zoom inset), n = 5. **t**, Representative images and quantification (n = 3,665 for sgNTC; 3,353 for sg*Vdac2*) of dsDNA (red) co-localization with mitochondria (based on TOMM20 staining; green) in control and VDAC2-deficient B16-OVA tumour cells. Scale bar, 20 μm. The same assay was used in Fig. 3o for IFNγ-treated samples. **u**, Relative cytosolic mtDNA levels (versus control at 0 h) in control and VDAC2-deficient B16-OVA tumour cells after treatment IFNγ for indicated timepoints (n = 3 per group). **v**, Cytosolic mtDNA levels in control and VDAC2-deficient B16-OVA tumour cells treated with ethidium bromide (EtBr, 200 ng ml^{-1}; denoted as "ρ^0" cells) for mtDNA depletion (n = 4 per group). **w**–**y**, Control and VDAC2-deficient B16-OVA tumour cells that lack or contain mtDNA were treated with or without IFNγ for 24 h. Immunoblot analysis of the indicated proteins, with densiometric quantification of phosphorylated p-TBK1 shown (**w**). IFNβ levels in culture supernatants (**x**, n = 4 per group) and relative *Ccl5* levels (versus non-treated control cells) (**y**, n = 3 per group). **z**, Bubble plot depicting upregulated pathways in VDAC2-deficient versus control LoVo tumour cells after treatment with IFNγ for 48 h (n = 3 samples per group). Data are representative of three (**h**, left panel), two (**f**; middle panel in **g**; middle and right panels of **h**; **m**–**o**, **r**–**y**) or one (**e**; left panel of **g**, **h**) independent experiments and are mean ± s.e.m. Two-tailed unpaired Student's *t*-test (**e**, **t**, **u**). One-way ANOVA (middle and right panels of **g**, **h**; **i**, **j**, **l**–**n**, **r**, **v**, **x**, **y**). Two-way ANOVA (**o**). Mantel–Cox test (**k**). Two-tailed Wilcoxon rank sum test (**p**, **q**). One sample *t*-test (**s**).

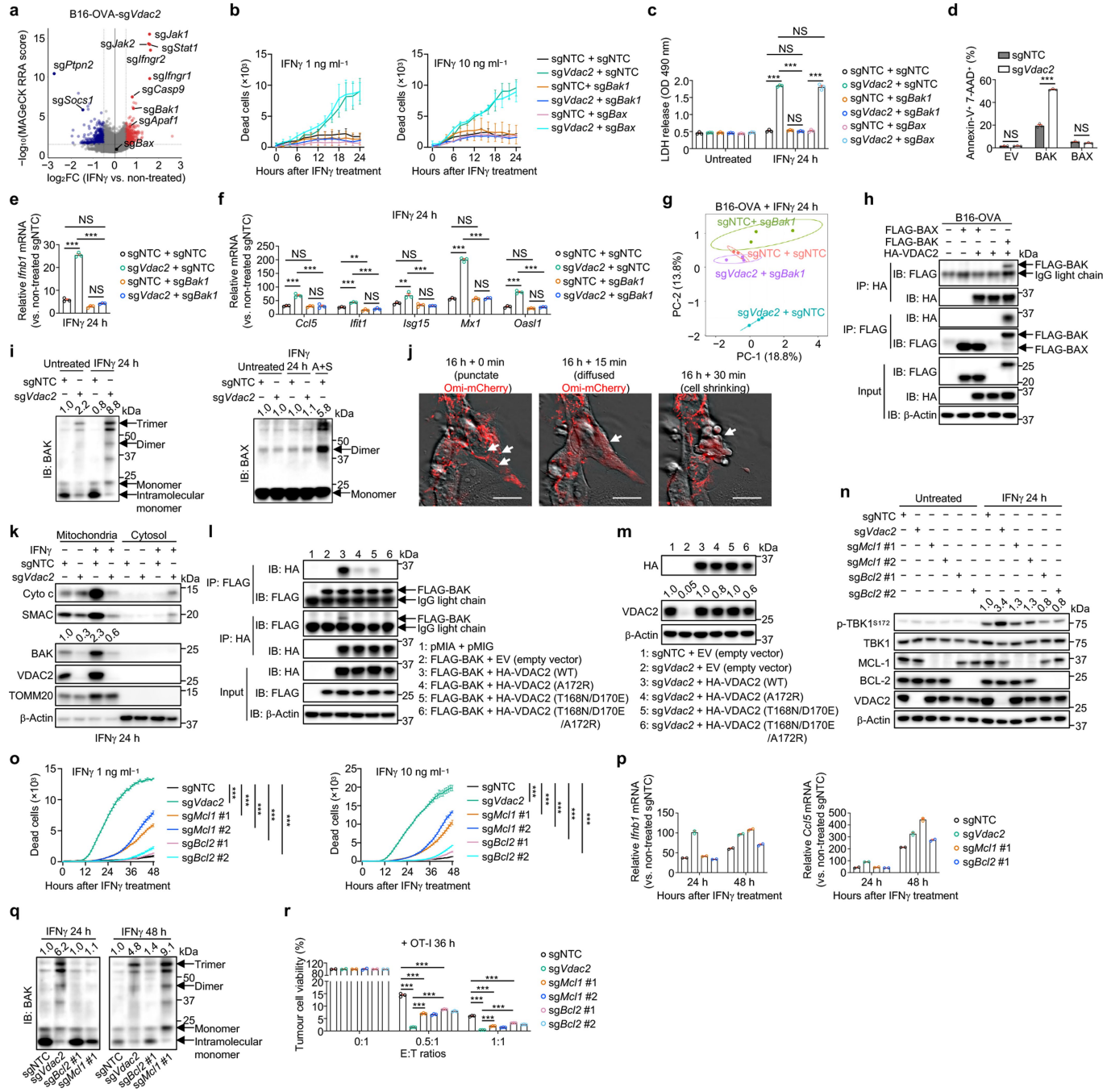

Extended Data Fig. 7 | See next page for caption.

Extended Data Fig. 7 | (related to Fig. 4). BAK-mediated MOMP occurs in the absence of VDAC2 and elicits tumour cell death and inflammation in response to IFNγ. a, Enriched (red) and depleted (blue) sgRNAs in IFNγ-treated versus non-treated VDAC2-deficient B16-OVA tumour cells in genome-scale genetic interaction CRISPR screen described in Fig. 4a. **b**, Real-time survival analysis control, VDAC2-deficient, BAK-deficient, BAX-deficient, VDAC2 and BAK co-deficient or VDAC2 and BAX co-deficient B16-OVA tumour cells after treatment with 1 ng ml^{-1} (left; n = 2 per group) and 10 ng ml^{-1} (right; n = 2 per group) of IFNγ. **c**, LDH release from indicated B16-OVA tumour cells treated with or without IFNγ (10 ng ml^{-1}) for 24 h (n = 3 per group). **d**, Control and VDAC2-deficient B16-OVA tumour cell death upon overexpression of BAK or BAX (as indicated) for 48 h (n = 3 per group). EV, empty vector. **e**, Relative *Ifnb1* levels (versus non-treated control cells) in indicated B16-OVA tumour cells treated with IFNγ treatment for 24 h (n = 3 per group). **f**, Relative levels (versus non-treated control cells) of indicated IFN-responsive genes in indicated B16-OVA tumour cells treated with IFNγ for 24 h (n = 3 per group). **g**, Principal component analysis (PCA) plot of each sample in the microarray data from Fig. 4f, with the percentage of variance shown (n = 3 per group). **h**, FLAG-BAK or FLAG-BAX were stably co-expressed with HA-VDAC2 (or EV) in B16-OVA cells. The interaction between HA-VDAC2 and FLAG-BAK or FLAG-BAX was analysed by anti-HA or anti-FLAG immunoprecipitation (IP) and immunoblot (IB) analysis for FLAG and HA as indicated. **i**, Control or VDAC2-deficient B16-OVA tumour cells were treated with or without IFNγ (in the presence of the pan-caspase inhibitor Q-VD-OPh to inhibit cell death of VDAC2-deficient cells) for 24 h, or control cells were treated with ABT-737 (BCL-2 inhibitor) + S63845 (MCL-1 inhibitor) + Q-VD-OPh (pan-caspase inhibitor) (A + S group) for 6 h. Mitochondrial fractions were isolated, followed by treatment with sulfhydryl reactive cysteine crosslinker (1,6-bis-maleimidohexane, BMH) to promote formation of intramolecularly linked monomers and intermolecularly linked dimers and trimers. BAK and BAX molecules without cross-linked cysteines are labelled as monomers. Samples were separated by SDS-PAGE under reducing conditions to resolve these different BAK and BAX complexes. Densiometric quantification of BAK trimers and BAX dimers is shown. **j**, Time-lapsed fluorescence microscopy images of VDAC2-deficient B16-OVA tumour cells (with stable Omi-mCherry expression, which localizes to mitochondria inter-membrane space and is released upon MOMP) following IFNγ treatment for 16 h. Images were acquired immediately at 16 h and for 2 additional 15-minute timepoints thereafter (labelled as 16 h + 0 min, 16 h + 15 min and 16 h + 30 min). Scale bar, 20 μm. **k**, Immunoblot analysis of cytochrome c (Cyto c) and SMAC protein levels in cytosolic and mitochondrial fractions of control or VDAC2-deficient B16-OVA tumour cells treated with or without IFNγ for 24 h. Densiometric quantification of BAK is shown. **l**, Interaction between HA-VDAC2 (wild-type (WT) or mutants) and FLAG-BAK in indicated B16-OVA tumour cells was analysed by anti-HA or anti-FLAG IP and IB analysis for FLAG and HA. **m**, Immunoblot analysis of HA-VDAC2 and total VDAC2 in indicated B16-OVA tumour cells, with densiometric quantification of total VDAC2 shown. **n**, Immunoblot analysis of indicated proteins in control, VDAC2-deficient, MCL-1-deficient, or BCL-2-deficient B16-OVA tumour cells treated with or without IFNγ for 24 h. Densiometric quantification of p-TBK1 is shown. **o**, Real-time survival analysis of control (sgNTC), VDAC2-deficient (sg*Vdac2*), MCL-1-deficient (sg*Mcl1* #1 or sg*Mcl1* #2) and BCL-2-deficient (sg*Bcl2* #1 or sg*Bcl2* #2) B16-OVA tumour cells treated with indicated concentrations of IFNγ (n = 4 per group). **p**, Relative *Ifnb1* and *Ccl5* levels (versus non-treated control cells) in control, VDAC2-deficient, BCL-2-deficient or MCL-1-deficient B16-OVA tumour cells treated with or without IFNγ (10 ng ml^{-1}) for 24 or 48 h (n = 2 per group). **q**, Indicated B16-OVA tumour cells were treated with IFNγ (in the presence of the pan-caspase inhibitor Q-VD-OPh to block cell death) for 24 or 48 h. Mitochondrial fractions were isolated, followed by treatment with sulfhydryl reactive cysteine crosslinker (1,6-bis-maleimidohexane, BMH) to promote formation of dimers and trimers as described in **i**. **r**, Indicated B16-OVA tumour cell viability after co-culture with OT-I cells for 36 h at the indicated E:T ratios (n = 2 per group for 0:1; 3 per group for other E:T ratios). Similar statistics were observed for the second sgRNA as the first sgRNA targeting *Mcl1* or *Bcl2* in indicated comparisons (not depicted for clarity). Data are representative of three (**h**, **i**, **k**) or two (**b**–**f**, **j**, **l**–**r**) independent experiments and are mean ± s.e.m. One-way ANOVA (**c**, **e**, **f**, **r**). Two-way ANOVA (**d**, **o**).

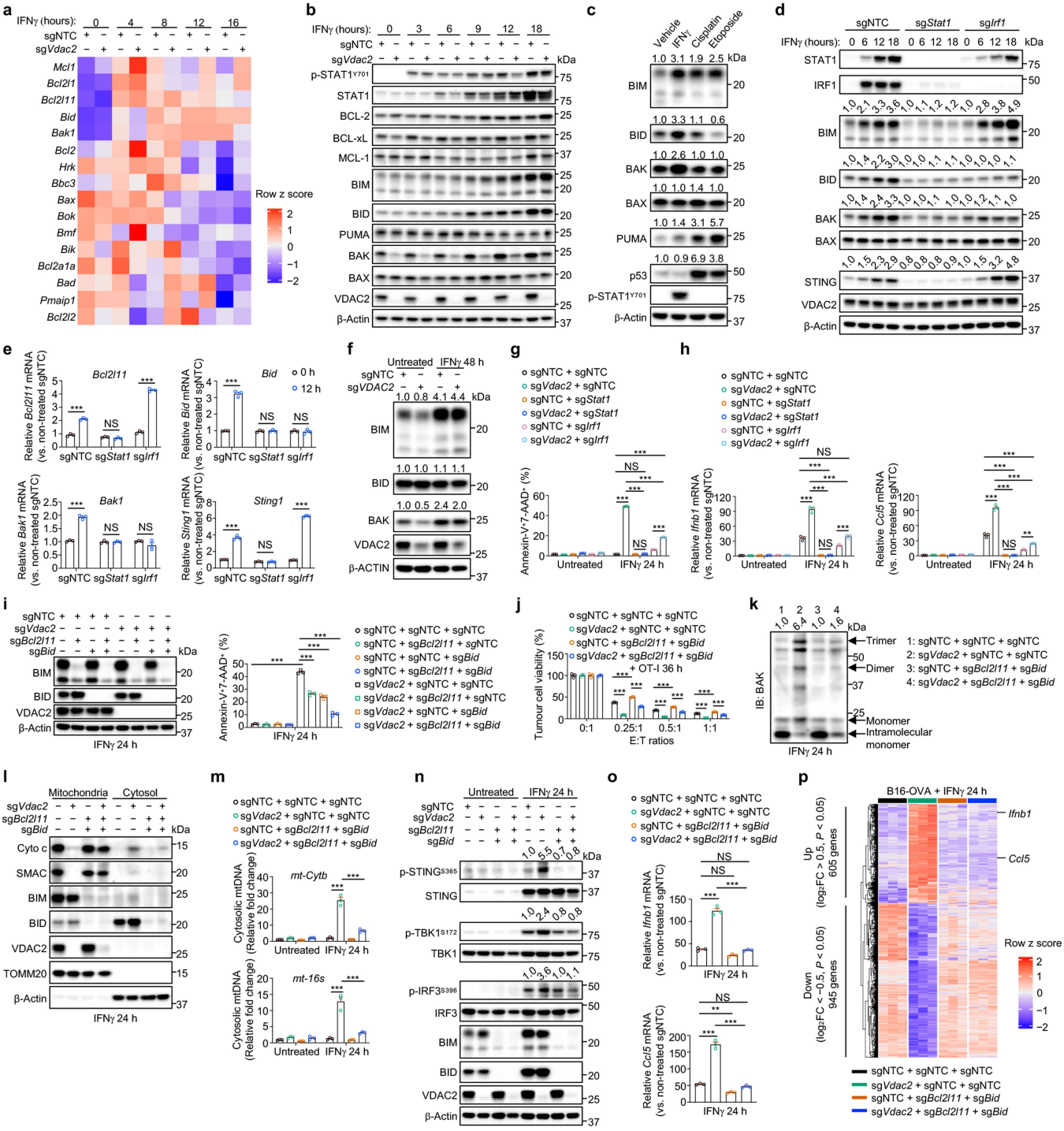

Extended Data Fig. 8 | See next page for caption.

Extended Data Fig. 8 | (related to Fig. 4). IFNγ-mediated coordinated upregulation of BIM, BID and BAK contributes to cell death of VDAC2-deficient cells. a, Relative gene expression of BCL-2 family proteins in control or VDAC2-deficient B16-OVA tumour cells after treatment with IFNγ for indicated timepoints (n = 4 per group). **b**, Immunoblot analysis of indicated proteins in B16-OVA tumour cells after treatment with IFNγ for indicated timepoints. The same VDAC2 and β-Actin blots were shown in Fig. 3i. **c**, Immunoblot analysis of indicated proteins in B16-OVA tumour cells treated with vehicle, IFNγ (10 ng ml^{-1}), cisplatin (20 μM), or etoposide (20 μM) for 12 h. Densiometric quantification of BIM, BID, BAK, BAX, PUMA, or p53 expression is shown. **d**, Immunoblot analysis of indicated proteins in control, STAT1-deficient or IRF1-deficient B16-OVA tumour cells treated with IFNγ for indicated timepoints. Densiometric quantification of BIM, BID, BAK and STING expression is shown. **e**, Relative *Bcl2l11*, *Bid*, *Bak1* and *Sting1* levels (versus non-treated control cells) in indicated B16-OVA tumour cells treated with or without IFNγ for 12 h (n = 3 per group). **f**, Immunoblot analysis of indicated proteins in control and VDAC2-deficient LoVo tumour cells treated with or without IFNγ for 48 h, with densiometric quantification of BIM, BID and BAK shown. The same VDAC2 and β-ACTIN blots were shown in Fig. 3s. **g**, Control, VDAC2-deficient, STAT1-deficient, VDAC2 and STAT1 co-deficient, IRF1-deficient or VDAC2 and IRF1 co-deficient (B16-OVA tumour cell survival after treatment with or without IFNγ (10 ng ml^{-1}) for 24 h (n = 3 per group). **h**, Relative *Ifnb1* and *Ccl5* levels (versus non-treated control cells) indicated B16-OVA tumour cells treated with or without IFNγ (10 ng ml^{-1}) for 24 h (n = 3 per group). **i**, Immunoblot analysis of BIM, BID and VDAC2 in control, VDAC2-deficient, BIM-deficient, BID-deficient, BIM and BID co-deficient, VDAC2 and BIM co-deficient, VDAC2 and BID co-deficient, or VDAC2, BIM, and BID co-deficient tumour cells (left). Cell death of indicated B16-OVA tumour cells treated with IFNγ (10 ng ml^{-1}) for 24 h (right; n = 3 per group). **j**, Control, VDAC2-deficient, BIM and BID co-deficient, or VDAC2, BIM and BID co-deficient B16-OVA cell viability after co-culture with OT-I cells at the indicated E:T ratios for 36 h (n = 3 per group). **k**, Indicated B16-OVA cells were treated with IFNγ for 24 h. Mitochondrial fractions were isolated and treated with 1,6-bis-maleimidohexane (BMH). Samples were separated by SDS-PAGE to resolve different BAK complexes (monomers, dimers, and trimers as indicated). Densiometric quantification of BAK trimers is shown. **l**, Expression of cytochrome c (Cyto c) and SMAC in cytosolic and mitochondrial fractions of indicated B16-OVA tumour cells treated with IFNγ for 24 h. **m**, Relative cytosolic mtDNA levels (versus non-treated control cells) in indicated B16-OVA tumour cells treated with or without IFNγ for 24 h (n = 3 per group). **n**, Immunoblot analysis of indicated proteins in B16-OVA tumour cells treated with or without IFNγ. Densiometric quantification of p-STING, p-TBK1 or p-IRF3 is shown. **o**, Relative *Ifnb1* and *Ccl5* levels (versus non-treated control cells) expression in indicated B16-OVA tumour cells treated with IFNγ for 24 h (n = 3 per group). **p**, Relative expression of genes (with differential expression ($|\log_2 FC| > 0.5$, P value < 0.05) in VDAC2-deficient versus control tumour cells in indicated B16-OVA tumour cells after treatment with IFNγ for 24 h (n = 3 per group). Data are representative of two (**b**–**o**) independent experiments and are presented mean ± s.e.m. One-way ANOVA (**g**, **h**; right panel for **i**; **j**, **m**, **o**). Two-way ANOVA (**e**).

Extended Data Fig. 9 | See next page for caption.

Extended Data Fig. 9 | (related to Fig. 4). Co-targeting APAF-1 or caspase-9 further enhanced STING activation in IFNγ-stimulated VDAC2-deficient tumour cells. a, Real-time survival analysis of control, VDAC2-deficient, APAF-1-deficient, caspase-9-deficient, VDAC2 and APAF-1 co-deficient or VDAC2 and caspase-9 co-deficient B16-OVA tumour cells after treatment with 1 ng ml^{-1} (left; n = 2 per group) or 10 ng ml^{-1} (right; n = 2 per group) of IFNγ. The same control and VDAC2-deficient B16-OVA tumour cells are presented in Extended Data Fig. 7b. **b**, **c**, Cell death (**b**) or LDH release (**c**) of control, VDAC2-deficient, BAK-deficient, APAF-1-deficient, caspase-9-deficient, VDAC2 and BAK co-deficient, VDAC2 and APAF-1 co-deficient or VDAC2 and caspase-9 co-deficient B16-OVA tumour cells treated with IFNγ (10 ng ml^{-1}) for 24 h (n = 3 per group). **d**, **e**, Cell death of control and VDAC2-deficient B16-OVA tumour cells treated with IFNγ (10 ng ml^{-1}) plus indicated pan-caspase inhibitors (or vehicle) for 24 h (**d**; n = 3 per group) or 72 h (**e**; n = 3 per group). **f**, **g**, Cell death (**f**) or LDH release (**g**) of indicated B16-OVA cells treated with IFNγ (10 ng ml^{-1}) for 72 h (n = 3 per group). **h**, Immunoblot analysis of indicated proteins in indicated B16-OVA tumour cells treated with or without IFNγ for 24 h. Densiometric quantification of p-TBK1 is shown. **i**, Relative *Ifnb1* levels (versus non-treated control cells) in indicated B16-OVA tumour cells treated with IFNγ for 24 h (n = 3 per group). **j**, IFNβ protein levels in culture supernatants from indicated B16-OVA tumour cells treated with IFNγ for 24 h (n = 3 per group). **k**, Relative levels of IFN-responsive genes (versus non-treated control cells) in indicated B16-OVA tumour cells treated with IFNγ for 24 h (n = 3 per group). **l**, Relative *Ifnb1* and *Ccl5* levels (versus non-treated control cells) in control, VDAC2-deficient, caspase-3-deficient, caspase-7-deficient, VDAC2 and caspase-3 co-deficient, or VDAC2 and caspase-7 co-deficient B16-OVA cells treated with or without IFNγ for 24 h (n = 3 per group). **m**, Relative *Ifnb1* and *Ccl5* levels in control and VDAC2-deficient B16-OVA tumour cells treated with IFNγ (10 ng ml^{-1}) plus indicated pan-caspase inhibitors (or vehicle) for 24 h. Vehicle label indicates no IFNγ treatment (n = 3 per group). **n**, Bubble plots showing upregulated (red; Up) and downregulated (blue; Down) pathways in IFNγ-treated VDAC2 and APAF-1 co-deficient B16-OVA tumour cells versus IFNγ-treated VDAC2-deficient B16-OVA tumour cells (n = 3 per group). **o**, C57BL/6 mice were inoculated with control (n = 8), VDAC2-deficient (n = 8), APAF-1-deficient (n = 7), caspase-9-deficient (n = 7), VDAC2 and APAF-1 co-deficient (n = 8) or VDAC2 and caspase-9 co-deficient (n = 8) B16-OVA tumour cells. Tumour growth (left) and mouse survival (right) were monitored. **p**, C57BL/6 mice were inoculated with control and VDAC2-deficient B16-OVA tumour cells, followed by vehicle or emricasan (i.p. 20 mg kg^{-1}, twice a day) treatment on days 8–10 after tumour inoculation (n = 10 per group). Tumour growth (left) and mouse survival (right) were monitored. **q**, Numbers of CD45$^+$ cells (left) and CD8$^+$ T cells (right) in control, VDAC2-deficient, BAK-deficient or VDAC2 and BAK co-deficient B16-OVA tumours on day 14 after tumour inoculation (n = 8 per group). **r**, Numbers of IFNγ$^+$TNF$^+$ (left) or GZMB$^+$ (right) CD8$^+$ T cells in tumours described in **q** (n = 8 per group). **s**, **t**, C57BL/6 mice were inoculated with control (n = 7), VDAC2-deficient (n = 8), BAK-deficient (n = 7), or VDAC2 and BAK co-deficient (n = 8) B16-OVA tumour cells in combination with isotype (left) or anti-PD-L1 (right) treatment on days 7, 10, and 13 after tumour inoculation. Tumour growth (**s**) and mouse survival (**t**) were monitored. Data are representative of two (**a**–**m**, **o**, **q**–**t**) or one (**p**) independent experiments and are mean ± s.e.m. One-way ANOVA (**b**, **c**, **f**, **g**, **i** – **l**, **q**, **r**). Two-way ANOVA (**d**, **e**, **m**; tumour size of **o**, **p**, **s**). Mantel–Cox test (survival of **o**, **p**, **t**).

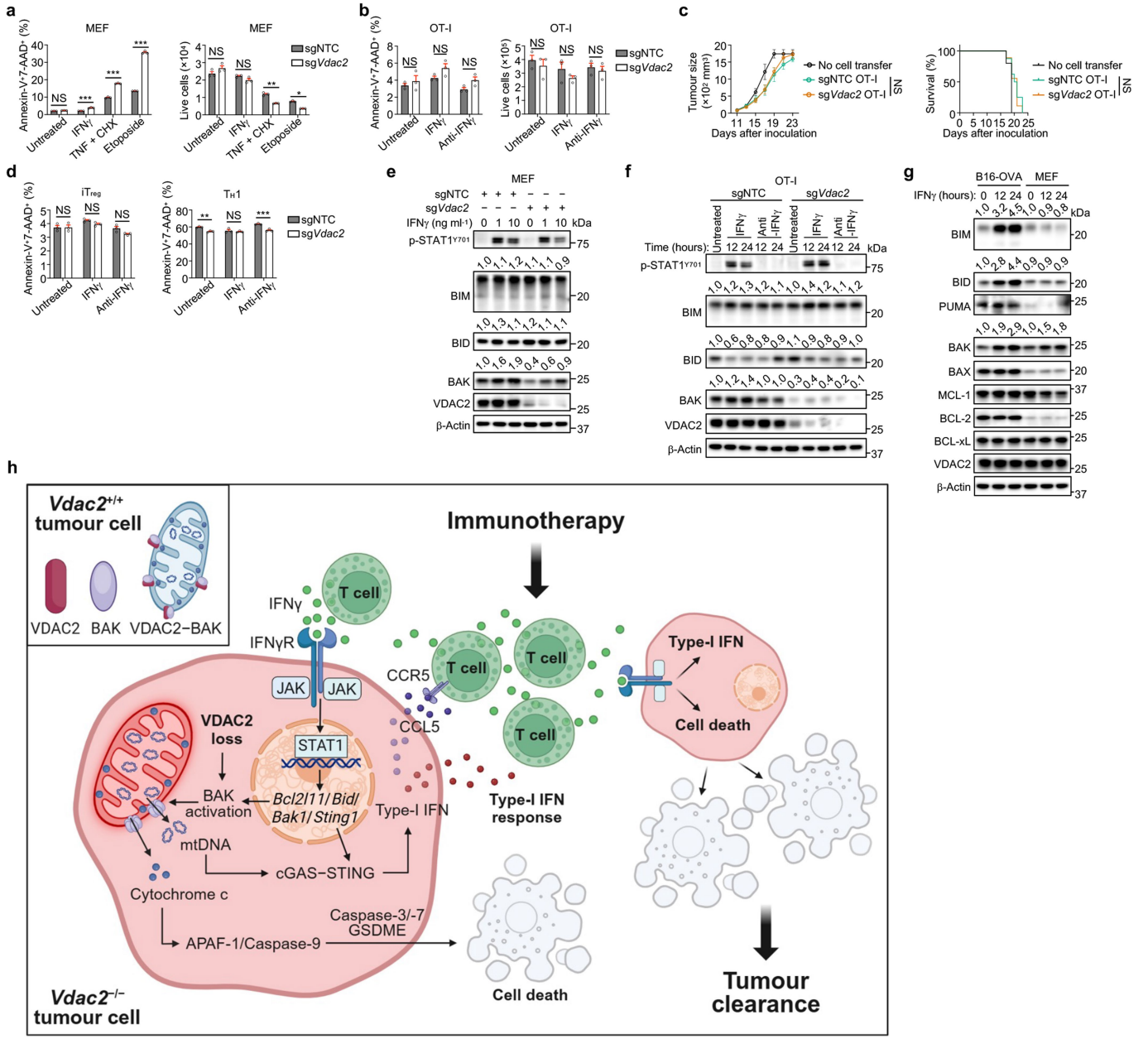

Extended Data Fig. 10 | (related to Fig. 4). IFNγ signalling does not induce cell death in non-tumorigenic cells lacking VDAC2. a, Cell death analysis of control and VDAC2-deficient MEFs treated with or without IFNγ (10 ng ml^{-1}, 24 h), TNF (10 ng ml^{-1}) plus cycloheximide (CHX, 5 μg ml^{-1}, 4 h), or etoposide (20 μM, 24 h), based on Annexin-V and 7-AAD co-staining (left; n = 3 per group) and live cell number counts (right; n = 3 per group). **b**, Cell death analysis of control and VDAC2-deficient OT-I cells treated with or without IFNγ (10 ng ml^{-1}) or anti-IFNγ (10 μg ml^{-1}) for 24 h, based on Annexin-V and 7-AAD co-staining (left; n = 3 per group) and live cell number counts (right; n = 3 per group). **c**, B16-OVA tumour growth (left) and mouse survival (right) in mice that received Cas9-expressing OT-I cells transduced with sgNTC (n = 8) or sg*Vdac2* (n = 9) on day 12 after tumour inoculation. No cell transfer group (n = 5) shows mice without adoptive transfer of OT-I cells. **d**, Cell death analysis of control and VDAC2-deficient iT$_{reg}$ (left; n = 3 per group) or T$_H$1 (right; n = 3 per group) CD4$^+$ T cells treated with or without IFNγ (10 ng ml^{-1}) or anti-IFNγ (10 μg ml^{-1}) for 24 h. **e**, Immunoblot analysis of indicated proteins in control or VDAC2-deficient MEFs treated with or without indicated concentrations of IFNγ, with densiometric quantification of BIM, BID or BAK expression shown. **f**, Immunoblot analysis of indicated proteins in control or VDAC2-deficient OT-I cells treated with or without IFNγ or anti-IFNγ. Densiometric quantification of BIM, BID or BAK expression is shown. **g**, Immunblot analysis of indicated proteins in B16-OVA tumour cells and MEFs treated with or without IFNγ (10 ng ml^{-1}) for 12 or 24 h, with densiometric quantification of BIM, BID, and BAK expression shown. **h**, Two-step model for IFNγ-dependent tumour cell destruction and inflammatory remodelling by the VDAC2–BAK axis. In both wild-type (not depicted) and VDAC2-deficient tumour cells, IFNγ signalling upregulates pro-apoptotic BIM, BID and BAK as well as STING, in a STAT1- and/or IRF1 (not depicted)-dependent manner. This coordinate upregulation sensitizes tumour cells to cell death and cGAS–STING activation that is tuned by the VDAC2–BAK axis. Specifically, in wild-type (depicted as *Vdac2*$^{+/+}$) cells, BAK co-localizes with and is inhibited by VDAC2, which acts to counterbalance IFNγ-induced sensitizing effects. Accordingly, wild-type cells are protected from these effects, thereby enabling tumour immune evasion. In the absence of VDAC2 (depicted as *Vdac2*$^{-/-}$), tumour cells respond to IFNγ stimulation by enhancing BIM- and BID-mediated BAK activation and MOMP, accompanied by uncontrolled mitochondrial cytochrome c release to the cytosol and subsequent cell death. In parallel, aberrant accumulation of cytosolic mtDNA activates cGAS–STING signalling, thereby triggering type-I IFN response and CCL5 production, which enhances CD8$^+$ T cell accumulation in the TME and promotes anti-tumour immunity. Created in BioRender. Yuan, S. (2025) https://BioRender.com/n19m747. Data are representative of two (**a**, **b**, **e**, **g**) or one (**c**, **d**, **f**) independent experiments and are mean ± s.e.m. Two-way ANOVA (**a**, **b**; tumour growth of **c**; **d**). Mantel–Cox test (survival of **c**).

nature portfolio

Corresponding author(s): Hongbo Chi

Last updated by author(s): Jan 27, 2025

Reporting Summary

Nature Portfolio wishes to improve the reproducibility of the work that we publish. This form provides structure for consistency and transparency in reporting. For further information on Nature Portfolio policies, see our Editorial Policies and the Editorial Policy Checklist.

Statistics

For all statistical analyses, confirm that the following items are present in the figure legend, table legend, main text, or Methods section.

n/a	Confirmed
☐	☒ The exact sample size (*n*) for each experimental group/condition, given as a discrete number and unit of measurement
☐	☒ A statement on whether measurements were taken from distinct samples or whether the same sample was measured repeatedly
☐	☒ The statistical test(s) used AND whether they are one- or two-sided *Only common tests should be described solely by name; describe more complex techniques in the Methods section.*
☐	☒ A description of all covariates tested
☐	☒ A description of any assumptions or corrections, such as tests of normality and adjustment for multiple comparisons
☐	☒ A full description of the statistical parameters including central tendency (e.g. means) or other basic estimates (e.g. regression coefficient) AND variation (e.g. standard deviation) or associated estimates of uncertainty (e.g. confidence intervals)
☐	☒ For null hypothesis testing, the test statistic (e.g. *F*, *t*, *r*) with confidence intervals, effect sizes, degrees of freedom and *P* value noted *Give P values as exact values whenever suitable.*
☒	☐ For Bayesian analysis, information on the choice of priors and Markov chain Monte Carlo settings
☒	☐ For hierarchical and complex designs, identification of the appropriate level for tests and full reporting of outcomes
☐	☒ Estimates of effect sizes (e.g. Cohen's *d*, Pearson's *r*), indicating how they were calculated

Our web collection on statistics for biologists contains articles on many of the points above.

Software and code

Policy information about availability of computer code

Data collection	BD FACSDIva software (v8) was used to collect flow cytometry data on LSRII, Fortessa or Symphony A3 cytometers (BD Biosciences).
Data analysis	FlowJo v10 (TreeStar) for flow cytometry results; IncuCyte S3 and IncuCyte S5 for cell death analysis; GraphPad Prism v10 for statistics; Affymetrix Expression console v1.4.1 for microarray; Limma R package v3.34.9, ComplexHeatmap R package v2.6.2 for microarray; CIBERSORTx algorithm (https://cibersortx.stanford.edu/, v1.05) for deconvolution of RNA-seq; GEPIA v2 (http://gepia2.cancer-pku.cn/) for calculating correlations of genes and signatures in TCGA datasets; trimmomatic v0.36, BWA v0.7.16, Picard v2.9.4, MACS2 v2.1.120160309, SAMtools v1.9, bedtools v2.25.0, MEME suite v4.11.3, DEseq2 v1.43.5 for ATAC-seq; Cell Ranger v6.0.0, Seurat R package v4.1, GSEA software v4.3.2, Ingenuity® Pathway Analysis (Qiagen, www.qiagen.com/ingenuity, v01-23-01), MSigDB v7.4, ggplot2 R package v3.3.5, inferCNV v1.3.5 and scRepertoire R package v1.3.5 for scRNA-seq; MAGeCK v0.5.9.4 software for bulk CRISPR screening; NIS Elements (64bit, v5.30.03) for imaging deconvolution. Imaris software (Bitplane, v9.5.1.x64) for imaging analysis. All codes used for analysis are available from the authors upon request (see Code Availability Statement).

For manuscripts utilizing custom algorithms or software that are central to the research but not yet described in published literature, software must be made available to editors and reviewers. We strongly encourage code deposition in a community repository (e.g. GitHub). See the Nature Portfolio guidelines for submitting code & software for further information.

Data

Policy information about availability of data

All manuscripts must include a data availability statement. This statement should provide the following information, where applicable:

- Accession codes, unique identifiers, or web links for publicly available datasets
- A description of any restrictions on data availability
- For clinical datasets or third party data, please ensure that the statement adheres to our policy

All microarray, scRNA-seq, and ATAC-seq data described in the manuscript have been deposited in the NCBI Gene Expression Omnibus (GEO) database and are accessible through the GEO SuperSeries access number GSE261554. Public scRNA-seq datasets are available through GSE217160 (https://www.ncbi.nlm.nih.gov/geo/query/acc.cgi?acc=GSE217160), GSE112865 (https://www.ncbi.nlm.nih.gov/geo/query/acc.cgi?acc=GSE112865), GSE121861 (https://www.ncbi.nlm.nih.gov/geo/query/acc.cgi?acc=GSE121861), GSE215121 (https://www.ncbi.nlm.nih.gov/geo/query/acc.cgi?acc=GSE215121) and GSE148071 (https://www.ncbi.nlm.nih.gov/geo/query/acc.cgi?acc=GSE148071). Hallmark, C2, and C5 collections were from the MSigDB (https://www.broadinstitute.org/gsea/msigdb/). Cancer DepMap (https://depmap.org/portal/gene/VDAC2?tab=dependency) and TCGA database (https://www.cancer.gov/ccg/research/genome-sequencing/tcga) are publicly available.

Research involving human participants, their data, or biological material

Policy information about studies with human participants or human data. See also policy information about sex, gender (identity/presentation), and sexual orientation and race, ethnicity and racism.

Reporting on sex and gender	The human samples that were collected for this study were blood samples to generate the B7-H3-CAR T cells. Fresh human peripheral blood leukopaks were purchased from Charles River. Purification of CD4+ and CD8+ T cells was performed at the Experimental Cellular Therapeutics Laboratory (ECTL) of St. Jude. ECT026 cells were from a female donor. ECT028 and ECT031 were from male donors.
Reporting on race, ethnicity, or other socially relevant groupings	Limited donor information was provided by Charles River. Donor for ECT026 is female, Hispanic. Donor for ECT028 and ECT031 are both male, Caucasian.
Population characteristics	This information was not available to the authors of this study.
Recruitment	The authors of this study were not involved with the recruitment of healthy donors used to obtain the commerically available leukopaks.
Ethics oversight	Since de-identified leukapheresis products were used, CAR T cell generation and experiments with these cells are considered non-human subject research. This determination was confirmed by the Institutional Review Board (IRB) at St. Jude Children's Research Hospital.

Note that full information on the approval of the study protocol must also be provided in the manuscript.

Field-specific reporting

Please select the one below that is the best fit for your research. If you are not sure, read the appropriate sections before making your selection.

☒ Life sciences ☐ Behavioural & social sciences ☐ Ecological, evolutionary & environmental sciences

For a reference copy of the document with all sections, see nature.com/documents/nr-reporting-summary-flat.pdf

Life sciences study design

All studies must disclose on these points even when the disclosure is negative.

Sample size	Sample sizes were selected based on those used in previous publications (Zhou et al. Nature 2023; Guo et al. Nature 2023; Tsai et al. Cell Metabolism 2023).
Data exclusions	No data were excluded.
Replication	All the experimental findings were reliably reproduced as validated by at least three biological replicates in at least three independent experiments unless otherwise noted.
Randomization	Age- and sex-matched mice were assigned randomly to experimental and control groups in vivo. Randomization was not applicable for in vitro studies.
Blinding	The investigators were not blinded to group allocation during data collection or analysis. This approach is considered standard for experiments of the type performed in this study, as genotypes of both mice and gene-targeted cells must be pre-determined prior to analysis. Researchers were not blinded to treatment groups for in vivo and in vitro studies because knowledge of this information was essential to conduct the studies.

Reporting for specific materials, systems and methods

We require information from authors about some types of materials, experimental systems and methods used in many studies. Here, indicate whether each material, system or method listed is relevant to your study. If you are not sure if a list item applies to your research, read the appropriate section before selecting a response.

Materials & experimental systems

n/a	Involved in the study
☐	☒ Antibodies
☐	☒ Eukaryotic cell lines
☒	☐ Palaeontology and archaeology
☐	☒ Animals and other organisms
☒	☐ Clinical data
☒	☐ Dual use research of concern
☒	☐ Plants

Methods

n/a	Involved in the study
☒	☐ ChIP-seq
☐	☒ Flow cytometry
☒	☐ MRI-based neuroimaging

Antibodies

Antibodies used

1. The following antibodies were used for cell culture: anti-CD3 (2C11; Bio X Cell, BE0001-1), anti-CD28 (37.51; Bio X Cell, BE0015-1, anti-IFNγ antibody (XMG1.2, Bio X Cell), anti-IFNAR1 antibody (MAR1-5A3, Bio X Cell) and IgG1 isotype control (HRPN, Bio X Cell).

2. The following antibodies were used for in vivo treatments: anti-PD-1 antibody (J43, Bio X Cell), anti-PD-L1 antibody (10F.9G2, Bio X Cell), anti-CD8α (2.43, Bio X Cell),rat IgG2b isotype control (LTF-2, Bio X Cell), anti-IFNγ antibody (XMG1.2, Bio X Cell) and IgG1 isotype control (HRPN, Bio X Cell).

3. For flow cytometry analysis: 7-AAD (A9400, 1:200, Sigma-Aldrich) or fixable viability dye (65-0865-18, 1:1000, eBioscience) was used for dead cell exclusion. The following antibodies were used: PE–anti-CD45 (1:400, 30-F11, 12-0451-83, eBioscience), FITC–anti-CD45.2 (1:400, 104, 109806, BioLegend), Brilliant Violet 785–anti-CD45.2 (1:400, 104, 109839, BioLegend), Alexa Fluor 700–anti-CD8α (1:400, 53-6.7, 100730, BioLegend), Brilliant Violet 605–anti-CD8α (1:400, 53-6.7, 100743, BioLegend), Alexa Fluor 650–anti-CD4 (1:400, GK1.5, 100469, BioLegend), Brilliant Violet 785–anti-TCRβ (1:400, H57-597, 109249, BioLegend),PE/DazzleTM 594–anti-PD-1 (1:400, 29F.1A12, Biolegend,135228), Brilliant Violet 711–anti-B220 (1:400, RA3-6B2, 103255, BioLegend), FITC–anti-CD19 (1:400, eBio1D3, 11-0193-85, eBioscience),PE/Cyanine7–anti-IFNγ (1:200, XMG1.2, 505826, BioLegend), Brilliant Violet 421–anti-TNF (1:200, MP6-XT22, 506328, BioLegend), Alexa Fluor 647–anti-granzyme B (1:100, GB11, 515406, BioLegend), FITC–anti-FOXP3 (1:200, FJK-16s, 11-5773-82, eBioscience), BV650–anti-Ki67 (1:100, B56, 563757, BD Biosciences), Alexa Fluor 647–anti-active caspase-3 (1:100, C92-605, 560626, BD Biosciences), PE–anti-IL-2 (1:200, JES6-5H4, 554428, BD Biosciences), APC–anti-Annexin V (1:50, BMS306APC-100, Invitrogen).

4. The following antibodies were used for immunoprecipitation or immunoblot analysis: anti-VDAC2 (1:1,000, PA5-28106, Invitrogen), anti-BCL-2 (1:1,000, sc-7382, Santa Cruz), anti-MCL-1 (1:1,000, ab32087, Abcam), anti-GSDME (1:1,000, ab215191, Abcam), anti-FLAG (1:5,000, F1804, Sigma-Aldrich); anti-BIM (1: 1,000, B7929, Sigma-Aldrich); anti-Cas9 (1:5,000, 14697), anti-β-Actin (1:5,000, 4970), anti-p-STAT1 Y701 (1:1,000, 9167), anti-STAT1 (1:1,000, 14994), anti-caspase-3 (1:1,000, 9662), anti-cleaved caspase-3 (1:1,000, 9661), anti-caspase-7 (1:1,000, 9492), anti-cleaved caspase-7 (1:1,000, 9491), anti-caspase-9 (1:1,000, 9504), anti-APAF-1 (1:1,000, 8969), anti-cGAS (1:1,000, 31659), anti-STING (1:1,000, 13647), anti-p-STING S365 for mouse cells (1:1,000, 72971), anti-p-STING S366 for human cells (1:1,000, 19781), anti-TBK1 (1:1,000, 38066), anti-p-TBK1 S172 (1:1,000, 5483), anti-IRF3 (1:1,000, 4302), anti-p-IRF3 S396 (1:1,000, 29047), anti-MAVS (1:1,000, 4983), anti-BAK (1:1,000, 12105), anti-BAX (1:1,000, 2772), anti-BCL-XL (1:1,000, 2764), anti-BID for mouse cells (1:1,000, 2003), anti-BID for human cells (1:1,000, 2002), anti-PUMA (1:1,000, 98672), anti-HA (1:5,000, 3724), anti-SMAC (1:1,000; 15108), anti-cytochrome c (1:1,000, 4280) and anti-TOMM20 (1:1,000, 42406) (all from Cell Signaling Technology). Secondary antibodies used for protein detection were HRP-conjugated anti-mouse IgG (1:3,000; W4021; Promega) or HRP-conjugated anti-rabbit IgG (1:3,000; W4011; Promega).

5. The following antibodies were used for image analysis: anti-dsDNA (1 µg/ml; MAB030, Millipore-Sigma), anti-TOMM20 (1 µg/ml; 186735, Abcam), anti-HA (1 µg/ml; 2367, Cell Signaling Technology) and anti-F-Actin (PHDG1, Cytoskeleton); secondary antibodies used were donkey anti-mouse (1:500; A32773, Thermo Fisher Scientific) and donkey anti-rabbit (1:500; A32795, Thermo Fisher Scientific).

Validation

1. The following antibodies were used for cell culture have been validated for the specificity and application by the manufacturers (see detailed reference on the website)
anti-mouse CD3: https://bioxcell.com/invivomab-anti-mouse-cd3-epsilon-be0001-1
anti-mouse CD28: https://bioxcell.com/invivomab-anti-mouse-cd28-be0015-1
anti-mouse IFNAR1: https://bioxcell.com/invivomab-anti-mouse-ifnar-1-be0241

2. The following antibodies were used for in vivo treatments have been validated for the specificity and application by the manufacturers (see detailed reference on the website)
anti-mouse PD-L1: https://bioxcell.com/invivomab-anti-mouse-pd-l1-b7-h1-be0101
anti-mouse PD-1: https://bioxcell.com/invivomab-anti-mouse-pd-1-cd279-be0033-2
anti-mouse IFNγ: https://bioxcell.com/invivomab-anti-mouse-ifn-gamma-be0055
anti-mouse CD8α: https://bioxcell.com/invivomab-anti-mouse-cd8-alpha-be0061
rat IgG2b isotype control: https://bioxcell.com/invivomab-rat-igg2b-isotype-control-anti-keyhole-limpet-hemocyanin-be0090

rat IgG1 isotype control: https://bioxcell.com/invivomab-rat-igg1-isotype-control-anti-horseradish-peroxidase-be0088

3. The following antibodies for flow cytometry have been validated for the specificity and application by the manufacturers (see detailed reference on the website):
7-AAD: https://www.sigmaaldrich.com/US/en/product/sigma/a9400
Fixable viability dye: https://www.thermofisher.com/order/catalog/product/65-0865-14?SID=srch-srp-65-0865-14
PE–anti-CD45: https://www.fishersci.se/shop/products/cd45-monoclonal-antibody-30-f11-pe-ebioscience-invitrogen/15278539
FITC–anti-CD45.2: https://www.biolegend.com/de-at/products/fitc-anti-mouse-cd45-2-antibody-6
Brilliant Violet 785–anti-CD45.2: https://www.biolegend.com/de-at/products/brilliant-violet-785-anti-mouse-cd45-2-antibody-8924
Alexa Fluor 700–anti-CD8α: https://www.biolegend.com/de-at/products/alexa-fluor-700-anti-mouse-cd8a-antibody-3387
Brilliant Violet 605–anti-CD8α: https://www.biolegend.com/de-at/products/brilliant-violet-605-anti-mouse-cd8a-antibody-7636
Alexa Fluor 650–anti-CD4: https://www.biolegend.com/de-at/products/brilliant-violet-650-anti-mouse-cd4-antibody-16780
Brilliant Violet 785–anti-TCRβ: https://www.biolegend.com/de-at/products/brilliant-violet-785-anti-mouse-tcr-b-chain-antibody-17614
PE/DazzleTM 594–anti-PD-1: https://www.biolegend.com/de-at/products/pe-dazzle-594-anti-mouse-cd279-pd-1-antibody-12090
Brilliant Violet 711–anti-B220: https://www.biolegend.com/de-at/products/brilliant-violet-711-anti-mouse-human-cd45r-b220-antibody-9692
FITC–anti-CD19 (1:400, eBio1D3, 11-0193-85, eBioscience):https://www.fishersci.at/shop/products/cd19-monoclonal-antibody-ebio1d3-1d3-fitc-ebioscience-invitrogen/15298039
PE/Cyanine7–anti-IFNγ: https://www.biolegend.com/de-at/products/pe-cyanine7-anti-mouse-ifn-gamma-antibody-5865
Brilliant Violet 421–anti-TNF: https://www.biolegend.com/de-at/products/brilliant-violet-421-anti-mouse-tnf-alpha-antibody-7336
Alexa Fluor 647–anti-granzyme B: https://www.biolegend.com/de-at/products/alexa-fluor-647-anti-human-mouse-granzyme-b-antibody-6067
FITC–anti-FOXP3: https://www.thermofisher.com/antibody/product/FOXP3-Antibody-clone-FJK-16s-Monoclonal/11-5773-82
BV650–anti-Ki67: https://www.bdbiosciences.com/ja-jp/products/reagents/flow-cytometry-reagents/research-reagents/single-color-antibodies-ruo/bv650-mouse-anti-ki-67.563757
Alexa Fluor 647–anti-active caspase-3: https://www.bdbiosciences.com/en-dk/products/reagents/flow-cytometry-reagents/research-reagents/single-color-antibodies-ruo/alexa-fluor-647-rabbit-anti-active-caspase-3.560626
PE–anti-IL-2: https://www.bdbiosciences.com/en-dk/search-results?searchKey=554428
APC–anti-Annexin V: https://www.thermofisher.com/proteins/product/Annexin-V-Recombinant-Protein/BMS306APC-100

4. The specificities of listed immunoblot antibodies have been validated by the manufacturer by western blot:
anti-VDAC2: https://www.thermofisher.com/antibody/product/VDAC2-Antibody-Polyclonal/PA5-28106
anti-BCL-2: https://www.scbt.com/p/bcl-2-antibody-c-2
anti-MCL-1: https://www.abcam.com/products/primary-antibodies/mcl1-antibody-y37-ab32087.html
anti-GSDME: https://www.abcam.com/products/primary-antibodies/dfna5gsdme-antibody-epr19859-n-terminal-ab215191.html
anti-FLAG: https://www.sigmaaldrich.com/US/en/product/sigma/f1804
anti-BIM: https://www.sigmaaldrich.com/US/en/product/sigma/b7929?srsltid=AfmBOopDztR4n-2XynJ9shXKPeyxc6SUPvUVwBp01ZEVGuzns-Jak04Y
anti-Cas9: https://www.cellsignal.com/products/primary-antibodies/cas9-s-pyogenes-7a9-3a3-mouse-mab/14697
anti-β-Actin: https://www.cellsignal.com/products/primary-antibodies/b-actin-13e5-rabbit-mab/4970
anti-p-STAT1 Y701:https://www.cellsignal.com/products/primary-antibodies/phospho-stat1-tyr701-58d6-rabbit-mab/9167
anti-STAT1:https://www.cellsignal.com/products/primary-antibodies/stat1-d1k9y-rabbit-mab/14994
anti-caspase-3: https://www.cellsignal.com/products/primary-antibodies/caspase-3-antibody/9662
anti-cleaved caspase-3: https://www.cellsignal.com/products/primary-antibodies/cleaved-caspase-3-asp175-antibody/9661
anti-caspase-7: https://www.cellsignal.com/products/primary-antibodies/caspase-7-antibody/9492
anti-cleaved caspase-7: https://www.cellsignal.com/products/primary-antibodies/cleaved-caspase-7-asp198-antibody/9491
anti-caspase-9: https://www.cellsignal.com/products/primary-antibodies/caspase-9-antibody/9504
anti-APAF-1: https://www.cellsignal.com/products/primary-antibodies/apaf-1-d5c3-rabbit-mab/8969
anti-cGAS: https://www.cellsignal.com/products/primary-antibodies/cgas-d3o8o-rabbit-mab/31659
anti-STING: https://www.cellsignal.com/products/primary-antibodies/sting-d2p2f-rabbit-mab/13647
anti-p-STING S365: https://www.cellsignal.com/products/primary-antibodies/phospho-sting-ser365-d8f4w-rabbit-mab/72971
anti-p-STING S366:https://www.cellsignal.com/products/primary-antibodies/phospho-sting-ser366-d7c3s-rabbit-mab/19781?srsltid=AfmBOopQmFJtCoB01JovrGNe_wW3-Z82lordZ3m6AXQJZeMqt1FM7Y8b
anti-TBK1: https://www.cellsignal.com/products/primary-antibodies/tbk1-nak-e8i3g-rabbit-mab/38066
anti-p-TBK1 S172: https://www.cellsignal.com/products/primary-antibodies/phospho-tbk1-nak-ser172-d52c2-xp-174-rabbit-mab/5483
anti-IRF-3: https://www.cellsignal.com/products/primary-antibodies/irf-3-d83b9-rabbit-mab/4302
anti-p-IRF3 S396: https://www.cellsignal.com/products/primary-antibodies/phospho-irf-3-ser396-d6o1m-rabbit-mab/29047
anti-MAVS: https://www.cellsignal.com/products/primary-antibodies/mavs-antibody/4983
anti-BAK: https://www.cellsignal.com/products/primary-antibodies/bak-d4e4-rabbit-mab/12105
anti-BAX: https://www.cellsignal.com/products/primary-antibodies/bax-antibody/2772
anti-BCL-XL: https://www.cellsignal.com/products/primary-antibodies/bcl-xl-54h6-rabbit-mab/2764
anti-BID: https://www.cellsignal.com/products/primary-antibodies/bid-antibody/2003?srsltid=AfmBOoq0aJG1nDHnnCwe8rwo5op2shZ-yCUf-5F4wMaRRZbF99HGccAZ
anti-BID:https://www.cellsignal.com/products/primary-antibodies/bid-antibody/2002?srsltid=AfmBOopPk09vGCnJx3-utBrFAtngdEOLfSRJaGXXvmcJV58dtVh9_unj
anti-PUMA: https://www.cellsignal.com/products/primary-antibodies/puma-e2p7g-rabbit-mab/98672?srsltid=AfmBOooyOeZ4JpB6Hoesf6Q42MGBXGihB3EgAe740OWWjvMP5PXCzuat
anti-HA: https://www.cellsignal.com/products/primary-antibodies/ha-tag-c29f4-rabbit-mab/3724
anti-SMAC: https://www.cellsignal.com/products/primary-antibodies/smac-diablo-d5s3r-rabbit-mab/15108
anti-cytochrome c: https://www.cellsignal.com/products/primary-antibodies/cytochrome-c-136f3-rabbit-mab/4280
anti-TOMM20: https://www.cellsignal.com/products/primary-antibodies/tom20-d8t4n-rabbit-mab/42406
HRP-conjugated anti-mouse IgG: https://www.promega.com/products/protein-detection/primary-and-secondary-antibodies/anti-rabbit-igg-h-and-l-hrp-conjugate/?catNum=W4011
HRP-conjugated anti-rabbit IgG: https://www.promega.com/products/protein-detection/primary-and-secondary-antibodies/

anti_mouse-igg-h-and-l-hrp-conjugate/?catNum=W4021

5. The following antibodies for image analysis have been validated for the specificity and application by the manufacturers (see detailed reference on the website):
anti-dsDNA: https://www.sigmaaldrich.com/US/en/product/mm/mab030
anti-TOMM20: https://www.abcam.com/products/primary-antibodies/tomm20-antibody-epr15581-54-mitochondrial-marker-ab186735.html
anti-HA: https://www.cellsignal.com/products/primary-antibodies/ha-tag-6e2-mouse-mab/2367
anti-F-Actin: https://www.cytoskeleton.com/phdg1
Donkey anti-Mouse IgG (H+L) Highly Cross-Adsorbed Secondary Antibody, Alexa Fluor™ Plus 555: https://www.thermofisher.com/antibody/product/Donkey-anti-Mouse-IgG-H-L-Highly-Cross-Adsorbed-Secondary-Antibody-Polyclonal/A32773
Donkey anti-Rabbit IgG (H+L) Highly Cross-Adsorbed Secondary Antibody, Alexa Fluor™ Plus 647:https://www.thermofisher.com/antibody/product/Donkey-anti-Rabbit-IgG-H-L-Highly-Cross-Adsorbed-Secondary-Antibody-Polyclonal/A32795

Eukaryotic cell lines

Policy information about cell lines and Sex and Gender in Research

Cell line source(s)	B16-OVA, MC38-OVA and MC38 cell lines were provided by D. Vignali (University of Pittsburgh). The HEK293T and LoVo cell lines were purchased from the American Type Culture Collection (ATCC). The Plat-E cell line was provided by Y.-C. Liu (La Jolla Institute of Immunology).
Authentication	The cell lines used were not authenticated.
Mycoplasma contamination	Cell lines were tested and determined to be free of mycoplasma contamination.
Commonly misidentified lines (See ICLAC register)	No commonly misidentified cell lines were used.

Animals and other research organisms

Policy information about studies involving animals; ARRIVE guidelines recommended for reporting animal research, and Sex and Gender in Research

Laboratory animals	C57BL/6 (stock number 000664), OT-I (stock number 003831), SMARTA (stock number 030450), Rosa26-Cas9 knock-in (stock number 026179), C57BL/6-Tg (Cd8a-cre)1Itan/J (Cd8Cre) (stock number 008766) and Rag1−/− mice (stock number 002216) were purchased from the Jackson Laboratory. We crossed OT-I mice with Rosa26-Cas9 knock-in mice to generate OT-I-Cas9 mice. To generate Ifngfl/fl mice, loxP sites were inserted into intron 1 and the 3′ UTR of the Ifng gene, resulting in Cre-mediated deletion of exons 2–4 (in the C57BL/6 background). These mice were outbred to C57BL/6 prior to any experimental crosses. Ifngfl/fl mice were crossed with the abovementioned Cd8Cre mice or WT C57BL/6 mice to generate Cd8CreIfngfl/fl or control Ifngfl/fl mice, respectively. To generate complete bone marrow chimeras, bone marrow cells from Cd8CreIfngfl/fl or control Ifngfl/fl mice were flushed from mouse tibias and femurs, and red blood cells were lysed using ACK lysis buffer, followed by intravenously injection into sublethally (5.5Gy) irradiated Rag1−/− recipient mice. Sex-matched mice were used at 6–10 weeks old. Animals were housed under 12 h light–dark cycles that coincide with daylight in Memphis, TN, USA (light on at 06:00 and off at 18:00). Food and water were provided ad libitum. The St. Jude Children's Research Hospital Animal Resource Center was maintained at 20–25 °C and 30–70% humidity.
Wild animals	The study did not involve wild animals.
Reporting on sex	Both male and female mice were included in all analyses reported in this manuscript, as there were no differences between sexes observed in any of our biological or functional assays.
Field-collected samples	The study did not involve samples collected from the field.
Ethics oversight	Experiments and procedures were performed in accordance with the Institutional Animal Care and Use Committee (IACUC) of St. Jude Children's Research Hospital.

Note that full information on the approval of the study protocol must also be provided in the manuscript.

Plants

Seed stocks	N/A
Novel plant genotypes	N/A
Authentication	N/A

Flow Cytometry

Plots

Confirm that:

☒ The axis labels state the marker and fluorochrome used (e.g. CD4-FITC).

☒ The axis scales are clearly visible. Include numbers along axes only for bottom left plot of group (a 'group' is an analysis of identical markers).

☒ All plots are contour plots with outliers or pseudocolor plots.

☒ A numerical value for number of cells or percentage (with statistics) is provided.

Methodology

Sample preparation	The spleens, peripheral lymph nodes (PLN) and mesenteric lymph nodes (MLN) were manually disrupted under nylon mesh using the flat end of a 3-mL syringes. Red blood cells were removed by ACK lysing buffer, followed by washing cells with isolation buffer. To isolate intratumoral lymphocytes, subcutaneous tumors were harvested on day 14 after inoculation, excised, minced and digested with 1 mg/ml collagenase IV (LS004188, Worthington Biochemicals) and 200 U/ml DNase I (DN25-1G, Sigma-Aldrich) for 1 hour at 37°C and then passed through 70-um filters to remove undigested tumor tissues.
Instrument	LSRII, Fortessa or Symphony A3 (BD Biosciences); Reflection cell sorter (i-Cyt).
Software	BD FACSDIva software (version 8) was used to collect flow cytometry data on LSRII, Fortessa or Symphony A3 cytometers (BD Biosciences). FlowJo v10 (TreeStar) for FACS results.
Cell population abundance	The purities of the sorted cells were more than 98%.
Gating strategy	For all experiments, FSC-A vs. SSC-A gates was used to identify population targeted viable cells. Singlet cells were separated from doublets using FSC-A vs. FSC-H gating. Live viability dye was used to eliminate dead cells. Target populations were further determined by specific antibodies, which were able to distinguish from negative populations.

☒ Tick this box to confirm that a figure exemplifying the gating strategy is provided in the Supplementary Information.